Title: Halibee fossil assemblages reveal later Pleistocene cercopithecins (Cercopithecidae: Primates) in the Middle Awash of Ethiopia

Running Title: New cercopithecin fossils from the Afar Rift, Ethiopia

Authors: Taylor, Catherine E.[1,2]; Brasil, Marianne F.[1,3]; Monson, Tesla A.[4]; Yohler, Ryan M.[1,2]; Hlusko, Leslea J.[1,2,5]

Affiliations: [1]Human Evolution Research Center, University of California, Berkeley; [2]Department of Integrative Biology, University of California, Berkeley; [3]Berkeley Geochronology Center, Berkeley, CA; Department of Anthropology, [4]Western Washington University; [5]Centro Nacional de Investigación sobre la Evolución Humana (CENIEH), Burgos, Spain

Corresponding author: Taylor, C.E. (email: catherine_taylor@berkeley.edu)

Target journal(s): American Journal of Biological Anthropology

1 | Introduction

We introduce here two new assemblages of cercopithecin fossils from the later Pleistocene of eastern Africa. These fossils belong to a Linnaean tribe with several challenging characteristics, namely: 1) an extensive amount of hybridization (Aldrich-Blake, 1968; de Jong & Butynski, 2010; Detwiler, 2004; 2010, Detwiler, Burrell, and Jolly, 2005; Struhsaker, Butynski, & Lwanga, 1988; Tapanes, 2016, Tosi, 2017); 2) remarkably conserved skeletal morphology (Arenson et al., 2020; Cardini & Elton, 2008; Sargis, Terranova, & Gebo, 2008; Gilbert et al., 2021; Szalay & Delson, 1979; Verheyen, 1962); and 3) a sparse fossil record. Before providing the paleontological description of these new fossils from the Middle Awash study area of Ethiopia's Afar Rift (Figure 1), we review the challenges that this tribe presents in both the neontological and paleontological realms.

1.1 | Extant guenons and their classification

Cercopithecin monkeys are among the most geographically widespread and taxonomically diverse primate groups alive today. These monkeys were some of the first to be extensively studied by primatologists (Elliot, 1911; Haughton, 1864; Jentink, 1886; Reuvens, 1890; Sclater, 1893; Stiles & Orleman, 1926). Tribe Cercopithecini contains ~35 species across six extant genera: *Allenopithecus, Allochrocebus*, *Cercopithecus*, *Chlorocebus*, *Erythrocebus*, and *Miopithecus* (Rowe & Myers, 2016; Turner, Schmitt, & Cramer, 2019). Often collectively referred to as the African guenons, this tribe is relatively diverse in its pelage (especially facial and genital coloration) and karyotype (Turner et al., 2019). The molecular phylogeny of this taxon has proven difficult to resolve (Arenson et al., 2020; Guschanski et al., 2013; Lo Bianco, Masters, & Sineo, 2017; Perelman et al., 2011; Tosi & Detwiler, 2016; Turner et al., 2019; Tosi, 2017; Xing et al., 2007), apparently the result of a long history of hybridization that occurs at both generic and specific levels of classification (Detwiler, 2004; Detwiler et al., 2005; de Jong & Butynski, 2010; Groves, 2018; Shurtliff, 2013).

Cercopithecin species also vary in their preferred habitat and locomotor substrates. The genera occupy three major ecological zones: semi-arid open savannah (*Erythrocebus*), swamp forests (*Allenopithecus*), and savannah woodland/shrub/gallery forest (*Allochrocebus/Cercopithecus/Chlorocebus/Miopithecus*) (Rowe & Myers, 2016). *Erythrocebus* is the largest genus in terms of body size and is almost completely terrestrial, and, consequently, this genus has the most distinctive postcranial morphology (Gebo & Sargis, 1994; Sargis et al., 2008).

The shrub/gallery forest group of genera are in the middle of the range of body size and fall into three subgroups that exhibit variation in locomotor behavior. The first and most distinct of these subgroups is often referred to as the 'L'hoesti's monkey group.' The species within this subset are largely terrestrial and have variably been assigned to *Chlorocebus* (Elton et al., 2016; Tosi, 2008), *Cercopithecus* (Cardini & Elton, 2008; Disotell, 2000; Grubb et al., 2003; Harrison, 1988; Motsch et al., 2015), and *Allochrocebus* (Lo Bianco et al., 2017; Rowe & Myers, 2016). The second subgroup, commonly referred to as 'vervets' or 'savannah monkeys,' are usually considered semi-terrestrial; they were first placed into their own separate genus (*Chlorocebus*) in 1870 (Gray, 1870) based primarily on fur and soft tissue differences, and on their semi-terrestrial habits. Now, species are usually assigned to *Chlorocebus* based on pelage, soft tissue, behavior, and genetic data. Though still often classified in their own genus, some researchers have grouped

the vervets with the third and most arboreal subgroup, *Cercopithecus*. While there is some variation in the taxonomy applied to these monkeys, most researchers today place the most terrestrial subgroup (L'hoesti's monkey group) into *Allochrocebus*, the semi-terrestrial savannah monkeys into *Chlorocebus*, and the most arboreal species into *Cercopithecus*. But, of course, there are exceptions.

While it is generally accepted that the more arboreal species of the savannah woodland/shrub/gallery forest group all belong in *Cercopithecus*, with the exception of the much smaller and genetically distinct *Miopithecus* (Lo Bianco et al., 2017), multiple species within *Cercopithecus* are consistently classified as semi-terrestrial (i.e., *Cercopithecus neglectus*; McGraw, 1994) or terrestrial (*Cercopithecus hamlyni*; Rowe & Myers, 2016). Additionally, recent research shows that *Cercopithecus lomamiensis*, which exclusively inhabits dense forest, is semi-terrestrial and likely spends a significant amount of time foraging on the ground (Arenson et al., 2020). This illustrates that the arboreal/semi-terrestrial genus dichotomization is a bit of an oversimplification. As for the ancestral cercopithecins, recent studies offer support for semi-terrestriality as the ancestral mode of locomotion, with terrestriality and arboreality evolving multiple times in different clades (Arenson et al., 2020; McGraw, 2004; Turner et al., 2019).

1.2 | Skeletal evidence

Most cercopithecin species are similar to each other in body size, with the notable exceptions being the larger Patas monkey (*Erythrocebus patas*), the much smaller talapoins (*Miopithecus*), and the slightly smaller *Cercopithecus dryas* (Gilbert et al., 2021). Cercopithecins are also very similar in craniodental and postcranial morphology, especially *Chlorocebus* and *Cercopithecus* (e.g., Arenson et al., 2020; Cardini & Elton, 2008; Gebo & Sarigs, 1994; Gilbert et al., 2021; Sargis et al., 2008; Szalay & Delson, 1979; Verheyen, 1962). While the teeth of *Allenopithecus* are somewhat distinctive, only the postcranial skeletons of the most terrestrial of the guenons – such as *Allochrocebus* and *Erythrocebus* – are readily distinguishable from other guenons (Gebo & Sargis, 1994; Strasser & Delson, 1987).

Many researchers report that craniodental traits can distinguish *Chlorocebus* and *Cercopithecus*, but diagnostic characters are limited and may not distinguish the two genera consistently (Gebo & Sargis, 1994; Cardini & Elton, 2008; Sargis et al., 2008; Szalay & Delson, 1979; Verheyen, 1962; Arenson et al., 2020; Gilbert et al., 2021). Orbital shape may be useful in distinguishing genera (Gilbert et al., 2021). Frost and Alemseged (2007) and Gilbert et al. (2021) also describe relative I^2 size (maxillary I^2 mesiodistal length / I^1 mesiodistal length) as a distinguishing characteristic, with *Chlorocebus* exhibiting larger lateral relative to medial maxillary incisors than *Cercopithecus*. Other traits suggested to separate the two genera include relative I^1 size (I^1 mesiodistal length/M^1 mesiodistal length), mandibular corpus height, and facial length (Gilbert et al., 2021). Cardini & Elton (2008) point out that cranial shape and facial length may distinguish species and genera, but large sample sizes and complete crania with numerous 3D landmarks are needed even for modest differentiation.

Postcranial traits claimed to distinguish between *Chlorocebus* and *Cercopithecus* based on locomotor habitus include aspects of scapular morphology, humeral head shape, distal humeral morphology, and head shape of the astragalus (Sargis et al., 2008; Arenson et al., 2020; Gilbert et al., 2021). However, Arenson et al. (2020) point out that it is highly likely that developmental plasticity contributes to the intraspecific variation observed in such traits.

Furthermore, the presence or absence of these traits has been used in taxonomic assessments even when the trait is not consistently present/absent within a single extant population. For example, the relative height of the humeral greater tubercle has been identified as a key trait in identifying locomotor habitus in guenons but differs even between the two extant lesula (*Cercopithecus lomamiensis*) individuals described by Arenson et al. (2020).

This example demonstrates that postcranial skeletal morphology also has a limited use in taxonomic identification because morphological traits associated with terrestriality/arboreality are not as discrete or invariable as would be needed. As another example, Nakatsukasa (1994) showed that observed locomotor behavior does not always correlate with the presence of morphological features claimed to be indicative of "locomotor type". Although the appendicular skeleton is often used to infer locomotor categories in guenons, the high levels of intraspecific variation in these regions of the skeleton complicate this endeavor (Buck, Stock, & Foley, 2010). The combination of highly conserved morphology and high levels of variation among this tribe's species, along with frequent changes in the tribe's taxonomic nomenclature, renders it difficult to conclusively and confidently infer either locomotor mode or substrate preference for fossil postcranial remains.

1.3 | Genetic evidence

Unlike their papionin and other anthropoid relatives, cercopithecins have considerable variation in chromosome number, with diploid numbers ranging from 48 to 72 (Chiarelli, 1968; Dutrillaux, 1988; Lo Bianco et al., 2017; Moulin, Gerbault-Seureau, Dutrillaux, & Richard, 2008; Sineo, 1990). Hybridization is known to occur across species with different chromosome numbers (Dugoujon, Moro & Larrouy, 1982; Sineo, 1990). After the recent publication of the *Chlorocebus* reference genome by Warren et al. (2015), Svardal et al. (2017) reported high levels of admixture between *Chlorocebus* species that diverged during the Late Pleistocene. Cercopithecins are known to commonly hybridize in the wild (Aldrich-Blake, 1968; Detwiler, 2004; 2010, Detwiler et al., 2005; Struhsaker et al., 1988; Tapanes, 2016), even inter-generically (between *Chlorocebus* and *Cercopithecus* in Kenya; de Jong & Butynski, 2010).

It is possible that these high levels of hybridization are responsible for the difficulty in resolving a clear pattern of phylogenetic branching based on genetic evidence. Attempts to resolve the phylogeny of this group have explored mtDNA (Raaum, Sterner, Noviello, Stewart, & Disotell, 2005; van der Kuyl, Kuiken, Dekker, & Goudsmit, 1995), X and Y chromosomes (Tosi, Buzzard, Morales, & Melnick, 2002; Tosi, Disotell, Morales, & Melnick, 2003; Tosi, Melnick, & Disotell, 2004a, Tosi, Buzzard, Morales, & Melnick, 2004b; Tosi, Detwiler, & Disotell, 2005a; Tosi, Detwiler, & Disotell, 2005b), serum proteins (Lucotte, Gautreau, Galat, & Galat-Luong, 1982), and next generation sequencing (Guschanski et al., 2013).

Despite these varied efforts, the guenon phylogeny is still largely unresolved (Arenson et al., 2020; Cardini & Elton, 2008; Detwiler et al., 2005; Disotell & Raaum, 2004; Guschanski et al., 2013; Lo Bianco et al., 2017; Perelman et al., 2011; Springer et al., 2012; Svardal et al., 2017; Tosi et al., 2005a; Tosi et al., 2005b; Xing et al., 2007). While inferences about the phylogenetic relationships among cercopithecins are as varied as the methods on which they are based, at this point in time, nuclear DNA studies are arguably the most robust and suggest that *Chlorocebus* is more closely related to the earlier diverging *Erythrocebus* and *Allochrocebus* than to *Cercopithecus* (Perelman et al., 2011; Springer et al., 2012).

1.4 | Fossil evidence

To add to the phylogenetic and taxonomic challenges, the cercopithecins are represented by only a sparse fossil record compared to papionins or colobines, with only a few dozen fragmentary specimens known prior to this publication (Cardini & Elton, 2008; Jablonski & Frost, 2010; Jablonski, 2002). The oldest fossil attributed to Tribe Cercopithecini is a single mandibular molar from the Baynunah Formation of Abu Dhabi, dated to 8.0 – 6.5 million years (Ma; Gilbert, Bibi, Hill, & Beech, 2014). There are several fragmentary guenons from the Shungura and Usno Formations (3.0 – 1.5 Ma) of southern Ethiopia, including two mandibular fragments with teeth assigned to *Cercopithecus* as well as two maxillary molars from the Usno Formation (~2.9 Ma; Eck & Howell, 1972; Eck, 1987; MacDougall et al., 2012).

Koobi Fora has produced a handful of fossils attributed to *Cercopithecus* from the KBS and Okote Members (~1.75 – 1.5 Ma), including a femur, a proximal ulna, isolated teeth, and a humerus from the Okote Member, as well as teeth attributed to *Nanopithecus* from the Kanapoi Formation (4.2 – 4.1 Ma; Frost, Ward, Manthi, & Plavcan, 2020a; Plavcan, Ward, Kay & Manthi, 2019; Pobiner, Rogers, Monahan, & Harris, 2008; Simons, Delson, Maglio, & Cooke, 1978). Koobi Fora has also yielded a *Nanopithecus* mandible fragment with two molars from the Tulu Bor Member (4.2 – 3.3 Ma; Jablonski et al., 2008; Plavcan et al., 2019). An Early Pleistocene juvenile mandible from Kanam is attributed to *Cercopithecus* sp. (Harrison & Harris, 1996). The lower Ngaloba Beds from Laetoli, Tanzania, have also yielded a recently named species of guenon, *Cercopithecus ngedere* (~1.7 – 1.2 Ma; Arenson et al., 2022). There are also a handful of isolated teeth from Olduvai Gorge and Loboi (Leakey, 1988).

The Middle Pleistocene Kapthurin Formation has also yielded cercopithecins (McBrearty, Bishop, & Kingston, 1996). Sediments from Asbole (~600 ka), near the Awash River in Ethiopia, yielded over a dozen cercopithecin fossils (Alemseged & Geraads, 2000; Frost & Alemseged, 2007). Of these specimens, eight were attributed to cf. *Chlorocebus* aff. *aethiops*, four to cf. *Chlorocebus* aff. *patas*, and five to cf. *Chlorocebus* sp. based mostly on dental characteristics and body size (Frost & Alemseged, 2007). Frost (2001) also assigns the "Andalee" and "Upper Andalee" cercopithecins to *Cercopithecus* sp. and suggests that they are most similar to *Cercopithecus aethiops*, which is now often referred to as *Chlorocebus aethiops*. We use quotations to refer to "Andalee" and "Upper Andalee" here because these names derive from the original fieldwork by the Rift Valley Research Mission in Ethiopia (RVRME; Frost, 2001; Kalb et al., 1982). Ongoing fieldwork has updated the names and geological placement originally inferred. We use these original names to maintain continuity with older literature but include them in quotation marks to indicate that these are historical terms.

The definition of *Chlorocebus aethiops* has also changed over time, previously including all species in the genus *Chlorocebus*. It is worth noting here that the fossil material from Omo, Koobi Fora, and Kanam were attributed to *Cercopithecus* at a time when few other cercopithecin genera were widely used. By assigning these fossils to *Cercopithecus*, the original authors were essentially identifying the material as cercopithecin but not belonging to *Allenopithecus*, *Erythrocebus*, or *Miopithecus*. It is possible that these authors may have identified these specimens differently if they were using the taxonomy widely used today.

1.5 | New cercopithecin fossils from the Middle Awash study area

Recent fieldwork in the Halibee member's Chai Baro (>158 ka) and Faro Daba (ca. 100 ka) beds in the Middle Awash study area yielded nearly 1,000 cercopithecid fossils. Hundreds of these fossils represent papionin and colobine individuals. The papionin and colobine assemblages are described in companion papers in the current issue (Brasil, Monson, Taylor, Yohler, & Hlusko Submitted A for papionins from Faro Daba; Brasil et al., Submitted B for colobines from Chai Baro).

Approximately one third of the fossils from these two beds (n=223 and n=105 from Faro Daba and Chai Baro, respectively) represent Cercopithecini, the only primate tribe present at both horizons. These cercopithecin fossil assemblages are each remarkable, both in terms of sample size and preservation (Figures 2 and 3). Both assemblages contain numerous partial skeletons (e.g., Figure 3) and exceptionally well-preserved craniodental (Figures 4 - 9) and postcranial elements (Figures 10 – 15).

2 | Geochronological and depositional contexts

The fossils described here were collected from localities in the Chai Baro and Faro Daba beds of the Halibee member of the Dawaitoli Formation (Figure 1; Niespolo et al., 2021) following standard Middle Awash project protocols (Gilbert & Asfaw, 2008).

The Faro Daba assemblage was collected immediately above and below a widespread basaltic tuff marker (the AFBT) that proved unsusceptible to Ar/Ar age determination. However, surface and *in situ* obsidian Middle Stone Age knapping debitage in stratigraphic association with the fossils from the Faro Daba beds were susceptible to this technique and combined with associated U/Th dates on ostrich eggshells, the age of these assemblages is now fixed at between 106 ± 20 ka and 96.4 ± 1.6 ka. These age determinations are compatible with the overall biochronology as well as the Middle Stone Age archaeological assemblages from the surface and excavations (Niespolo et al., 2021). The Chai Baro fossil assemblage is stratigraphically below, and therefore older than, the Faro Daba assemblage and derives from sediments ~9m below a volcanic tuff (the DGST) dated to 158.1 ± 11ka (Niespolo et al., 2021). The archaeology of the Chai Baro beds is also Middle Stone Age.

The primate fossils from localities in both areas were embedded within a few meters of overbank silts rapidly deposited atop higher energy cobble conglomerates (Niespolo et al., 2021). These silts were deposited in low energy or still water at some distance from the main channel of a paleo-Awash river. Their fossil and archaeological contents show little sign of predepositional displacement. Abundant associated paleobotanical and vertebrate fossil material at Faro Daba is commensurate with deposition in a wooded riverine-proximal ecotype, whereas the geologically earlier Chai Baro fossils appear to have accumulated farther from the main channel (Niespolo et al., 2021).

3 | Hypothesis-testing

The size of the Halibee fossil assemblage is unprecedented in the paleontological record of cercopithecins. It is uncommon for an assemblage of newly discovered fossils representing just one taxon to have more than 100 specimens recovered during limited fieldwork, and many specimens from both Faro Daba and Chai Baro are well-preserved (e.g., Figures 2 and 3). Rather

than describing the fossil specimens one-by-one, as is the traditional method, we approach the Halibee cercopithecin assemblage as two populations (Chai Baro and Faro Daba). Because the geological ages of the two samples are recent in time, we focus our comparison of the fossil populations primarily with extant cercopithecins and the most recent part of the cercopithecin fossil record. Two hypotheses guide our research:

Hypothesis 1: Neither the Chai Baro nor the Faro Daba assemblage is anatomically distinct from one of the extant guenons.

Hypothesis 2: The Chai Baro and Faro Daba assemblages sample the same taxon.

The decision to take a population-based approach is warranted by three key factors: 1) these fossils are nearly modern, and therefore their anatomies are so similar to modern cercopithecins that it is more useful to frame the variation reflected in this fossil assemblage relative to the ranges of variation observed for extant populations; 2) the Halibee cercopithecin fossils, while not a true biological population in a neontological sense, comprise two discrete geochronological snapshots of population-level variation in stratigraphic succession; and 3) the scientific insight to be gained from a lengthy, detailed specimen-by-specimen descriptive approach would be relatively minor and restricted relative to our population-based approach employing a comparative analysis of the new paleobiological evidence. Given this hypothesis-testing framework and population-based approach, our research focuses on the analysis of quantitative and qualitative data. The morphology of the fossils is primarily shown through photographic comparisons with extant and fossil taxa.

4 | Materials

4.1 | Overview of the fossil assemblages

A total of 973 cercopithecid fossils were recovered from the Faro Daba and Chai Baro beds. The 143 *Papio* and 360 *Colobus* fossils are described in Brasil et al., (Submitted A, B). Of the other 474 fossils, 328 were identified as cercopithecins (223 from Faro Daba and 105 from Chai Baro). The remaining 142 fossils (124 from Faro Daba and 18 from Chai Baro) were too poorly preserved to be attributed to a more specific taxon but do not evince morphologies or sizes that deviate significantly from those described here or in Brasil et al., (A, B). These specimens are cataloged as Cercopithecidae indet. (Appendix 3 and 4) and are not included in any figures or analyses in this paper.

4.2 | Overview of extant comparative samples

For comparison with the cercopithecin fossils from Faro Daba (n = 223) and Chai Baro (n = 105), we collected data from fossil and extant taxa. Extant comparative data were collected by the authors from museum specimens and derived from published data (Arenson et al., 2020; Gilbert et al., 2021; PRImate Morphometrics Online). Data for a total of 430 individuals representing 25 species of extant cercopithecin were used in our comparative analyses (Table 1). Taxa were chosen for inclusion in this study based on availability, and morphological and geographical proximity to the Halibee fossil cercopithecin assemblages. Because so many

comparative taxa are included, species were grouped following Arenson et al. (2020) to simplify data visualizations and make results easier to interpret.

4.3 | Comparative fossils

We also compared the Faro Daba and Chai Baro assemblages to the cercopithecin fossils recovered from Middle Pleistocene deposits in the adjacent Asbole area of the Afar, as well as later Pleistocene fossils from "Andalee" and "Upper Andalee" (Table 1). Quantitative measurements and qualitative descriptions of the Asbole, "Andalee", and "Upper Andalee" fossils derive primarily from those published by Frost & Alemseged (2007) and Frost (2001). Photos and data for cercopithecins from Asbole were pulled from Frost & Alemseged (2007). We also made qualitative observations on the original Asbole fossils housed at the National Museum of Ethiopia in Addis Ababa.

5 | Methods

5.1 | Data collection methods

Craniodental and postcranial measurements were chosen for their diagnostic utility in taxonomic assignment and locomotor inference, as well as for comparison with other cercopithecid fossils from Faro Daba and Chai Baro. We also collected data on sex and age at death to characterize the demographic composition of the assemblages. The data collection methods described herein are consistent with those employed by Brasil et al. (Submitted A, B).

5.1.1 | Cranial and mandibular anatomy

Cranial measurements were collected by TAM using dialMax analog calipers following standard protocols (see Monson, 2020; Monson, Brasil, Stratford & Hlusko, 2017). The following 17 cranial measurements were collected: calvarial length, facial length, facial width, interorbital breadth, maximum cranial breadth, maximum calvarial width, maximum cranial length, maximum width at the upper canines, muzzle width at ectomolare, muzzle width at the maxillary fossae, nasal height, nasal width, orbital height, orbital width, palatal length, palatal width at the third molars, and palatal width at the upper canines. Craniodental measurements were chosen for inclusion based on 1) utility in taxonomic identification, and 2) to provide data relevant to other research questions. Definitions for all measurements, and a visual description of measurements taken, can be found in Monson et al. (2017).

Mandibular corpus height measurements were taken by CET from standardized photographs using ImageJ (Schneider, Rasband, & Eliceiri, 2012). Mandibular height at M_1, M_2, and M_3 were measured at the midpoint of each molar, following the methodology of Gilbert et al. (2021). Analyses of mandibular height were performed following Gilbert et al. (2021) as a mechanism of assigning the Faro Daba and Chai Baro cercopithecins to genus.

5.1.2 | Dental anatomy

Dental measurements were collected for each tooth whose positions could be unambiguously determined. Dental measurements were taken following standard protocols (e.g., Grieco, Rizk, &

Hlusko, 2013). All maxillary dental measurements were taken by a single observer (TAM) using dialMax analog calipers. All mandibular dental measurements were taken by a single observer (MFB) using Mitutoyo digital calipers. Collected measurements include mesiodistal length, anterior and posterior buccolingual widths of the molars, and mesiodistal length and buccolingual width of the premolars, canines, and incisors. Mesiodistal length at the cementum-enamel junction (CEJ) was also measured on the incisors. Mesiodistal length of the mandibular third premolar was measured in both occlusal and lateral views to capture the length of the honing flange. Measurements from the right side of the dentition were included in analyses unless they were unavailable, in which case measurements from the left side were included.

Measurements were estimated only in cases where they could be made with a high degree of confidence (e.g., in cases where weathering and/or breakage was minimal, and the crown outline could be easily extrapolated); these estimated measurements are included in analyses. Measurements were not adjusted for interproximal wear. It should be noted that the measurement protocols employed in the description of the Asbole fossils (Frost & Alemseged, 2007) do not specify whether adjustments were made for interproximal wear, and this may affect the comparability of measurements between the two samples (e.g., if adjustments were made for the Asbole fossils, those measurements would be inflated relative to the Chai Baro and Faro Daba fossils).

Comparative extant dental data were collected following the same standard protocols (e.g., Grieco et al., 2013) as the fossil data collection with the exception of those data pulled from the PRIMO database and Gilbert et al. (2021). Our extant dental dataset overlaps with the dataset used in Hlusko et al. (2016), and augments the dataset compiled by Grieco et al. (2013) and archived online (Dryad doi:10.5061/dryad.693j8).

We abbreviate the terminology for teeth by using I for incisor, C for canine, P for premolar, and M for molar. Tooth position is indicated with a number, such that I2 is the second (lateral) incisor. We indicate maxillary and mandibular arches within the text rather than through abbreviation.

5.1.3 | Postcranial anatomy

Postcranial fossils were examined for qualitative traits widely used to infer locomotor adaptation to terrestrial versus arboreal substrates (Anapol, Turner, Mott, & Jolly, 2005; Arenson et al., 2020; Elton et al., 2016; Frost & Delson, 2002; Frost et al., 2020b; Gebo & Sargis, 1994; Sargis et al., 2008). Following Frost et al. (2020b), CET collected several postcranial metrics (humeral epicondyle ratio, humeral relative flange length, humeral distal articular surface dimensions, femoral relative greater trochanter projection, femoral patellar groove width), each of which has been considered useful for inferring locomotor modes in catarrhine monkeys. While each of the studies above referred to subtle morphological differences between species that were characterized as more arboreal or more terrestrial, we included only those features that were preserved in the Halibee assemblages, for which clear definitions have been published, and for which measurements were found to be replicable between our observers (details below). We also measured maximum lengths of all long bones. However, none of the cercopithecin partial skeletons from Faro Daba or Chai Baro preserve more than a single complete long bone, so we did not calculate limb indices (intermembral, humerofemoral, crural, brachial) in this study. Reconstructions of long bones and estimation of limb indices will be pursued in subsequent studies.

In light of previous reports of challenges in accurately measuring the femoral neck-shaft angle in humans (e.g., Bizdikian et al., 2018; Bonneau et al., 2012), we assessed interobserver error for the two angular measurements that we include in our comparisons (i.e., humeral epicondyle angle and femoral neck-shaft angle). These measurements were collected by CET, MFB, and RMY from standardized photographs of Chai Baro *Papio* fossils using ImageJ (see Brasil et al., Submitted A for sample details; Schneider et al., 2012). Average interobserver error was found to be high for the femoral neck-shaft angle (5.5%) and especially for the humeral epicondyle angle (15.6%). Since these two measurements are commonly assessed in studies of cercopithecid postcrania (e.g., Frost, 2007; Frost & Delson, 2002; Frost et al., 2020b), we report these measurements in our dataset [reference number to be specified immediately prior to publication]. However, considering the high degree of inter-observer error observed in *Papio*, we strongly caution against drawing firm conclusions from these metrics, particularly as they compare to measurements published by other researchers as their data collection protocol may have differed substantially from ours.

Measurements and qualitative observations of postcranial fossils were taken following the methodologies of previous publications on cercopithecin monkeys (Arenson et al., 2020; Delson, Terranova, Jungers, Sargis, & Jablonski, 2000; Elton et al., 2016; Frost & Delson, 2002; Gilbert et al., 2021; Sargis et al., 2008). Linear measurements were taken by CET using Mitutoyo digital calipers. Extant comparative postcranial measurements were taken by CET and derived from published data (Arenson et al., 2020; Frost et al., 2020b).

Postcranial analyses were employed to quantitatively determine the affinities of each bed with comparative taxa. The aim of these analyses was to document the morphological traits in the Faro Daba and Chai Baro assemblages that are associated with locomotor habitus and substrate use.

5.1.4 | Sex

Sex was estimated independently by two observers (MFB and LJH) based on the C/P3 honing complex. Sex assignments were then checked against each other and discussed when individual assignments from the two authors disagreed. If agreement was not reached, individuals were marked as “uncertain”.

5.1.5 | Ontogenetic age

We used tooth eruption and occlusal wear to estimate ontogenetic age on a scale of one to six for all craniodental specimens for which postcanine tooth position could be ascertained with absolute confidence (i.e., a specimen with at least one of the following: more than one postcanine tooth, a complete third molar with distinctive morphology, or with the postcanine tooth/teeth in the jaw; Table 2). We report dental eruption rather than estimates of chronological age because of the amount of variation in timing of primate tooth eruption (Bolter & Zihlman, 2003; Harvati, 2000; Hlusko & Mahaney, 2009; Jogahara & Natori, 2012; Monson and Hlusko, 2018).

5.2 | Analytical methods

5.2.1 | Approach to taxonomic identification

Our approach to the taxonomic assignments for these two cercopithecin assemblages was carried out using the following steps:

Step 1. We first performed an initial taxonomic sorting of the 973 cercopithecid fossils from Faro Daba and Chai Baro, based on cranial and dental morphology, and overall size. Both papionins and cercopithecins are present in the Chai Baro sample. Here, cercopithecins were differentiated form papionins based on the presence of relatively large upper incisors, a spatulate upper central incisor with a widening crown from the cervix to the incisal edge in anterior view, a conical upper lateral incisor, distally reduced upper and lower third molars, the absence of a hypoconulid on the mandibular third molar, and size of the postcrania (following Frost & Alemseged, 2007). Both cercopithecins and colobines are present in the Faro Daba sample. Since cercopithecins and colobines are roughly similar in size, we relied on craniodental features to identify cercopithecins in the Faro Daba sample. Cercopithecins can be distinguished from colobines by a narrow interorbital pillar, low postcanine cusps relative to crown height, and a low degree of occlusal relief (Brasil et al., Submitted B; Groves, 2007).

Step 2. After we identified fossils as either papionin, cercopithecin, or colobine, we compared the morphological variation within each fossil taxon against observed variation in extant species. We first assessed morphological variation separately in each geologically contemporaneous sample (Faro Daba and Chai Baro) to determine whether the observed variation could fit within expectations of a single species. We then compared morphological variation across the Faro Daba and Chai Baro samples to assess whether they likely represent the same or different species. Qualitative and quantitative results and comparisons with extant taxa are detailed below and in the accompanying papers on papionins and colobines (Brasil et al., Submitted A, B).

Step 3. Individual specimens were given a taxonomic designation to the lowest, most specific level possible. We first focused on the taxonomic assignment of those specimens with sufficiently preserved craniodental material. We then used these well-preserved specimens to aid in identifying the more limited craniodental remains, and we used those biological individuals for which postcrania were associated as comparative standards to identify other isolated postcrania lacking associated craniodental material.

5.2.2 | Statistics

Descriptive statistics were calculated using Microsoft Excel. Bivariate plots and craniodental boxplots were created using *ggplot2* (v3.3.0; Wickham, 2016) in the R statistical environment and compiled in Adobe Illustrator CC 2019 (Adobe, Inc.). Extant species with large sample sizes were chosen for inclusion in descriptive statistics tables. Distribution figures were created using the *dplyr* package in R to illustrate distributions of traits that distinguish *Cercopithecus* and *Chlorocebus* (Wickham, François, Henry, & Müller, 2022). Postcranial boxplots were also visualized using *ggplot2* and were then overlain on excerpts of published figures from Frost & Delson (2002) and Frost (2020b) using Adobe Illustrator CC 2019 to produce figures that match the format presented in those publications.

Statistical analyses of quantitative data were performed in the R statistical environment v3.6.1 (R Core Team, 2019). Traits used for statistical analyses focus on those identified in the literature as useful for differentiating guenon genera and species. To test Hypothesis 1, each assemblage was individually compared to each extant species of *Chlorocebus* and *Cercopithecus* in an attempt to assign each assemblage to a more specific taxonomic level within

Cercopithecini. We first tested for normality using Shapiro-Wilk tests, and we then employed Kruskal-Wallis non-parametric tests at the species level (due to small and unevenly distributed sample sizes) to test for significant differences between sample means. We used the Dunn's *post hoc* test with a Bonferroni correction for pairwise comparisons between each assemblage and extant and fossil samples. We report only the uncorrected significance for these species-level analyses, as the correction overwhelmed nearly all statistical signal. For all statistical analyses, significance was set at $p<0.05$.

To test Hypothesis 2, we assessed the similarities between the Faro Daba and Chai Baro cercopithecins using Kruskal-Wallis non-parametric tests. For genus-level analyses, *post hoc* tests were not necessary, as each assemblage was assessed against each genus individually.

6 | Results

6.1 | Test of Hypothesis 1: comparing the Halibee cercopithecins to extant taxa

The Faro Daba and Chai Baro cercopithecin assemblages exhibit craniodental morphology typical of the tribe. Size and morphology within the two assemblages excludes *Erythrocebus, Miopithecus,* or *Nanopithecus* as candidates. These two assemblages are also clearly not sampling *Allochrocebus* based on mandibular morphology, and neither assemblage exhibits the distinct molar morphology or extreme molar flare of *Allenopithecus.* Thus, both the Faro Daba and Chai Baro assemblages represent either *Cercopithecus* or *Chlorocebus*. We turn our focus to comparing the Halibee cercopithecin fossils with these two genera to further test Hypothesis 1: that neither the Chai Baro nor the Faro Daba assemblage is anatomically distinct from one of these extant guenons.

There are several features that have been reported to distinguish *Cercopithecus* and *Chlorocebus*, including, relative incisor size, mandibular corpus height, and orbital shape (Gilbert et al., 2021). There are several scapular features shown by Arenson et al. (2020) that may also distinguish the two genera, but the fossil assemblages described here do not preserve scapular morphology sufficient for meaningful comparisons. For the craniodental traits examined, the Chai Baro and Faro Daba individuals do not consistently fall with one genus over another (Tables 3 – 5; Figures 17 – 22). In nearly all features investigated, both the Chai Baro and Faro Daba assemblages plot most closely with *Cercopithecus nictitans* and *Chlorocebus aethiops*. In terms of mandibular height, the Chai Baro and Faro Daba assemblages fall within the range of nearly every cercopithecin included (Table 6; Figure 18). *Chlorocebus*, *Cercopithecus*, and the Faro Daba and Chai Baro cercopithecins have very similar ranges and distributions in nearly every trait examined (Tables 3 – 6, 8; Figures 16 – 22). The only trait for which *Chlorocebus* and *Cercopithecus* do not completely overlap in their ranges and distributions is orbital shape, for which we could measure one undistorted individual from each assemblage. The Faro Daba specimen falls outside the range of *Cercopithecus* and at the lower end of *Chlorocebus*, whereas the Chai Baro specimen falls toward the upper range of *Chlorocebus* and within the range of *Cercopithecus* (Figure 17).

Both the Faro Daba and Chai Baro assemblages show some significant differences when compared to specific species of *Cercopithecus*, but neither assemblage shows significant differences when compared to individual species of *Chlorocebus* (Supplementary Table 1). Because neither assemblage shows a consistently significant statistical similarity to a single species of *Chlorocebus* or *Cercopithecus*, but both show more differences with more species of

Cercopithecus, we attribute the Faro Daba and Chai Baro assemblages to genus but not species. Although the ranges and distributions of craniodental metrics are similar for *Chlorocebus*, *Cercopithecus*, and the fossil assemblages (Figures 17 – 20), the Faro Daba and Chai Baro assemblages show the most statistical similarity to *Chlorocebus* (Table 7, Supplementary Table 1).

Therefore, results from the test of Hypothesis 1 indicate that both the Faro Daba and Chai Baro cercopithecin samples are similar but not identical to either *Cercopithecus* or *Chlorocebus*, and show stronger affinities to *Chlorocebus* than *Cercopithecus*. Therefore, we refer these specimens to cf. *Chlorocebus*. The rationale for this is described in more detail in the following section.

6.2 | Test of Hypothesis 2: comparing the Faro Daba and Chai Baro assemblages

Having established that both the Faro Daba and Chai Baro samples demonstrate the strongest affinities to *Chlorocebus* among the extant guenons, we turn to testing Hypothesis 2: the Chai Baro and Faro Daba assemblages sample the same taxon.

Body size. Size metrics do not notably differ between the Faro Daba and Chai Baro samples. Both assemblages fall towards the lower end of both *Chlorocebus* and *Cercopithecus* in both craniodental and postcranial size (Figure 6 for craniodental comparisons, Figures 10, 11, 12, and 14 for postcranial comparisons).

Craniodental and mandibular anatomy. There is only one individual from each assemblage without obvious deformation for which we could measure both orbital height and orbital width. These two individuals fall on opposite ends of the range of variation of extant *Chlorocebus* for orbital shape (Figure 17). Mandibular measurements for both Faro Daba and Chai Baro fall squarely within the range of both *Chlorocebus* and *Cercopithecus*, with no notable qualitative difference or significant quantitative differences between the two beds (Table 6; Figure 18). As for the dental comparisons, the Chai Baro cercopithecins have slightly more flared molars than those from Faro Daba (i.e., they have a crown that bulges more on the buccolingual aspects; Figures 6 and 7). This trait is seen in occlusal view as a greater distance between the occlusal fovea and the base of the crown on both the lingual and labial aspects of the crown. While this trait can sometimes be quantified using an index of molar flare (Benefit, 1993; Delson, 1973; Frost, 2001; Singleton, 2003), we were not able to quantitatively capture our observation, perhaps due to the subtlety of the trait and the confounding effects of tooth wear. The subtle variation in molar flare between the two assemblages is a qualitative frequency difference and can be seen in Figures 6 and 7. It is possible that the slightly increased molar flare in the Chai Baro assemblage is related to increased enamel thickness, a line of investigation we intend to pursue in further studies.

Results of craniodental statistical comparisons among the Faro Daba and Chai Baro samples, as well as *Cercopithecus* and *Chlorocebus*, are shown in Table 7 and Supplementary Table 1. These results indicate that the Faro Daba and Chai Baro assemblages are not significantly different for any of the traits examined (Table 7). Statistical comparisons were also made for linear dental metrics (e.g., those shown in Figures 21 and 22) and no significant differences were detected (results are not presented as they are all insignificant).

Relative to other recent fossil cercopithecin samples, both Faro Daba and Chai Baro are similar to the Asbole and "Andalee" fossils in some traits and somewhat offset in others. The Asbole cf. *Chlorocebus* aff. *aethiops* and Chai Baro cf. *Chlorocebus* individuals are within the

range of the Faro Daba cf. *Chlorocebus* sample in mandibular height at M_1 and M_3 (Figure 18). In relative I^2 length, the Chai Baro and Faro Daba ranges overlap, and the "Andalee" individual falls within the range of both Halibee assemblages, while the Asbole individual does not (Figure 19). In relative I^1 length, the Asbole cf. *Chlorocebus* aff. *patas* and the "Andalee" *Cercopithecus* sp. fossils fall within the range of the Faro Daba sample, the Chai Baro individuals overlap the upper end of the Faro Daba range, and the Asbole cf. *Chlorocebus* aff. *aethiops* overlap with the Chai Baro sample (Figure 20).

Postcranial anatomy. The Faro Daba and Chai Baro cercopithecin assemblages both have the generalized postcranial skeleton typical of the tribe. The Faro Daba and Chai Baro humeri exhibit a range of variation (Figures 10 – 12). The Chai Baro humeri are slightly more medially curved (laterally bowing) than those from Faro Daba (Figure 11). Chai Baro distal humeri are slightly more square in shape than Faro Daba, but the variation is continuous between the two beds with no noticeable break in morphology (Figure 11 and 12). Humeri from both assemblages have weak trochlear ridges that are slightly more noticeable in some individuals from Faro Daba. The greater tubercle and the crest of the *triceps brachii* are roughly equal in size in humeri from both beds. The ulnae from both assemblages are straight (Figure 13), and the radii have a robust interosseous crest. The superior aspect of the greater trochanter curves medially (Figures 14 and 15) and the femoral epicondyles are roughly symmetrical in size and shape. The degree of femoral trochanteric projection for both assemblages falls towards the lower end of the *Chlorocebus aethiops* and *Cercopithecus mitis* ranges (Figure 16). The Chai Baro femora have somewhat more narrow patellar grooves than the Faro Daba femora, but not remarkably or significantly so (results are not presented as they are insignificant).

The two assemblages show minor differences in humeral curvature, distal humeral articular surface morphology, and patellar groove width, all of which may be associated with locomotion. The Chai Baro individuals show some morphological traits that are associated with more terrestrial taxa, such as slightly more medially curved humeri, narrow patellar grooves, and more square distal humeri. The Faro Daba individuals are more similar to arboreal species in those traits, but have a stronger humeral trochlear ridge than those from Chai Baro, which is also associated with more terrestrial species (Arenson et al., 2020). These features differ in frequency in Faro Daba and Chai Baro. However, such a mosaic of more terrestrial and more arboreal features occurs even within single species of extant guenons (Arenson et al., 2020; Gebo & Sargis, 1994). Considering that such traits are likely highly influenced by behavior (Arenson et al., 2020), the observations described above do not falsify the null hypothesis that the Faro Daba and Chai Baro assemblages sample one species lineage. Furthermore, there are no statistically significant differences between the two beds in any of the postcranial measurements, and their ranges overlap (Table 8).

Comparisons across the craniodental, mandibular, and postcranial morphology fail to reject the hypothesis that the Faro Daba and Chai Baro assemblages represent the same species lineage of guenon. In addition to the comparisons presented above, the case for the common taxonomic attribution of the two assemblages stems from three major observations, namely: 1) the combined dental variation in these two fossil assemblages does not exceed that of a modern guenon species (Tables 3 and 4); 2) the postcranial size variation also does not exceed that of a modern guenon species (Figure 16); and 3) there is not a mean or range of variation shift between the two samples through time that would suggest that the two beds sample different cercopithecin taxa. Considering how much variation there is within and among extant species of cercopithecin monkeys, we do not interpret the observed minor variations between the Faro Daba

and Chai Baro assemblages as justification for formal taxonomic distinction. Furthermore, we think that dichotomizing substrate use based on a few postcranial characters is a hazardous undertaking given the flexibility of the extant relatives of these fossil guenons in both locomotion and preferred substrate.

6.3 | Systematic paleontology

Family Cercopithecidae Gray, 1821
Subfamily Cercopithecinae Gray, 1821
Tribe Cercopithecini Gray, 1821
Genus *Chlorocebus*, Gray 1870
cf. *Chlorocebus*

We identified 328 cercopithecins in total from the Halibee assemblages, 223 from Faro Daba and 105 from Chai Baro. Dentally, the Faro Daba and Chai Baro assemblages are similar to modern *Cercopithecus* and *Chlorocebus* (Tables 3 and 4). Figures 21 and 22 further show that both the Faro Daba and Chai Baro assemblages fall within the range of variation of extant *Chlorocebus* and *Cercopithecus* in all dental metrics studied (Figures 19 – 22). However, relative I^1 length is significantly different between extant *Cercopithecus* and our Faro Daba cercopithecin assemblage (Table 7). As such, the Halibee fossil sample demonstrates slightly more statistical similarity with extant *Chlorocebus* (Supplementary Table 1). Therefore, 296 specimens were assigned to cf. *Chlorocebus* based on dental traits, as described in section 6.1, as well as their statistical similarity in cranial features to extant *Chlorocebus*.

In comparisons with other fossil material, the Faro Daba and Chai Baro assemblages fall within the dental range of the Asbole individuals (except for one outlier in the Asbole sample; Frost & Alemseged, 2007). The Halibee samples are also similar to the cf. *Chlorocebus* aff. *aethiops* individuals from Asbole in mandibular corpus height (Figure 18).

We also refer 32 postcranial specimens to cf. *Chlorocebus*. For the Faro Daba assemblage, isolated cercopithecin postcranial elements were differentiated from colobines and assigned to cf. *Chlorocebus* based on comparison with individuals that preserve both craniodental and postcranial material (e.g., Figure 2). In contrast to Faro Daba, the Chai Baro cercopithecid assemblage only includes cercopithecins and *Papio* (Brasil et al., Submitted A). Because of the significant size difference between the cercopithecin and papionin specimens in the Chai Baro assemblage, isolated cercopithecid postcranial specimens (n = 32) within the size range of the specimens with craniodental material were attributed to cf. *Chlorocebus*.

Family Cercopithecidae Gray 1821

In addition to the Halibee fossils identified as cercopithecins, papionins (Brasil et al., Submitted A), and colobines (Brasil et al., Submitted B), 124 specimens from Faro Daba and 18 from Chai Baro were too fragmentary and/or ambiguous to assign to a more specific taxonomic category and were attributed to Cercopithecidae indet. (Appendix 3 and Appendix 4, respectively). Individuals attributed to Cercopithecidae indet. are not included in any analyses or figures in this paper.

6.4 | Population characteristics

6.4.1 | Sex

Of the 182 cf. *Chlorocebus* craniodental specimens that preserve part of the canine honing complex, we were able to estimate sex for nearly half (n = 86). The number of males and females is fairly even for both beds (Table 9).

6.4.2 | Demography

Of the 328 cercopithecin specimens, we were able to score age for 115 Faro Daba and 50 Chai Baro cf. *Chlorocebus* specimens using the criteria detailed in the Methods (Tables 2 and 10). Age categories four, five, and six are the most well represented for both assemblages (spanning young to old adult ages).

7 | Discussion

The Faro Daba and Chai Baro assemblages provide the opportunity to study two geographically proximate and chronologically sequential populations of cercopithecin monkeys. Our research demonstrates that both Halibee assemblages show similarities with *Cercopithecus* and *Chlorocebus*. However, they both have slightly stronger affinities with *Chlorocebus* than *Cercopithecus*. Therefore, we refer the 328 cercopithecin specimens from Halibee to cf. *Chlorocebus*. The morphological similarity between *Chlorocebus* and *Cercopithecus*, and the lack of significant differences between the two assemblages and extant species of *Chlorocebus*, lead us to conclude that it is inappropriate to give these fossils a species designation.

We also see overwhelming similarity between the cf. *Chlorocebus* fossils in the Faro Daba and Chai Baro assemblages. We find no evidence that rejects the hypothesis that these two populations belong to a single species lineage. Considering the morphological similarity across most extant guenon skeletons, and the sympatry observed among modern guenon species (Arenson et al., 2020; Rowe & Myers, 2016), it is possible that there are multiple species present in the Halibee assemblages. However, as we cannot reject the null hypothesis, there is not support for an alternative hypothesis of multiple genera or species. Therefore, we assign all 328 specimens across both assemblages, Faro Daba and Chai Baro, to the same cf. *Chlorocebus*.

It has long been recognized that fossil taxa require different criteria for species delimitation compared to extant organisms. In vertebrate paleontology, we are forced to rely on skeletal data. However, skeletal features do not clearly and consistently differentiate the extant mid-sized cercopithecins *Cercopithecus* and *Chlorocebus*. Rather, pelage and behavioral phenotypes are the most diagnostic features. While there are statistically significant differences between these two genera for a handful of skeletal features, the distributions and ranges of variation overlap completely for nearly every single trait (Figures 17 – 20). When a fossil assemblage consists of just one or two specimens preserving some aspect of anatomy, variation is often overlooked in order to facilitate taxonomy. However, when confronted with a large fossil assemblage, like the present one from Halibee, it becomes clear that the presence/absence dichotomization of characters is insufficient for taxonomic identification. Our results show that skeletally and dentally – and therefore paleontologically – *Cercopithecus* and *Chlorocebus* are nearly indistinguishable.

The strong skeletal similarities between *Cercopithecus* and *Chlorocebus* ultimately result from their similarity in body size and generalist adaptations, and are likely also due in part to

their long history of hybridization (Aldrich-Blake, 1968; Detwiler, 2004; 2010, Detwiler et al., 2005; Dugoujon et al., 1982; Sineo, 1990; Struhsaker et al., 1988; Tapanes, 2016). It is remarkable that even the unusually high variation in karyotype does not prevent these different species from hybridizing (Detwiler, 2019). So-called 'hybrid swarms' occur where there is no reproductive isolation between species, and cross-breeding and backcrossing with parent species are common (Butynski & De Jong, 2022; Tapanes, 2016). This results in high levels of genetic and phenotypic variation such as what is observed in cercopithecin populations (Booth, 1968; Cortes-Ortiz, Roos, & Zinner, 2019; Napier, 1976). Because most extant hybrids are identified in the wild by pelage and behavior (Struhsaker et al., 1988; Tapanes, 2016), it may well be impossible to discern hybridization between cercopithecins through the skeletal, and therefore paleontological evidence, (but see arguments for the ability to identify hybrids in other primate taxa; Ackermann, 2010; Ackermann, Rogers, & Cheverud, 2006; Ackermann, Schroeder, Rogers, & Cheverud, 2014; and Cortés-Ortiz, 2017). Although the effects of hybridization on postcranial morphology in cercopithecins are not well understood, hybrid studies in pedigreed papionins show that hybrids typically display high levels of variability and may have postcranial morphology that is intermediate between parental forms (Jolly et al., 1997). Hybridization events, conserved skeletal morphology, and high levels of intraspecific variation combine in the case of cercopithecin monkeys to demonstrate that a strictly cladogenetic approach to primate evolution may not always be appropriate.

From a microevolutionary perspective, the minor morphological differences between the Faro Daba and Chai Baro assemblages are insufficient to confirm that the two assemblages contain two different species lineages, let alone chronospecies. Within the postcranial skeleton, Chai Baro cercopithecins have a slightly more curved humeral shaft (Figure 11), slightly more square distal humeri (Figure 12), and more narrow patellar grooves (Figure 14) than those from the Faro Daba assemblage, which are more common in terrestrial species of cercopithecin monkeys (Gebo & Sargis, 1994; Sargis et al., 2008; Lo Bianco et al., 2017). However, the Faro Daba individuals tend to have stronger humeral trochlear ridges, which are also associated with more terrestrial species (Arenson et al., 2020). Overall, the results suggest that both the Faro Daba and Chai Baro cercopithecins are neither extremely terrestrial nor extremely arboreal. If the two assemblages are, as seems plausible, sampling one species lineage, these differences could be evidence of phyletic evolution or phenotypic plasticity. More information about the developmental underpinnings of postcranial morphology is needed to evaluate the relative contributions of phyletic evolution versus developmental plasticity for these traits. Either way, the differences in humeral curvature, distal humeral morphology, and patellar notch width might indicate a response to changing substrate use between the populations sampled at what are effectively geological snapshots at ~100,000 and >158,000 years ago.

Ecological interpretations of fossil primates are often drawn from postcranial differences thought to vary with use and/or locomotor mode. We urge caution on such inferences for two reasons. First, making inferences about locomotory habit, substrate preference, or even arboreal cover based on minor postcranial variation is tenuous due to the variability of the postcranial skeleton. For example, Buck et al. (2010) found that intraspecific variation is greatest in the appendicular skeletons of catarrhines (including guenons). Guenon appendicular skeletons exhibit highly conserved skeletal morphology across taxa, and high levels of intraspecific variation (Buck et al., 2010). Additionally, these animals are highly flexible in their substrate use and locomotor activities (Anapol et al., 2005; Arenson et al., 2020; McGraw, 2004).

Attempts to infer ecological variables from fossil guenon postcranial remains are perhaps even more tenuous compared to other primate taxa. For example, "terrestrial", "semi-terrestrial", and "arboreal" categorizations among guenons are often based on non-discrete behavioral variation (Motsch et al., 2015). For instance, Arenson et al. (2020) define 'arboreal' as spending less than 20% of time on the ground, 'semi-terrestrial' as spending 20-40% of time on the ground, and 'terrestrial' as spending over 40% of time on the ground. Depending on the researcher's definition of semi-terrestrial, some species of cercopithecin have been considered as both arboreal and semi-terrestrial (e.g., Cardini & Elton, 2008 v.s. Arenson et al. 2020), or both semi-terrestrial and terrestrial (e.g., Arenson et al., 2020 and Arenson et al., 2022 v.s. Gebo & Sargis, 1994 and Cardini & Elton, 1998). *Cercopithecus hamlyni* is even categorized as "terrestrial" by Arenson et al. (2020), "semi-terrestrial" by Gebo & Sargis (1994), and "arboreal" by Cardini & Elton (2008). Arenson et al. (2020) evaluated the postcranial skeletons of two *Cercopithecus lomamiensis* individuals and found that they overlapped with both the "semi-terrestrial" and "terrestrial" categories, despite their dense forest habitat.

Neither the Faro Daba nor Chai Baro cercopithecins have morphology consistent with highly terrestrial or highly arboreal cercopithecins. It is therefore unsurprising that the Faro Daba and Chai Baro cercopithecin assemblages both exhibit the most similarity with "semi-terrestrial" extant species. However, it is important to note that nearly all cercopithecins exhibit a similar semi-terrestrially adapted postcranium, with the exception of the few extremely terrestrial and extremely arboreal species. The inference of paleoenvironment from *Chlorocebus* and *Cercopithecus* postcranial morphology is further complicated by the fact that some "semi-terrestrial" species are known to exclusively inhabit dense forests (Arenson et al., 2020; Hart et al., 2012), and many semi-terrestrial-to-terrestrial guenon species share habitats with arboreal species (Rowe & Meyers, 2016). The presence of more terrestrially adapted features in the Chai Baro assemblage compared to the Faro Daba assemblage therefore does not necessarily indicate an ecological shift, but may suggest a behavioral shift in time-successive populations of the same species.

8 | Conclusion

The cercopithecin fossil assemblages described here are remarkable for their sheer sizes. These two samples increase the number of known cercopithecin fossils from the African Pleistocene by hundreds of individuals. The Faro Daba and Chai Baro assemblages therefore provide insight into cercopithecin populational variation, diachronic stasis, and demography. We assign individuals from both the Faro Daba (ca. 100 ka) and Chai Baro (>158 ka) beds to the same indeterminate species within the genus cf. *Chlorocebus*. Craniodentally, the Faro Daba and Chai Baro assemblages together fall within the range of variation observed for a single extant species of cercopithecin. There are some postcranial differences that suggest that the Chai Baro population may have been more terrestrial than the Faro Daba population. Given the modern biogeography of cercopithecin monkeys, and the geographic position of these fossils in Afar Rift of Ethiopia, our data support that these fossil populations may be ancestral to living cercopithecins.

Acknowledgements

We are grateful to the members of the Middle Awash research team, especially the project co-directors B. Asfaw, Y. Beyene, T. White, and G. WoldeGabriel, without whose efforts this research could not have occurred. We thank the Human Evolution Research Center at the University of California Berkeley and its donors for funding our research. We thank the National Museum of Ethiopia for providing permissions and access to the fossils. We are also grateful to the Afar Regional Government and the Afar people of the Middle Awash, as well as the hundreds of individuals comprising the field crews that worked at Halibee for their ongoing collaboration, sacrifices, and contributions to the fieldwork behind this fossil assemblage. We thank the staff of the Authority for Research and Conservation of Cultural Heritage and the National Museum of Ethiopia for permission to study fossils in their care, particularly W. Amerga, Y. Assefa, M. Endalamaw, T. Gebremedhin, T. Getachew, and G. Tekle for laboratory and/or field assistance. Some data for this project were downloaded from PRIMO, the NYCEP PRImate Morphology Online database (http://primo.nycep.org). We thank Dr. Eric Delson and colleagues for access to these data.

We also thank the following repositories for providing access to extant specimens included in this study: the American Museum of Natural History, the Cleveland Museum of Natural History, the Smithsonian Institution's National Museum of Natural History, and the Anthropological Museum at the University of Zurich. Collection of the comparative dental and cranial data was supported by NSF grants 0500179, 0616308, 1025263, 0327208, 0130277, 1720128 awarded to LJH, as well as NSF DGE 1752814 awarded to CET. CET, MFB, RMY, and TAM were partially supported by Desmond Clark Graduate Fellowships from the Human Evolution Research Center, UC Berkeley. MFB was partially supported by a Chancellor's Fellowship and the Portuguese Studies Program at UC Berkeley, and by the John Templeton Foundation. During the course of this study, TAM was partially supported by the National Science Foundation in Switzerland, the Department of Anthropology at Western Washington University, and by the Human Evolution Research Center, the Museum of Vertebrate Zoology, the Department of Integrative Biology, and the Museum of Paleontology at the University of California at Berkeley, CA. We thank J. Carlson, M. Krouse, A. Peck, A. Weitz, and T. White for helpful feedback and discussion.

Data Availability Statement

The data that support the findings of this study are openly available in *figshare* at http://doi.org/[doi to be specified immediately prior to publication], reference number [reference number to be specified immediately prior to publication].

References

Ackermann, R. R., Rogers, J., & Cheverud, J. M. (2006). Identifying the morphological signatures of hybridization in primate and human evolution. *Journal of Human Evolution*, *51*(6), 632-645. https://doi.org/10.1016/j.jhevol.2006.07.009

Ackermann, R. R. (2010). Phenotypic traits of primate hybrids: Recognizing admixture in the fossil record. *Evolutionary Anthropology: Issues, News, and Reviews*, *19*(6), 258-270. https://doi.org/10.1002/evan.20288

Ackermann, R. R., Schroeder, L., Rogers, J., & Cheverud, J. M. (2014). Further evidence for phenotypic signatures of hybridization in descendant baboon populations. *Journal of Human Evolution*, *76*, 54-62. https://doi.org/10.1016/j.jhevol.2014.05.004

Alemseged, Z., & Geraads, D. (2000). A new Middle Pleistocene fauna from the Busidima–Telalak region of the Afar, Ethiopia. *Comptes Rendus de l'Académie des Sciences-Series IIA-Earth and Planetary Science*, *331*(8), 549-556. https://doi.org/10.1016/S1251-8050(00)01450-

Aldrich-Blake, F.P.G. (1968). A fertile hybrid between two *Cercopithecus* spp. in the Budongo Forest, Uganda. *Folia Primatologica*, 9, 15-21. https://doi.org/10.1159/000155165

Anapol, F., Turner, T. R., Mott, C. S., & Jolly, C. J. (2005). Comparative postcranial body shape and locomotion in *Chlorocebus aethiops* and *Cercopithecus mitis*. *American Journal of Physical Anthropology, 127*(2), 231-239. https://doi.org/10.1002/ajpa.20055

Arenson, J. L., Sargis, E. J., Hart, J. A., Hart, T. B., Detwiler, K. M., & Gilbert, C. C. (2020). Skeletal morphology of the lesula (*Cercopithecus lomamiensis*) and the evolution of guenon locomotor behavior. *American Journal of Physical Anthropology*, *172*(1), 3-24. https://doi.org/10.1002/ajpa.24025

Arenson, J. L., Harrison, T., Sargis, E. J., Taboada, H. G., & Gilbert, C. C. (2022). A new species of fossil guenon (Cercopithecini, Cercopithecidae) from the Early Pleistocene Lower Ngaloba Beds, Laetoli, Tanzania. *Journal of Human Evolution*, *163*, 103136. https://doi.org/10.1016/j.jhevol.2021.103136

Benefit, B. K. (1993). The permanent dentition and phylogenetic position of Victoriapithecus from Maboko Island, Kenya. *Journal of Human Evolution*, *25*(2), 83-172.

Bizdikian, A. J., Assi, A., Bakouny, Z., Yared, F., Saghbini, E., Bakhos, G. E., . . . Ghanem, I. (2018). Validity and reliability of different techniques of neck–shaft angle measurement. *Clinical Radiology, 73*(11), 984.e981-984.e989. doi:10.1016/j.crad.2018.06.006

Bolter, D. R., & Zihlman, A. L. (2003). Morphometric analysis of growth and development in wild-collected vervet monkeys (*Cercopithecus aethiops*), with implications for growth patterns in Old World monkeys, apes and humans. *Journal of Zoology*, *260*(1), 99-110.

Bonneau, N., Libourel, P. A., Simonis, C., Puymerail, L., Baylac, M., Tardieu, C., & Gagey, O. (2012). A three-dimensional axis for the study of femoral neck orientation. *Journal of Anatomy, 221*(5), 465-476. doi:10.1111/j.1469-7580.2012.01565.x

Booth, C. P. (1968). Taxonomic studies of *Cercopithecus mitis wolf* (East Africa). *National Geographic Society., Research Report*.

Brasil, M. F., Monson, T. A., Taylor, C. E., Yohler, R. M., & Hlusko, L. J. (Submitted A). A fossil assemblage of near-modern *Papio hamadryas* from the Afar Depression of Ethiopia. *American Journal of Biological Anthropology*, *present issue*.

Brasil, M. F., Monson, T. A., Taylor, C. E., Yohler, R. M., & Hlusko, L. J. (Submitted B). Hundreds of newly-recovered *Colobus* (Cercopithecidae: Primates) fossils from the Late Pleistocene of the Afar Depression, Ethiopia. *American Journal of Biological Anthropology*, *present issue*.

Brasil, M. F., Monson, T. A., Taylor, C. E., Yohler, R. M., & Hlusko, L. J. To be made available on figshare immediately prior to the publication of this manuscript.

Buck, L. T., Stock, J. T., & Foley, R. A. (2010). Levels of intraspecific variation within the catarrhine skeleton. *International Journal of Primatology*, *31*(5), 779-795. DOI 10.1007/s10764-010-9428-0

Butynski, T. M., & De Jong, Y. A. (2020). Taxonomy and biogeography of the gentle monkey Cercopithecus mitis Wolf, 1822 (Primates: Cercopithecidae) in Kenya and Tanzania, and designation of a new subspecies endemic to Tanzania. *Primate Conservation*, *34*, 71-127.

Cardini, A., & Elton, S. (2008). Variation in guenon skulls (I): species divergence, ecological and genetic differences. *Journal of Human Evolution*, *54*(5), 615-637. https://doi.org/10.1016/j.jhevol.2007.09.022

Chiarelli, B. (1968). Chromosome polymorphism in the species of the genus *Cercopithecus*. *Cytologia*, *33*(1), 1-16. https://doi.org/10.1508/cytologia.33.1

Cortés-Ortiz, L. (2017). Hybridization and hybrid zones. *The international encyclopedia of primatology*, 1-5. https://doi.org/10.1002/9781119179313.wbprim0380

Cortés-Ortiz, L., Roos, C., & Zinner, D. (2019). Introduction to special issue on primate hybridization and hybrid zones. *International Journal of Primatology*, *40*(1), 1-8. https://doi.org/10.1007/s10764-019-00076-z

de Jong Y.A., Butynski T.M. (2010)….. Three Sykes's monkey *Cercopithecus mitis* × vervet monkey *Chlorocebus pygerythrus* hybrids in Kenya. *Primate Conservation, 25*: 43- 56. https://doi.org/10.1896/052.025.0109

Delson, E. (1973). *Fossil colobine monkeys of the circum-Mediterranean region and the evolutionary history of the Cercopithecidae (Primates, Mammalia)*. Columbia University.

Delson, E., Terranova, C. J., Jungers, W. L., Sargis, E. J., & Jablonski, N. G. (2000). Body mass in Cercopithecidae (Primates, Mammalia): estimation and scaling in extinct and extant taxa. New York: American Museum of Natural History.

Detwiler, K.M. (2004). Hybridization between red-tailed monkeys (*Cercopithecus ascanius*) and blue monkeys (*C. mitis*) in East African forests. In ME Glenn, M Cords, editors. *The guenons: diversity and adaptation in African monkeys*. New York: Kluwer Academic/Plenum Publishers. p 79- 97. https://doi.org/10.1007/0-306-48417-X_7

Detwiler, K.M, Burrell, A.S., Jolly, C.J. (2005). Conservation implications of hybridization in African cercopithecine monkeys. *International Journal of Primatology,* 26: 661- 684. https://doi.org/10.1007/s10764-005-4372-0

Detwiler, K. M. (2010). Natural hybridization between *Cercopithecus mitis x C. ascanius* in Gombe National Park, Tanzania (Doctoral dissertation, New York University).

Detwiler, K. M. (2019). Mitochondrial DNA analyses of Cercopithecus monkeys reveal a

localized hybrid origin for *C. mitis doggetti* in Gombe National Park, Tanzania. *International Journal of Primatology*, *40*(1), 28-52. https://doi.org/10.1007/s10764-018-0029-7

Disotell, T. R. (2000). Molecular systematics of the Cercopithecidae. P.F Whitehead, C. Jolly (Eds). *Old World Monkeys.* Cambridge University Press, Cambridge, 29-56.

Disotell, T. R., & Raaum, R. L. (2004). Molecular timescale and gene tree incongruence in the guenons. In *The guenons: Diversity and adaptation in African monkeys* (pp. 27-36). Springer, Boston, MA.

Dugoujon, J. M., Moro, F., & Larrouy, G. (1982). Cytogenetic study of *Cercopithecus pogonias grayi*× *Cercopithecus ascanius katangae* hybrids. *Folia Primatologica*, *38*(3-4), 269-274.

Dutrillaux, B. (1988). Chromosomal evolution of Cercopithecinae. *A primate radiation: evolutionary biology of the African guenons*. Cambridge University Press.

Eck, G. G. (1987). Plio-Pleistocene specimens of Cercopithecus from the Shungura Formation, southwestern Ethiopia. In *Cercopithecidae de la Formation de Shungura* (pp. 141-146).

Eck, G., & Howell, F. C. (1972). New fossil Cercopithecus material from the lower Omo basin, Ethiopia. *Folia Primatologica*, *18*(5-6), 325-355. https://doi.org/10.1159/000155492

Elliot, D. G. (1911). The generic name *Cercopithecus*. New York: American Museum of Natural History.

Elton, S., Jansson, A. U., Meloro, C., Louys, J., Plummer, T., & Bishop, L. C. (2016). Exploring morphological generality in the Old World monkey postcranium using an ecomorphological framework. *Journal of Anatomy*, *228*(4), 534-560. https://doi.org/10.1111/joa.12428

Frost, S. R. (2001). Fossil Cercopithecidae from the Afar depression, Ethiopia: Species systematics and comparison to the Turkana Basin (Doctoral dissertation). City University of New York, New York.

Frost, S. R., & Delson, E. (2002). Fossil Cercopithecidae from the Hadar Formation and surrounding areas of the Afar Depression, Ethiopia. *Journal of Human Evolution*, *43*(5), 687-748. doi:10.1053/jhev.2002.0603

Frost, S. R., & Alemseged, Z. (2007). Middle Pleistocene fossil Cercopithecidae from Asbole, Afar Region, Ethiopia. *Journal of Human Evolution*, *53*(3), 227-259. https://doi.org/10.1016/j.jhevol.2007.02.003

Frost, S. R. (2007). Fossil Cercopithecidae from the Middle Pleistocene Dawaitoli Formation, Middle Awash Valley, Afar Region, Ethiopia. *American Journal of Physical Anthropology*, *134*(4), 460-471. https://doi.org/10.1002/ajpa.20688

Frost, S. R., Simpson, S. W., Levin, N. E., Quade, J., Rogers, M. J., & Semaw, S. (2020a). Fossil Cercopithecidae from the Early Pliocene Sagantole Formation at Gona, Ethiopia. *Journal of Human Evolution, 144*, 102789. doi:10.1016/j.jhevol.2020.102789

Frost, S. R., Ward, C. V., Manthi, F. K., & Plavcan, J. M. (2020b). Cercopithecid fossils from Kanapoi, West Turkana, Kenya (2007–2015). *Journal of Human Evolution*, *140*, 102642. https://doi.org/10.1016/j.jhevol.2019.102642

Gebo, D. L., & Sargis, E. J. (1994). Terrestrial adaptations in the postcranial skeletons of guenons. *American Journal of Physical Anthropology*, *93*(3), 341-371. https://doi.org/10.1002/ajpa.1330930306

Gilbert, W.H. and Asfaw, B. eds., (2008). Homo erectus: Pleistocene Evidence from the Middle

Awash, Ethiopia (Vol. 1). Univ of California Press.
Gilbert, C. C., Bibi, F., Hill, A., & Beech, M. J. (2014). Early guenon from the late Miocene Baynunah Formation, Abu Dhabi, with implications for cercopithecoid biogeography and evolution. *Proceedings of the National Academy of Sciences*, *111*(28), 10119-10124. https://doi.org/10.1073/pnas.1323888111
Gilbert, C. C., Gilissen, E., Arenson, J. L., Patel, B.A., Nakatsukasa, M., Hart, T. B., ... & Sargis, E. J. (2021). Morphological analysis of new Dryas Monkey specimens from the Central Congo Basin: Taxonomic considerations and an emended diagnosis. *American Journal of Physical Anthropology*. https://doi.org/10.1002/ajpa.24278
Gray, J. E. (1821). Cercopithecidae. *London Medical Repository*, *15*, 297.
Gray, J. E. (1870). Catalogue of monkeys, lemurs, and fruit-eating bats in the collection of the British Museum. *Catalogue of mammalia.* British Museum (Natural History), London, UK.
Grieco, T. M., Rizk, O. T., & Hlusko, L. J. (2013). A modular framework characterizes micro- and macroevolution of old world monkey dentitions. *Evolution: International Journal of Organic Evolution*, *67*(1), 241-259. https://doi.org/10.1111/j.1558- 5646.2012.01757.x
Groves, C. P. (2007). The taxonomic diversity of the Colobinae of Africa. *Journal of Anthropological Sciences, 85*, 7-34.
Groves, C. (2018). An Overview of the Primates. Burke, M., Ptito, M. (Eds.) *Primates*, 11. https://dx.doi.org/10.5772/intechopen.70264
Grubb, P., Butynski, T. M., Oates, J. F., Bearder, S. K., Disotell, T. R., Groves, C. P., & Struhsaker, T. T. (2003). Assessment of the diversity of African primates. *International Journal of Primatology*, *24*(6), 1301-1357. https://doi.org/10.1023/B:IJOP.0000005994.86792.b9
Guschanski, K., Krause, J., Sawyer, S., Valente, L. M., Bailey, S., Finstermeier, K., ... & Lenglet, G. (2013). Next-generation museomics disentangles one of the largest primate radiations. *Systematic Biology*, *62*(4), 539-554. https://doi.org/10.1093/sysbio/syt018
Hart, J. A., Detwiler, K. M., Gilbert, C. C., Burrell, A. S., Fuller, J. L., Emetshu, M., ... & Tosi, A. J. (2012). Lesula: a new species of *Cercopithecus* monkey endemic to the Democratic Republic of Congo and implications for conservation of Congo's central basin. *PloS one*, *7*(9), e44271. https://doi.org/10.1371/journal.pone.0044271
Harrison, M. J. (1988). A new species of guenon (genus *Cercopithecus*) from Gabon. *Journal of Zoology*, *215*(3), 561-575. https://doi.org/10.1111/j.1469-7998.1988.tb02860.x
Harrison, T., & Harris, E. E. (1996). Plio-Pleistocene cercopithecids from Kanam East, western Kenya. *Journal of Human Evolution*, *30*(6), 539-561. https://doi.org/10.1006/jhev.1996.0042
Harvati, K. (2000). Dental eruption sequence among colobine primates. *American Journal of Physical Anthropology: The Official Publication of the American Association of Physical Anthropologists*, *112*(1), 69-85.
Haughton, S. (1864). Notes on Animal Mechanics: No. 8. Further Comparison of the Hip Joint and Knee Joint Muscles in the *Cercopithecus*, *Cynocephalus*, and *Macacus*. *Proceedings of the Royal Irish Academy (1836-1869)*, *9*, 287-294.
Hlusko, L. J., & Mahaney, M. C. (2009). The baboon model for dental development. In *The*

Baboon in Biomedical Research (pp. 207-223). Springer, New York, NY.
Hlusko, L. J., Schmitt, C. A., Monson, T. A., Brasil, M. F., & Mahaney, M. C. (2016). The Integration of quantitative genetics, paleontology, and neontology reveals genetic underpinnings of primate dental evolution. *Proceedings of the National Academy of Sciences*, *113*(33), 9262-9267. https://doi.org/10.1073/pnas.1605901113
Jablonski, N. G. (2002). Fossil Old World monkeys: the late Neogene radiation. *The primate fossil record*, 255-299. Cambridge University Press.
Jablonski N.G., Leakey M.G., and Anton, M. (2008). Systematic paleontology of the cercopithecines. In: *Koobi Fora Research Project: Volume 6. The Fossil Monkeys*. San Francisco: California Academy of Sciences
Jablonski, N. G., & Frost, S. R. (2010). Cercopithecoidea. In L. Werdelin & W. J. Sanders (Eds.), *Cenozoic Mammals of Africa* (pp. 393-428). Berkeley: University of California Press.
Jentink, F. A. (1886). On two new species of *Cercopithecus*. *Notes from the Leyden Museum*, *8*(1), 55-57.
Jogahara, Y. O., & Natori, M. (2012). Dental eruption sequence and eruption times in *Erythrocebus patas*. *Primates*, *53*(2), 193-204.
Leakey, M. (1988). Fossil evidence for the evolution of the guenons. *A primate radiation: Evolutionary biology of the African guenons*, 7-12.
Jolly, C. J., Woolley-Barker, T., Beyene, S., Disotell, T. R., & Phillips-Conroy, J. E. (1997). Intergeneric hybrid baboons. *International Journal of Primatology*, *18*(4), 597-627.
Kalb, J. E., Wood, C. B., Smart, C., Oswald, E. B., Mabrete, A., Tebedge, S., & Whitehead, P. (1980). Preliminary geology and palaeontology of the Bodo D'ar hominid site, Afar, Ethiopia. *Palaeogeography, Palaeoclimatology, Palaeoecology, 30*, 107-120. doi:10.1016/0031-0182(80)90052-8
Leakey, M. (1988). Fossil evidence for the evolution of the guenons. *A primate radiation: Evolutionary biology of the African guenons*, 7-12.
Lo Bianco, S., Masters, J. C., & Sineo, L. (2017). The evolution of the Cercopithecini: a (post) modern synthesis. *Evolutionary Anthropology: Issues, News, and Reviews*, *26*(6), 336-349. https://doi.org/10.1002/evan.21567
Lucotte, G., Gautreau, C., Galat, G., & Galat-Luong, A. (1982). Polymorphisme électrophorétique des différentes sous-espèces de *Cercopithecus aethiops*. *Folia Primatologica*, *38*(3-4), 183-195. https://doi.org/10.1159/000156056
McBrearty, S., Bishop, L., & Kingston, J. (1996). Variability in traces of Middle Pleistocene hominid behavior in the Kapthurin Formation, Baringo, Kenya. *Journal of Human Evolution*, *30*(6), 563-580.
McDougall, I., Brown, F. H., Vasconcelos, P. M., Cohen, B. E., Thiede, D. S., & Buchanan, M. J. (2012). New single crystal 40Ar/39Ar ages improve time scale for deposition of the Omo Group, Omo–Turkana Basin, East Africa. *Journal of the Geological Society*, *169*(2), 213-226.
McGraw, S. (1994). Census, habitat preference, and polyspecific associations of six monkeys in the Lomako Forest, Zaire. *American Journal of Primatology*, *34*(4), 295-307. https://doi.org/10.1002/ajp.1350340402
McGraw, W. S. (2004). Diversity of guenon positional behavior. In *The guenons: Diversity and adaptation in African monkeys* (pp. 113-131). Springer, Boston, MA. https://doi.org/10.1007/0-306-48417-X_9

Monson, T. A., Brasil, M. F., Stratford, D. J., & Hlusko, J. (2017). Patterns of craniofacial variation and taxonomic diversity in the South African Cercopithecidae fossil record. *Palaeontologica Electronica, 20,* 1-20.

Monson, T. A., & Hlusko, L. J. (2018). Breaking the rules: Phylogeny, not life history, explains dental eruption sequence in primates. *American Journal of Physical Anthropology*, *167*(2), 217-233.

Monson, T. A. (2020). Patterns and magnitudes of craniofacial covariation in extant cercopithecids. *The Anatomical Record*, 1-17. https://doi.org/10.1002/ar.24398

Motsch, P., Le Flohic, G., Dilger, C., Delahaye, A., Chateau-Smith, C., & Couette, S. (2015). Degree of terrestrial activity of the elusive sun-tailed monkey (*Cercopithecus solatus*) in Gabon: Comparative study of behavior and postcranial morphometric data. *American Journal of Primatology*, *77*(10), 1060-1074. https://doi.org/10.1002/ajp.22441

-Moulin, S., Gerbault-Seureau, M., Dutrillaux, B., & Richard, F. A. (2008). Phylogenomics of African guenons. *Chromosome Research*, *16*(5), 783. https://doi.org/10.1007/s10577-008-1226-6

Nakatsukasa, M. (1994). Intrageneric variation of limb bones and implications for positional behavior in Old World monkeys. *Zeitschrift für Morphologie und Anthropologie*, 125-136. https://www.jstor.org/stable/25757422

Napier, P. H. (1976). *Catalogue of Primates in the British Museum (Natural History) and Elsewhere in the British Isles: Family Cercopithecidae, Subfamily Colobinae* (Vol. 3). British Museum (Natural History), London, UK.

Niespolo, E. M., WoldeGabriel, G., Hart, W. K., Renne, P. R., Sharpe, W. D, Shackley, S. M., … White, T. D. (2021). Integrative geochronology calibrates the Middle and Late Stone Ages of Ethiopia's Afar Rift. *Proceedings of the National Academy of Sciences, in press.*

Perelman, P., Johnson, W. E., Roos, C., Seuánez, H. N., Horvath, J. E., Moreira, M. A., ... & Schneider, M. P. C. (2011). A molecular phylogeny of living primates. *PLoS Genetics*, *7*(3), e1001342. https://doi.org/10.1371/journal.pgen.1001342

Plavcan, J. M., Ward, C. V., Kay, R. F., & Manthi, F. K. (2019). A diminutive Pliocene guenon from Kanapoi, West Turkana, Kenya. *Journal of human evolution*, *135*, 102623. https://doi.org/10.1016/j.jhevol.2019.05.011

Pobiner, B. L., Rogers, M. J., Monahan, C. M., & Harris, J. W. (2008). New evidence for hominin carcass processing strategies at 1.5 Ma, Koobi Fora, Kenya. *Journal of Human Evolution*, *55*(1), 103-130. https://doi.org/10.1016/j.jhevol.2008.02.001

R Core Team. (2019). *R: A language and environment for statistical computing*. Retrieved from https://www.R-project.org/

Raaum, R. L., Sterner, K. N., Noviello, C. M., Stewart, C. B., & Disotell, T. R. (2005). Catarrhine primate divergence dates estimated from complete mitochondrial genomes: concordance with fossil and nuclear DNA evidence. *Journal of human evolution*, *48*(3), 237-257. https://doi.org/10.1016/j.jhevol.2004.11.007

Reuvens, C. L. (1890). On *Cercopithecus talapoin* Erxleben. *Notes from the Leyden Museum*, *12*(1/2), 41-46.

Rowe, N., & Myers, M. (2016). All the world's primates. *The International Encyclopedia of Primatology*, 1-4. https://doi.org/10.1002/9781119179313.wbprim0086

Sargis, E. J., Terranova, C. J., & Gebo, D. L. (2008). Evolutionary morphology of the

guenon postcranium and its taxonomic implications. In Sargis, E.J., Dagosto, M. (Eds) *Mammalian evolutionary morphology* (pp. 361-372). Springer, Dordrecht. https://doi.org/10.1007/978-1-4020-6997-0_16

Schneider, C. A., Rasband, W. S., & Eliceiri, K. W. (2012). NIH Image to ImageJ: 25 years of image analysis. *Nature methods*, *9*(7), 671-675. https://doi.org/10.1038/nmeth.2089

Sclater, P. L. (1893). On a new African monkey of the genus *Cercopithecus*, with a list of the known species. In *Proceedings of the Zoological Society of London* (pp. 243-258).

Shurtliff, Q. R. (2013). Mammalian hybrid zones: a review. *Mammal Review*, *43*(1), 1-21. https://doi.org/10.1111/j.1365-2907.2011.00205.x

Singleton, M. (2003). Functional and phylogenetic implications of molar flare variation in Miocene hominoids. *Journal of Human Evolution*, *45*(1), 57-79. https://doi.org/10.1016/S0047-2484(03)00086-1

Simons, E. L., Delson, E., Maglio, V. J., & Cooke, H. S. B. (1978). Cercopithecidae and Parapithecidae. *Evolution of African mammals*, 100-119.

Sineo, L. (1990). The banded karyotype of *Cercopithecus mitis maesi* compared with the karyotypes of *C. albogularis samango* and *C. nictitans stampflii*. *International Journal of Primatology*, *11*(6), 541-552.

Springer, M. S., Meredith, R. W., Gatesy, J., Emerling, C. A., Park, J., Rabosky, D. L., ... & Fisher, C. A. (2012). Macroevolutionary dynamics and historical biogeography of primate diversification inferred from a species supermatrix. *PloS One*, *7*(11), e49521. https://doi.org/10.1371/journal.pone.0049521

Stiles, C. W., & Orleman, M. B. (1926). Retention of *Cercopithecus*, Type Diana, for the Guenons. *Journal of Mammalogy*, *7*(1), 48-53. https://doi.org/10.2307/1373595

Strasser, E., & Delson, E. (1987). Cladistic analysis of cercopithecid relationships. *Journal of Human Evolution*, *16*(1), 81-99. https://doi.org/10.1016/0047-2484(87)90061-3

Struhsaker, T.T., Butynski, T.M., Lwanga, J.S. (1988). Hybridization between redtail (*Cercopithecus ascanius schmidti*) and blue (*C. mitis stuhlmanni*) monkeys in the Kibale Forest, Uganda. In A Gautier-Hion, F Bourlière, J-P Gautier, et al., editors. *A primate radiation: evolutionary biology of the African guenons*. Cambridge, UK: Cambridge University Press. p 477- 497.

Svardal, H., Jasinska, A. J., Apetrei, C., Coppola, G., Huang, Y., Schmitt, C. A., ... & Weinstock, G. (2017). Ancient hybridization and strong adaptation to viruses across African vervet monkey populations. *Nature Genetics*, *49*(12), 1705-1713. https://doi.org/10.1038/ng.3980

Szalay, F. S., & Delson, E. (1979). *Evolutionary history of the primates*. Academic Press.

Tapanes, E. (2016). Coat Color Variation Between Red-tailed Monkeys (*Cercopithecus ascanius*), Blue Monkeys (*C. mitis*), and Hybrids (*C. ascanius* x *C. mitis*) in Gombe National Park, Tanzania. Florida Atlantic University.

Tosi, A. J., Buzzard, P. J., Morales, J. C., & Melnick, D. J. (2002). Y-chromosome data and tribal affiliations of *Allenopithecus* and *Miopithecus*. *International Journal of Primatology*, *23*(6), 1287-1299. https://doi.org/10.1023/A:1021178904824

Tosi, A. J., Disotell, T. R., Morales, J. C., & Melnick, D. J. (2003). Cercopithecine Y-chromosome data provide a test of competing morphological evolutionary hypotheses. *Molecular Phylogenetics and Evolution*, *27*(3), 510-521. https://doi.org/10.1016/S1055-7903(03)00024-1

Tosi, A. J., Melnick, D. J., & Disotell, T. R. (2004a). Sex chromosome phylogenetics indicate a single transition to terrestriality in the guenons (tribe Cercopithecini). *Journal of Human Evolution*, *46*(2), 223-237. https://doi.org/10.1016/j.jhevol.2003.11.006

Tosi, A. J., Buzzard, P. J., Morales, J. C., & Melnick, D. J. (2004b). Y-chromosomal window onto the history of terrestrial adaptation in the Cercopithecini. In: Glenn, M. E., Cords, M. (Eds.), The Guenons: Diversity and Adaptation in African Monkeys. Kluwer/Plenum, New York, pp. 15–26. https://doi.org/10.1007/0-306-48417-X_2

Tosi, A. J., Detwiler, K. M., & Disotell, T. R. (2005a). Y-chromosomal markers suitable for noninvasive studies of guenon hybridization. *International Journal of Primatology*, *26*(3), 685-696. https://doi.org/10.1007/s10764-005-4374-y

Tosi, A. J., Detwiler, K. M., & Disotell, T. R. (2005b). X-chromosomal window into the evolutionary history of the guenons (Primates: Cercopithecini). *Molecular Phylogenetics and Evolution*, *36*(1), 58-66. https://doi.org/10.1016/j.ympev.2005.01.009

Tosi, A. J. (2008). Forest monkeys and Pleistocene refugia: a phylogeographic window onto the disjunct distribution of the *Chlorocebus lhoesti* species group. *Zoological Journal of the Linnean Society*, *154*(2), 408-41. https://doi.org/10.1111/j.1096-3642.2008.00419.x

Tosi, A. J., & Detwiler, K. M. (2016). The efficacy of sex-chromosomal markers in studies of Cercopithecus hybridization: Discovery of a captive hybrid and applications in wild populations. *Zoo Biology*, *35*(1), 61-64. https://doi.org/10.1002/zoo.21259

Tosi, A. J. (2017). Phylogenetic tests of a Cercopithecus monkey hybrid reveal X-chromosomal polyphyly of *C. cephus* and emerging patterns in the *cephus* species group radiation. *African Zoology*, *52*(3), 177-181. https://doi.org/10.1080/15627020.2017.1369363

Turner, T. R., Schmitt, C. A., & Cramer, J. D. (2019). *Savanna Monkeys: The Genus Chlorocebus*. Cambridge University Press.

van der Kuyl, A. C., Kuiken, C. L., Dekker, J. T., & Goudsmit, J. (1995). Phylogeny of African monkeys based upon mitochondrial 12S rRNA sequences. *Journal of Molecular Evolution*, *40*(2), 173-180.

Verheyen, W. N. (1962). Contribution à la craniologie comparée des primates: les genres Colobus Illiger 1811 et Cercopithecus Linné 1758. *Annal. Koninklijk Mus. voor Midden-afrika Ser. 8, Sci. Zool.*, *105*, 1-255.

Warren, W. C., Jasinska, A. J., García-Pérez, R., Svardal, H., Tomlinson, C., Rocchi, M., ... & Kyung, K. (2015). The genome of the vervet (*Chlorocebus aethiops sabaeus*). *Genome Research*, *25*(12), 1921-1933.

Wickham, H. (2016). *ggplot2: elegant graphics for data analysis*. Springer.

Wichkam, François, Henry, & Müller, 2022. Dplyr: A Grammar of Data Manipulation. https.//dplyr.tidyverse.org

Xing, J., Wang, H., Zhang, Y., Ray, D. A., Tosi, A. J., Disotell, T. R., & Batzer, M. A. (2007). A mobile element-based evolutionary history of guenons (tribe Cercopithecini). *BMC Biology*, *5*(1), 5. https://doi.org/10.1186/1741-7007-5-5

Figure Legends

Figure 1. Map showing the location of the Middle Awash study area, indicated on the left by the grey rectangle. The research area is enlarged in the inset map on the right with the location of the Halibee area indicated. The modern Awash River is visible as the dark green strip of vegetation running approximately north-south. Map data ©2018 Google.

Figure 2. Element counts for Faro Daba and Chai Baro cf. *Chlorocebus*. (a) Element preservation by type. Each specimen is included once. (b) Element count by region – if an individual preserves fossils from multiple regions, they are included in each region count.

Figure 3. The partial male skeleton HAL-VP-9/650 from Faro Daba.

Figure 4. Crania from Chai Baro (a & b) and Faro Daba (c & d). Each individual is shown in anterior (left) and superior (right) views. a) HAL-VP-5/150, female; b) HAL-VP-5/293, female; c) HAL-VP-9/650, male; d) HAL-VP-9/13, sex uncertain.

Figure 5. Maxilla and mandible of HAL-VP-9/634, male from Faro Daba in lateral view (left) and occlusal view (right).

Figure 6. Maxillae from Faro Daba with fossil and extant comparisons. Each individual is shown in lateral (top) and occlusal (bottom) views. (a) HAL-VP-9/650, male; (b) HAL-VP-9/1452, male; (c) HAL-VP-9/865, female; (d) HAL-VP-9/446, female; (e) HAL-VP-9/335, female; (f) ASB-87-1, female; (g) ASB-89, male; (h) ASB-254-1; (i) Michigan Museum of Zoology 9207 (*Chlorocebus pygerythrus*), male; (j) MMZ 86350 (*Cercopithecus mona*), sex uncertain. Photos for (i) and (j) photos by Phil Myers (licensed http://creativecommons.org/licenses/by-nc-sa/3.0/). Scale is the same for both panels.

Figure 7. Occlusal views of maxillae from Chai Baro (a-g, j) and Faro Daba (h & i). Anterior is up. Bottom row individuals are juveniles. (a) HAL-VP-5/150, female; (b) HAL-VP-6/144, female; (c) HAL-VP-5/43, female; (d) HAL-VP-5/63, male; (e) HAL-VP-5/26, male; (f) HAL-VP-5/164, female; (g) HAL-VP-6/263, sex uncertain; (h) HAL-VP-9/13, male; (i) HAL-VP-9/385, sex uncertain; (j) HAL-VP-5/157, sex uncertain.

Figure 8. Mandibles in occlusal (top) and lateral (bottom) views from Faro Daba (a-h), Chai Baro (i), Asbole (j-l), and extant cercopithecins (m, n). Anterior is to the right except for lateral views of (c), (d), (f), (g), and (l). (a) HAL-VP-9/1617, female; (b) HAL-VP-2/67, female; (c) HAL-VP-9/865, female; (d) HAL-VP-9/439, female; (e) HAL-VP-9/446, female; (f) HAL-VP-9/716, sex uncertain; (g) HAL-VP-9/670, male; (h) HAL-VP-2/135, male; (i) HAL-VP-8/100, male; (j) ASB-79 (*Chlorocebus* aff. *aethiops*), female; (k) ASB-58 (*Chlorocebus* aff. *aethiops*), female; (l) ASB-254-3 (*Chlorocebus* aff. *aethiops*), female; (m) HTB 0147 (*Cercopithecus mona*), male; (n) HTB 0827 (*Chlorocebus aethiops*), female. Scale is the same for both panels. H – j are taken from Frost and Alemseged (2007).

Figure 9. Mandibles from Chai Baro and Faro Daba in occlusal view. Anterior is up. Top row, from left to right: HAL-VP-5/108, Chai Baro, female; HAL-VP-9/846, Faro Daba, female; HAL-VP-5/102, Chai Baro, female; HAL-VP-5/81, Chai Baro, sex uncertain. Bottom row, from left to right: HAL-VP-9/313, Faro Daba, sex uncertain; HAL-VP-5/77, Chai Baro, male; HAL-VP-6/257, Chai Baro, male; HAL-VP-5/26, Chai Baro, male.

Figure 10. Humeri from Faro Daba (a & c) and Chai Baro (b) with extant comparisons (d – f); medial and lateral views. (a) HAL-VP-9/650, male; (b) HAL-VP-5/148, sex uncertain; (c) HAL-VP-9/865, female; (d) HTB 2138 (*Cercopithecus mitis*), male; (e) HTB 0147 (*Cercopithecus mona*), male; (f) HTB 1162 (*Chlorocebus aethiops*), female.

Figure 11. Fossil and extant humeri in (a) anterior and (b) proximal views. (a) Fom left to right: HTB 1162 (*Chlorocebus aethiops*), female; HTB 2138 (*Cercopithecus mitis*), male; HTB 0147 (*Cercopithecus mona*), male; HAL-VP-5/21, Chai Baro, sex uncertain; HAL-VP-5/300, Chai Baro, sex uncertain; HAL-VP-5/287, Chai Baro, sex uncertain; HAL-VP-9/416, Faro Daba, sex uncertain (mirrored); HAL-VP-9/591, Faro Daba, sex uncertain; HAL-VP-9/661, Faro Daba, sex uncertain (mirrored); HAL-VP-9/734, Faro Daba, male; HAL-VP-9/508, sex uncertain; HAL-VP-9/813, sex uncertain. (b) from left to right; HTB 2138 (*Cercopithecus mitis*), male; HTB 1162 (*Chlorocebus aethiops*), female; HAL-VP-5/148, Chai Baro, sex uncertain; HAL-VP-9/697, Faro Daba, sex uncertain; HAL-VP-9/650, Faro Daba, male; HAL-VP-9/1154, Faro Daba, sex uncertain.

Figure 12. Distal humeri in inferior view, anterior is up. All humeri are from the right side unless otherwise stated. Sex is uncertain unless otherwise indicated. Column (a) from top to bottom (Chai Baro): HAL-VP-6/112 (mirrored); HAL-VP-6/105; HAL-VP-5/287; HAL-VP-5/113, male. Column (b) from top to bottom: HTB 1044 (*Chlorocebus aethiops*), male; HTB 0147 (*Cercopithecus mona*), male; HTB 2138 (*Cercopithecus mitis*), male. Column (c) from top to bottom (Faro Daba): HAL-VP-9/813; HAL-VP-9/1154, female; HAL-VP-9/661; HAL-VP-14/20.

Figure 13. cf. *Chlorocebus* ulnae from Faro Daba in lateral view, seriated by size from largest (left) to smallest (right). From left to right: HAL-VP-9/600, male; HAL-VP-9/650, male; HAL-VP-9/734, male; HAL-VP-2/147, female; HAL-VP-9/865, female; HAL-VP-9/1637, sex uncertain.

Figure 14. Femora from Faro Daba (left panel), Chai Baro (middle panel), and extant comparative specimens (right panel). Sex is uncertain unless otherwise indicated. (a) HAL-VP-9/740; (b) HAL-VP-9/1137; (c) HAL-VP-9/734, male; (d) HAL-VP-9/1154; (e) HAL-VP-9/1637; (f) HAL-VP-6/231; (g) HAL-VP-5/288; (h) HAL-VP-5/241; (i) HAL-VP-6/246; (j) HAL-VP-5/101; (k) HTB 0147 (*Cercopithecus mona*), male; (l) HTB 0827 (*Chlorocebus aethiops*), female.

Figure 15. cf. *Chlorocebus* femora from Faro Daba (a) and Chai Baro (b) in posterior view, seriated by size from largest (left) to smallest (right). Sex is uncertain unless otherwise indicated. Left to right (largest to smallest): HAL-VP-9/600; HAL-VP-9/734, male; HAL-VP-9/650, male;

HAL-VP-9/1637; HAL-VP-9/1137; HAL-VP-9/1154. HAL-VP-6/51; HAL-VP-6/246; HAL-VP-5/241.

Figure 16. Three traits often considered indicative of locomotor habitus in cercopithecid monkeys with visual descriptions of each measurement on the right. The Faro Daba means fall closer to the arboreal end of the extant species, whereas the Chai Baro fossils are more similar to extant terrestrial and semi-terrestrial taxa. However, considerable overlap exists, complicated by the small sample sizes of both the extant and fossil taxa. Boxplots for modern species are modified from Frost et al. (2020b).

Figure 17. Boxplot of orbital shape (orbital height/orbital width, left) and distribution plot (right).

Figure 18. Boxplots of mandibular corpus height at the midpoint of M_1 (top left) and M_3 (bottom left) with corresponding distribution plots (right).

Figure 19. Boxplot of relative I^2 size (maxillary I^2 mesiodistal length / I^1 mesiodistal length; left) and corresponding distribution plot (right).

Figure 20. Boxplot of relative I^1 size (maxillary I^1 mesiodistal length / M^1 mesiodistal length; left) and corresponding distribution plot (right).

Figure 21. Maxillary dental plots of the Middle Awash fossil assemblages and fossil and extant comparative data. Measurements are in millimeters. A) M^1 maximum length vs. P^4 maximum length. B) M^3 maximum length vs. M^1 maximum length. C) M^1 anterior width vs. M^1 length. D) M^3 anterior width vs. M^1 anterior width. Abbreviations: L is mesiodistal crown length; AW is buccolingual width of the anterior loph; P4, M1, M2, and M3 refer to the fourth premolar and first, second, and third molars, respectively.

Figure 22. Mandibular dental plots of the Middle Awash fossil assemblages and comparative fossil and extant data. Measurements are in millimeters. A) M_1 maximum length vs. P_4 maximum length. B) M_3 maximum length vs. M_1 maximum length. C) M_1 anterior width vs. M_1 length. D) M_3 anterior width vs. M_1 anterior width. Abbreviations: L is mesiodistal crown length; AW is buccolingual width of the anterior loph; P4, M1, M2, and M3 refer to the fourth premolar and first, second, and third molars, respectively.

FIGURES & TABLES: Halibee fossil assemblages reveal later Pleistocene cercopithecins (Cercopithecidae: Primates) in the Middle Awash of Ethiopia

Table 1. Comparative samples included in this study.

Taxon	Number of individuals	Repository/Reference
Extant		
Allenopithecus nigroviridis	17	Arenson et al. (2020), Gilbert et al. (2021)
Allochrocebus lhoesti	24	PRIMO, Arenson et al. (2020), Gilbert et al. (2021)
Allochrocebus preussi	4	Arenson et al. (2020), Gilbert et al. (2021)
Cercopithecus albogularis	10	ADZ, Arenson et al. (2020), Gilbert et al. (2021)
Cercopithecus ascanius	32	PRIMO, Arenson et al. (2020), Gilbert et al. (2021)
Cercopithecus campbelli	13	ADZ, Arenson et al. (2020), Gilbert et al. (2021)
Cercopithecus cephus	13	Arenson et al. (2020), Gilbert et al. (2021)
Cercopithecus denti	10	PRIMO, Arenson et al. (2020), Gilbert et al. (2021)
Cercopithecus diana	10	Arenson et al. (2020), Gilbert et al. (2021)
Cercopithecus dryas	3	Arenson et al. (2020), Gilbert et al. (2021)
Cercopithecus erythrotis	1	Arenson et al. (2020), Gilbert et al. (2021)
Cercopithecus hamlyni	20	Arenson et al. (2020), Gilbert et al. (2021)
Cercopithecus lomamiensis	6	Arenson et al. (2020), Gilbert et al. (2021)
Cercopithecus mitis	107	AMNH, MVZ, NMNH, CMNH, Arenson et al. (2020)
Cercopithecus mona	11	PRIMO, Arenson et al. (2020), Gilbert et al. (2021)
Cercopithecus neglectus	19	Arenson et al. (2020), Gilbert et al. (2021)
Cercopithecus nictitans	5	Arenson et al. (2020), Gilbert et al. (2021)
Cercopithecus petaurista	7	Arenson et al. (2020), Gilbert et al. (2021)
Cercopithecus pogonias	17	PRIMO, Arenson et al. (2020), Gilbert et al. (2021)
Cercopithecus wolfi	7	Arenson et al. (2020), Gilbert et al. (2021)
Chlorocebus aethiops	28	ADZ, MVZ, CMNH
Chlorocebus cynosuros	15	Arenson et al. (2020), Gilbert et al. (2021)
Chlorocebus pygerythrus	36	PRIMO, Arenson et al. (2020), Gilbert et al. (2021)

Chlorocebus tantalus	3	Arenson et al. (2020), Gilbert et al. (2021)
Erythrocebus patas	2	ADZ
Fossil		
cf. *Chlorocebus* aff. *aethiops*	8	Frost & Alemseged (2007)
cf. *Chlorocebus* cf. *patas*	4	Frost & Alemseged (2007)
Cercopithecus ("Andalee")	30	Frost (2001)
Cercopithecus ("Upper Andalee")	5	Frost (2001)

Abbreviations: N, sample size; ADZ, Anthropology Department, Zurich; AMNH, American Museum of Natural History; CMNH, Cleveland Museum of Natural History; MVZ, Museum of Vertebrate Zoology; NME, National Museum of Ethiopia; NMNH, Smithsonian's National Museum of Natural History; PRIMO, PRImate Morphometrics Online.

Table 2. Age scoring criteria.

Score	Description
1	Individual only has deciduous dentition
2	Individual has mixed dentition[1]
3	Individual has permanent dentition, but the third molar is not fully erupted
4	Individual has permanent dentition with only light wear[2]
5	Individual has permanent dentition with moderate wear[3]
6	Individual has permanent dentition with heavy wear[4]

[1]Instances where both deciduous and permanent dentition are present.
[2]No dentine exposure that exceeds 1 millimeter in diameter.
[3]Exposed dentine on the first and second molars does not connect between cusps.
[4]Dentine is exposed on all three molars and the exposures connect between cusps.

Table 3. Descriptive statistics for maxillary dental metrics of Faro Daba and Chai Baro fossils and comparative samples. Range is presented as minimum measurement – maximum measurement.

		Faro Daba cf. *Chlorocebus*	Chai Baro cf. *Chlorocebus*	cf. *Chlorocebus* aff. *aethiops* (Asbole)	*Cercopithecus* spp.	*C. mitis*	*Chlorocebus* spp.	*Ch. aethiops*
M^3L	*Mean*	5.62 (22)	5.63 (12)	5.37 (3)	5.39 (109)	5.74 (75)	5.71 (33)	5.81 (25)
	Range	5.01 – 6.3	5.08 – 6.5	4.9 – 5.6	3.43 – 6.65	4.74 - 6.65	4.6 – 8.24	4.61 - 8.24
M^3AW	*Mean*	5.39 (22)	5.51 (11)	5.73 (3)	5.32 (106)	5.57 (72)	5.87 (33)	5.89 (25)
	Range	4.82 – 6.09	5.2 – 6.22	5.6 – 5.8	4 – 6.56	4.77 - 6.56	4.95 – 8.79	4.95 - 8.79
M^3PW	*Mean*	4.49 (22)	4.75 (10)	4.53 (3)	4.13 (104)	4.46 (70)	4.75 (33)	4.79 (25)
	Range	3.71 – 5.1	4.25 – 5.7	4.4 – 4.8	2.06 – 5.86	3.66 - 5.86	3.52 – 7.52	3.52 - 7.52
M^2L	*Mean*	6.26 (33)	6.29 (13)	6.47 (3)	6.26 (119)	6.56 (84)	6.48 (39)	6.52 (28)
	Range	5.32 – 7.07	5.82 – 6.6	6.3 – 6.6	4.9 – 7.58	5.8 - 7.58	5.07 – 8.57	5.07 - 8.57
M^2AW	*Mean*	5.97 (29)	6.23 (14)	6.47 (3)	5.97 (112)	6.21 (77)	6.37 (38)	6.39 (27)
	Range	5.22 – 6.5	5.51 – 6.66	6 – 6.9	4.59 – 7.46	5.24 - 7.46	5.5 – 9.02	5.51 - 9.02
M^2PW	*Mean*	5.45 (29)	5.64 (13)	5.93 (3)	5.36 (108)	5.58 (73)	5.79 (39)	5.77 (28)
	Range	4.87 – 6.1	5.29 – 6.01	5.8 – 6.1	4.03 – 6.71	4.7 - 6.56	5 – 8.09	5.08 - 8.09
M^1L	*Mean*	5.69 (36)	5.81 (14)	5.75 (2)	5.66 (223)	6.05 (97)	5.84 (70)	5.97 (31)
	Range	5.12 – 6.01	5.4 – 6.39	5.4 – 6.1	4.1 – 6.9	5.07 - 6.89	4.65 – 8.3	4.65 - 8.3
M^1AW	*Mean*	5.27 (32)	5.39 (15)	5.4 (1)	4.73 (210)	5.33 (85)	5.01 (71)	5.42 (32)
	Range	4.6 – 5.97	5 – 5.81	–	3.5 – 6.28	4.0 - 6.28	3.94 – 8.05	3.94 - 8.05
M^1PW	*Mean*	5.02 (32)	5.12 (15)	4.8 (1)	4.89 (101)	5.13 (69)	5.26 (38)	5.29 (28)
	Range	4.29 – 5.51	4.62 – 5.61	–	3.65 – 5.93	4.64 - 5.93	4.5 – 7.63	4.5 - 7.63
P^4L	*Mean*	4.09 (32)	4.15 (13)	3.63 (3)	4.20 (118)	4.40 (84)	4.49 (27)	4.49 (26)
	Range	3.62 – 4.78	3.81 – 4.5	3.4 – 3.9	3.06 – 5.15	3.86 - 5.15	3.68 – 6.01	3.68 - 6.01
P^4W	*Mean*	4.61 (32)	4.88 (12)	5 (2)	4.73 (119)	4.93 (84)	5.15 (28)	5.16 (27)
	Range	3.8 – 5.17	4.5 – 5.36	–	2.92 – 5.96	4.33 - 5.96	4.31 – 7.06	4.31 - 7.06
P^3L	*Mean*	3.81 (27)	3.65 (9)	3.1 (2)	3.90 (118)	4.1 (84)	4.07 (27)	4.11 (26)
	Range	3.17 – 4.38	3.34 – 3.92	2.9 – 3.3	2.8 – 4.9	3.35 - 4.9	3.11 – 5.35	3.43 - 5.35
P^3W	*Mean*	3.94 (27)	4.28 (7)	4.35 (2)	3.99 (113)	4.2 (79)	4.54 (27)	4.56 (26)
	Range	2.9 – 4.88	3.66 – 4.92	4 – 4.7	2.5 – 5.21	3.51 - 5.21	3.82 – 6.29	3.82 - 6.29
CL	*Mean*	6.42 (15)	6.15 (9)	–	1.26 (23)	–	6.04 (1)	–
	Range	4.7 – 9.7	4.57 – 7.33	–	3.7 – 6.94	–	–	–
CW	*Mean*	4.84 (15)	4.54 (9)	6.2 (1)	3.91 (23)	–	5.1 (1)	–
	Range	3.49 – 6.8	3.72 – 5.36	–	3.21 – 4.77	–	–	–
I^2L	*Mean*	3.39 (11)	3.52 (3)	2.9 (2)	1.84 (16)	–	–	–
	Range	2.9 – 4.17	3.1 – 3.86	2.5 – 3.3	1.46 – 2.59	–	–	–
I^2W	*Mean*	2.49 (14)	2.24 (3)	3.95 (2)	2.88 (22)	–	2.86 (1)	–
	Range	2 – 4.73	1.72 – 2.78	3.8 – 4.1	2.29 – 3.41	–	–	–
I^1L	*Mean*	4.76 (12)	5.13 (3)	4.9 (1)	5.34 (13)	–	–	–
	Range	3.98 – 5.31	4.17 – 5.3	-	4.84 – 5.78	–	–	–

I¹W	*Mean*	3.2 (12)	3.28 (3)	4.5 (2)	4.08 (22)	–	4.76 (1)	–
	Range	2.31 – 3.73	2.83 – 3.9	4.2 – 4.8	3.65 – 4.62	–	–	–

Means are reported in millimeters. Sample sizes are in parentheses adjacent to the mean for each measurement. Abbreviations: L = mesiodistal length of the crown; W = buccolingual width of the crown; AW = buccolingual width across the anterior (mesial) loph of the crown; PW = buccolingual width across the posterior (distal) loph of the crown. *Ch.* Indicated *Chlorocebus* and *C.* indicates *Cercopithecus.* Extant comparative species were chosen due to their large sample size.

Table 4. Descriptive statistics for mandibular dental metrics of Faro Daba and Chai Baro fossils and comparative samples. Range is presented as minimum measurement – maximum measurement.

		Faro Daba cf. *Chlorocebus*	Chai Baro cf. *Chlorocebus*	cf. *Chlorocebus* aff. *aethiops* (Asbole)	*Cercopithecus* spp.	*C. mitis*	*Chlorocebus* spp.	*Ch. aethiops*
M_3L	*Mean*	6.56 (49)	6.32 (20)	5.97 (3)	6.25 (111)	6.62 (78)	6.48 (33)	6.52 (25)
	Range	5.85 – 7.54	5.59 – 6.75	5.8 – 6.2	4.58 – 7.68	5.69 - 7.68	5.21 – 9.81	5.21 - 9.8
M_3AW	*Mean*	5.30 (44)	5.33 (20)	5.1 (3)	4.86 (107)	5.11 (74)	5.46 (33)	5.51 (25)
	Range	4.63 – 6.39	4.88 – 5.69	5.0 – 5.30	3.6 – 6.09	4.31 - 6.09	4.58 – 7.58	4.58 - 7.5
M_3PW	*Mean*	4.48 (43)	4.66 (20)	4.1 (3)	4.38 (98)	4.6 (75)	4.55 (18)	4.56 (10)
	Range	3.39 – 5.49	4.14 – 5.14	3.9 – 4.3	3.19 – 5.43	3.94 - 5.43	3.73 – 5.41	3.73 - 5.4
M_2L	*Mean*	6.61 (69)	6.54 (30)	6.13 (3)	6.38 (117)	6.64 (84)	6.50 (38)	6.51 (28)
	Range	5.98 – 8.32	5.88 – 7.30	5.8 – 6.4	4.6 – 7.7	5.97 - 7.7	5.26 – 8.62	5.26 - 8.6
M_2AW	*Mean*	5.31 (57)	5.41 (23)	5.33 (3)	4.93 (105)	5.13 (72)	5.39 (37)	5.38 (27)
	Range	4.52 – 5.97	4.68 – 6.01	5.1 – 5.5	3.77 – 6.11	4.58 - 6.11	4.42 – 7.43	4.42 - 7.4
M_2PW	*Mean*	5.12 (55)	5.31 (23)	5.13 (3)	4.95 (97)	5.1 (75)	5.12 (22)	5.13 (12)
	Range	4.53 – 5.89	4.69 – 6.07	4.8 – 5.4	3.79 – 5.96	4.3 - 5.96	4.44 – 6.19	4.44 - 5.9
M_1L	*Mean*	5.95 (69)	5.79 (27)	5.1 (3)	5.73 (115)	6.05 (82)	5.99 (35)	6.02 (26)
	Range	5.25 – 7.58	5.6 – 6.56	4.4 – 5.6	4.06 – 6.81	5.29 - 6.81	4.99 – 7.89	4.99 - 7.8
M_1AW	*Mean*	4.43 (57)	4.47 (23)	4.23 (3)	3.99 (103)	4.21 (70)	4.50 (36)	4.54 (27)
	Range	3.85 – 4.96	3.98 – 4.9	4.2 – 4.3	2.88 – 4.93	3.71 - 4.93	3.73 – 6.64	3.73 - 6.6
M_1PW	*Mean*	4.52 (55)	4.65 (22)	4.37 (3)	4.20 (90)	4.36 (67)	4.50 (36)	4.36 (11)
	Range	4.03 – 5.37	4.05 – 4.97	4.2 – 4.6	3.25 – 5.05	3.8 - 5.05	3.75 – 5.21	3.75 - 4.8
P_4L	*Mean*	5.02 (41)	4.99 (17)	4.3 (3)	5.15 (111)	5.47 (78)	5.51 (27)	5.54 (26)
	Range	4.36 – 6.36	4.35 – 5.67	4.2 – 4.4	3.63 – 6.31	4.27 - 6.31	4.41 – 6.93	4.41 - 6.9
P_4W	*Mean*	3.71 (36)	3.8 (11)	3.53 (3)	3.41 (108)	3.58 (75)	3.76 (29)	3.75 (28)
	Range	3.23 – 4.63	3.55 – 4.18	3.5 – 3.6	2.11 – 4.13	3.04 - 4.13	3.07 – 5.56	3.07 - 5.5
P_3L	*Mean*	6.72 (29)	6.27 (13)	4.43 (3)	6.35 (9)	–	7.63 (15)	7.63 (15)
	Range	4.64 – 8.46	4.95 – 7.73	4.1 – 4.6	4.5 – 8.1	–	5.91 – 9.32	5.91 - 9.3
P_3W	*Mean*	3.72 (28)	3.52 (12)	2.97 (3)	2.7 (32)	–	3.91 (16)	3.95 (15)

	Range	2.83 – 4.91	3.01 – 3.87	2.7 – 3.2	1.65 - 4.21	–	2.77 – 4.7	2.77 - 4.7
P_3FL	*Mean*	6.65 (32)	6.33 (14)	–	–	–	–	–
	Range	5.37	4.95 – 8.69	–	–	–	–	–
CL	*Mean*	4.10 (9)	3.65 (9)	–	2.89 (23)	–	3.97 (1)	–
	Range	3.12 – 5.3	2.88 – 4.27	–	2.05 – 3.99	–	–	–
CW	*Mean*	6.37 (14)	5.48 (8)	4.3 (1)	4.49 (23)	–	6.97 (1)	–
	Range	4.50 – 7.33	4.25 – 6.51	–	2.69 – 6.27	–	–	–
I_2L	*Mean*	3.24 (8)	3.33 (4)	–	2.74 (10)	–	2.27 (1)	–
	Range	2.84 – 3.75	3.18 – 3.66	–	1.79 – 3.46	–	–	–
I_2W	*Mean*	4.03 (6)	3.94 (3)	3.5 (1)	3.68 (22)	–	–	–
	Range	3.48 – 4.81	3.32 – 4.57	–	3.04 – 5.11	–	–	–
I_1L	*Mean*	3.38 (14)	3.39 (7)	2.7 (1)	3.10 (10)	–	–	–
	Range	2.82 – 3.79	3.09 – 3.67	–	2.63 – 3.73	–	–	–
I_1W	*Mean*	4.23 (6)	4.06 (2)	3.7 (1)	3.72 (22)	–	3.81 (1)	–
	Range	3.75 – 4.9	3.55 – 4.56	–	3.01 – 4.27	–	–	–

Means are reported in millimeters. Sample sizes are in parentheses adjacent to the mean for each measurement. Abbreviations: L = mesiodistal length of the crown; W = buccolingual width of the crown; AW = buccolingual width across the anterior (mesial) loph of the crown; PW = buccolingual width across the posterior (distal) loph of the crown; FL = mesiodistal length of the crown, taken in lateral view and including the mesial extension of the flange on the buccal side. *Ch.* indicates *Chlorocebus* and *C.* indicates *Cercopithecus.* Extant comparative species were chosen due to their large sample size.

Table 5. Descriptive statistics for cranial measurements of Faro Daba and Chai Baro cf. *Chlorocebus* fossils. Means and ranges are reported in millimeters. Range is presented as minimum measurement – maximum measurement. *Ch.* indicates *Chlorocebus* and *C.* indicates *Cercopithecus.* Extant comparative species were chosen due to their large sample size.

Measurement		Faro Daba cf. *Chlorocebus*	Chai Baro cf. *Chlorocebus*	*Cercopithecus* spp.	*C. mitis*	*Chlorocebus* spp.	*Ch. aethiops*
Orbital width	Mean	22.83 (1)	19.38 (1)	21.36 (117)	21.66 (38)	21.65 (41)	21.74 (16)
	Range	–	–	17 – 25.4	18.9 – 24.48	19.7 – 24.51	19.7 – 24.51
Orbital height	Mean	18.54 (1)	20.41 (1)	21.76 (117)	21.66 (38)	20.24 (41)	21.74 (16)

	Range	–	–	18.1 – 25.65	19.94 – 25.65	17.67 – 23	17.37 – 21.92
Interorbital breadth	Mean	5.25 (5)	5.69 (3)	6.59 (39)	6.87 (29)	5.93 (15)	5.93 (15)
	Range	4.5 - 5.53	5.12 - 6.71	4.77 – 8.3	5.04 – 8.3	4.21 – 8.07	4.21 – 8.07
Nasal width	Mean	8.55 (4)	7.81 (1)	9.67 (39)	9.79 (29)	9.55 (15)	9.55 (15)
	Range	7.71 – 9.26	–	7.16 – 13.19	7.16 – 13.19	7.8 – 12.97	7.8 – 12.97
Nasal height	Mean	–	13.53 (1)	18.21 (39)	18.87 (29)	16.58 (15)	16.58 (15)
	Range	–	–	11.39 – 24.88	15.04 – 22.01	13.83 – 19.59	13.83 – 19.59
Muzzle width (at ectomolare)[a]	Mean	33.71 (1)	29.3 (1)	33.14 (34)	33.66 (28)	33.75 (15)	33.75 (15)
	Range	–		28.9 –37.72	30.54 – 37.72	27.98 – 40.01	27.98 – 40.01
Muzzle width (at max. fossae)	Mean	–	18.11 (1)	24.57 (39)	24.56 (19)	26.33 (15)	26.33 (15)
	Range	–	–	18.92 – 30.4	18.92 – 30.4	21.44 – 31.33	21.44 – 31.33
Maximum width (at C^1)	Mean	–	19.89 (1)	25.90 (38)	26.23 (28)	25.96 (15)	25.96 (15)
	Range	–	–	22.4 – 32.65	22.56 – 32.65	21 – 31.28	21 – 31.28
Palatal width (at M^3)	Mean	–	12.11 (1)	16.83 (39)	16.84 (29)	16.35 (14)	16.35 (14)
	Range	–	–	13.98 – 19.99	13.99 – 19.99	13.51 - 19.2	13.51 - 19.2
Palatal width (at C^1)	Mean	16.6 (1)	–	14.88 (38)	14.83 (29)	15.08 (15)	15.08 (15)
	Range	–	–	11.53 – 19.37	11.53 – 19.37	11.71 – 18.61	11.71 – 18.61
Palatal length	Mean	–	26.03 (1)	33.02 (39)	33.80 (29)	33.64 (15)	33.64 (15)
	Range	–	–	25.28 – 41.96	28.81 – 41.96	24.9 – 41.62	24.9 – 41.62
Facial Length	Mean	–	39.63 (2)	44.32 (117)	49.49 (38)	40.88 (40)	43.72 (15)
	Range	–	37.8 – 41.4	30.1 – 61.97	38.2 – 61.97	29.7 – 54.07	34.73 – 54.07

Note: Measurement definitions are reported in Monson et al. (2017).
Abbreviations: *n*, sample size; C^1, maxillary canine; M^3, maxillary third molar.
[a]Maximum width of the muzzle, measured at the superior border of the maxillary fossae.

Table 6. Descriptive statistics for mandibular measurements of Faro Daba (FD) and Chai Baro (CB) cf. *Chlorocebus* fossils. Means and ranges are reported in millimeters. Range is presented as minimum measurement – maximum measurement.

Measurement		Faro Daba cf. *Chlorocebus*	Chai Baro cf. *Chlorocebus*	*Cercopithecus* spp.	*Chlorocebus* spp.	Asbole *Chlorocebus* aff. *aethiops*
Mandibular corpus height at M1	Mean	15.6 (15)	16.4 (1)	14.81 (84)	15.07 (32)	14.65 (2)
	Range	11.9 – 19.2	–	9.7 – 21.72	10.9 – 20.4	14.28 – 15.02
Mandibular corpus height at M2	Mean	14.34 (14)	–	15.84 (7)	15.28 (6)	13.69 (2)
	Range	11.7 –16.7	–	11.94 – 20.63	13.2 – 16.66	12.95 – 14.43
Mandibular corpus height at M3	Mean	14.69 (8)	14.6 (1)	14.59 (84)	14.57 (32)	13.93 (3)
	Range	11.9 – 17.1	–	9.4 – 20.52	10.6 – 19.3	13.46 – 14.24

Abbreviations: M_1, mandibular first molar; M_2, mandibular second molar; M_3, mandibular third molar. Species are grouped into genera due to small sample sizes.

Table 7. Results of Kruskal-Wallis non-parametric statistical analyses. P values are presented and bolded when the result is statistically significant ($p<0.05$).

	Cercopithecus vs. *Chlorocebus*	Faro Daba vs. Chai Baro	Faro Daba vs. *Cercopithecus*	Faro Daba vs. *Chlorocebus*	Chai Baro vs. *Cercopithecus*	Chai Baro vs. *Chlorocebus*
Relative I1 size	**0.001**	>0.05	**0.006**	>0.05	>0.05	>0.05
Relative I2 size	**<0.001**	>0.05	**<0.001**	**0.01**	>0.05	>0.05
Orbital Shape	**<0.001**	-	-	-	-	-
Facial Length	**0.006**	>0.05	>0.05	>0.05	>0.05	>0.05

Table 8. Descriptive statistics for postcranial metrics of Faro Daba (FD) and Chai Baro (CB) cf. *Chlorocebus* fossils. Means and ranges are reported in millimeters, except those indicated by [2] or [3]. Range is presented as minimum measurement – maximum measurement.

Measurement		Faro Daba cf. *Chlorocebus*	Chai Baro cf. *Chlorocebus*
Humeral maximum length	*Mean*	–	104.56 (1)
	Range	–	–
Humeral head diameter	*Mean*	13.07 (9)	11.92 (1)
	Range	11.76 – 14.61	–
Humeral epicondyle angle[2]	*Mean*	47.09 (11)	42.13 (7)
	Range	35.85 – 59.28	35.48 – 47.81
Humeral epicondyle ratio[1,3]	*Mean*	16.26 (11)	14.41 (8)
	Range	11.9 – 19.43	8.37 – 19.38
Humeral relative flange length[1,3]	*Mean*	72.75 (11)	71.83 (8)
	Range	62.47 – 82.1	68.17 – 79.69
Ulnar maximum length	*Mean*	138.48 (2)	–
	Range	138.38 – 138.57	–

Femoral maximum length	*Mean*	154.56 (1)	–
	Range	–	–
Femoral head diameter	*Mean*	11.83 (18)	11.52 (7)
	Range	10.97 – 13.83	10.97 – 12.87
Femoral neck-shaft angle[2]	*Mean*	118.85 (18)	14.58 (7)
	Range	107.4 – 138.76	104.68 – 122.63
Femoral relative greater trochanter projection[1, 3]	*Mean*	44.67 (17)	48.67 (6)
	Range	30.11 – 51.65	40.02 – 59.5

Note: Additional postcranial measurements and measurement definitions are provided in the dataset associated with this manuscript ([*reference online location in data repository here*]). Sample sizes are in parentheses adjacent to the mean for each measurement.
[1]See Figure 16 for comparison with extant samples.
[2]These measurements are angles – means and ranges are reported in degrees.
[3]These measurements are indices – see Figure 16 for calculations.

Table 9. Sex breakdown of fossils from Faro Daba and Chai Baro.

Sex	**Faro Daba cf. *Chlorocebus* Number of individuals (frequency)**	**Chai Baro cf. *Chlorocebus* Number of individuals (frequency)**
F	25 (21%)	12 (21%)
M	36 (28%)	13 (23%)
Uncertain	64 (51%)	32 (56%)
Total	125	57

Table 10. Age category breakdown from Faro Daba and Chai Baro.

Age Score/Category	Faro Daba cf. *Chlorocebus* Number of individuals	Chai Baro cf. *Chlorocebus* Number of individuals
1	4	1
2	8	3
3	3	3
4	43	9
5	39	25
6	17	9
Total	114	50

Appendices

Appendix 1. Inventory of specimens from Faro Daba referred to cf. *Chlorocebus*

Specimen ID	Sex	Element(s)
HAL-VP-2/23	U	R. UM3
HAL-VP-2/24	M	(A) L. MAN (C-M1); (B) CRA + PES frags. (MTC 2) (>1 MNI)
HAL-VP-2/31 *	–	R. RAD (prox. shaft)
HAL-VP-2/44 *	–	L. TIB (dist.); R. FIB (prox.); 2 shaft frags.
HAL-VP-2/58 *	–	L. FEM (prox.)
HAL-VP-2/67	F	R. + L. MAN (L. I1-M2, R. I1-I2, R. P3-M3); OCX; FEM
HAL-VP-2/86	–	OCX (partial); shaft frags.; L. ULN (prox.)
HAL-VP-2/134	U	L. MAN (M1-M3)
HAL-VP-2/135	M	R. + L. MAN (R. I1-M3; L. I1, P3-M1)
HAL-VP-2/136	U	R. MAN (M1-M2 frag.)
HAL-VP-2/146 *	–	Partial skull (no dental material); R. FEM (prox.); L. FEM (partial prox.); R. + L. FEM (dist.); TIB (dist.); R. CAL with partial TAL attached; OCX frag.; TIB (prox.); 3 VER; RIB frags.; several long bone and other associated frags.
HAL-VP-2/147	F	MAN w/ symph. (L. P4-M2, partial R. C, R. P3, and roots of L. I2-P3 and R. P4-M1); R. + L. HUM (dist.); L. ULN (prox.); R. HUM (prox.); 4 VER; misc. frags.
HAL-VP-2/155	M	R. MAN (P3); L. MAN (edent.); L. LC; L. UM3; R. + L. TAL; R. TIB (dist.)
HAL-VP-2/195	–	2 M's; I
HAL-VP-3/12	U	R. MAN (M1-M2)
HAL-VP-3/65	U	L. MAN (dC-M1)
HAL-VP-3/100	U	R. MAN (M2-M3)
HAL-VP-3/133	U	R. MAX (P3-M2)
HAL-VP-3/183	–	L. FEM (prox.)
HAL-VP-3/186	–	LM
HAL-VP-3/189	U	L. MAN (M2-M3)
HAL-VP-3/228	M	R. + L. MAN (R. I1 root, L. I1-P3); L. MAN frag. (M3 root)
HAL-VP-3/250 *	–	L. HUM (dist.)
HAL-VP-9/13	M	MAX (R. + L. P3-M3); R. MAN (C-M1); M3s erupting; CRA frags.; MAN frags. (incl. condyle)
HAL-VP-9/216 *	–	FRO

HAL-VP-9/220 *	–	R. MAN (edent.)
HAL-VP-9/222	–	R. UM
HAL-VP-9/247	U	L. MAN (M1-M3)
HAL-VP-9/253	F	L. MAX (C-M1)
HAL-VP-9/259	U	L. MAN (M3)
HAL-VP-9/263 *	–	L. HUM (dist.); R. HUM (prox.); R. SCA (w/ glenoid fossa)
HAL-VP-9/291	F	R. + L. MAN (L. partial P3-M2, L. M3, R. partial P3-M3)
HAL-VP-9/300	U	L. MAN (P4)
HAL-VP-9/302	M	L. MAX (P4-M1)
HAL-VP-9/308	U	R. MAN (dM2-M1)
HAL-VP-9/313	U	MAN (R. dM1-M2; R. + L. I1-I2, L. P4-M2)
HAL-VP-9/320 *	–	FEM (dist.)
HAL-VP-9/321	–	R. UM1 or 2
HAL-VP-9/322	F	L. MAX (P3-M3); ZYG
HAL-VP-9/329 *	–	L. TIB (prox.); L. HUM (dist.)
HAL-VP-9/330	U	MAX (R. + L. P3-M2)
HAL-VP-9/333	F	R. MAN (P3-M3)
HAL-VP-9/334	–	L. FEM (prox.)
HAL-VP-9/335	F	L. MAX (I1-I2, P3-M3)
HAL-VP-9/336	U	R. MAX (M3)
HAL-VP-9/337	M	R. MAX (C-M1)
HAL-VP-9/343	F	MAN (L. I1-M1; R. I1-M3)
HAL-VP-9/345	U	R. MAN (M2-M3)
HAL-VP-9/346 *	–	R. HUM (prox.)
HAL-VP-9/351	M	L. MAN (I2-C, P4-M2)
HAL-VP-9/356	U	L. MAN (P4-M3); R. MAN (P4-M3)
HAL-VP-9/366	M	R. MAX (I1, partial I2-P4, M1, partial M2, M3)
HAL-VP-9/380 *	–	L. MAN (dM1-dM2)
HAL-VP-9/385	U	R. MAX w/ ZYG (dM1-dM2, M1-M2); L. TEM frag.; TIB (prox., imm.); CRA and long bone frags.
HAL-VP-9/393	U	L. MAN (M2-M3)

HAL-VP-9/397	U	R. MAN (M2-M3)
HAL-VP-9/416	–	R. HUM (dist.); ULN; RAD (prox.); misc. frags.
HAL-VP-9/432	M	R. MAN (C-M3)
HAL-VP-9/433	F	L. MAN (M1)
HAL-VP-9/439	F	MAN (R. I1-I2, M1-M3; L. P3-M3); L. UM3
HAL-VP-9/442	–	R. FEM (prox.)
HAL-VP-9/445	U	L. MAN (M1, M3)
HAL-VP-9/446	F	L. MAX (C, P4-M3); MAN (R. I1, P4-M3; L. C-M3)
HAL-VP-9/450	F	R. MAX (edent.)
HAL-VP-9/470	U	R. MAN (partial M1-M2); L. MAN (partial M1 and M3)
HAL-VP-9/477	–	R. FEM (prox.)
HAL-VP-9/478 *	–	L. TIB (dist.)
HAL-VP-9/486	U	FRO w/ NAS; 2 R. MAX frags. (partial I1-M3); CRA frags.
HAL-VP-9/487	U	L. MAX (P3-M2)
HAL-VP-9/498	M	MAN symph. (incisor and R. C and R. P roots); R. MAN (M1-M3); L. MAN (M2); R. MAX (P3-M3); L. MAX (partial M1-M2); L. MAX (partial C and P3); R. MAX (I1-I2); palate frag.; L. HUM (dist.)
HAL-VP-9/501	U	R. + L. MAN (dM1-dM2); isolated L. LM1; isolated R. + L. LdC; isolated R. LdI2
HAL-VP-9/507	M	MAN (L. P3, R. M2)
HAL-VP-9/508	–	R. HUM (dist. w/ shaft); R. TIB (prox. w/ shaft, shaft frag.); L. FIB (prox.); VER frag.; misc. frag.
HAL-VP-9/511 *	–	R. ULN (prox.)
HAL-VP-9/512	U	R. MAN (M1-M3); L. MAN (P3-M3 roots); MAX (L. I1, M1; R. I1, P3-M1)
HAL-VP-9/516	M	MAN (R. P3-M3; L. P4); L. HUM (dist.)
HAL-VP-9/523	U	R. MAN (M1-M3)
HAL-VP-9/528	M	MAN (R. P3-M3; L. C-P3, M1-M3)
HAL-VP-9/532	U	L. MAN (M2-M3)
HAL-VP-9/535	U	L. MAN (dM2, M1)
HAL-VP-9/545	–	L. FEM (prox.)
HAL-VP-9/562 *	–	R. MAN (P3)
HAL-VP-9/566	U	L. MAN (P4-M3)

HAL-VP-9/567 *	–	R. TIB (dist. and prox.)
HAL-VP-9/572	F	MAX (L. I1-M3; R. I1-I2, M2-M3); isolated L. LP3-M2; isolated L. + R. LI1-I2; isolated R. LP3; MAN frag. (R. M1); MAN frag. (R. M2-M3); FRO frag.; L. ZYG; MAN (condyle); 2 pelvis frags.; 6 tooth frags.; misc. frags.
HAL-VP-9/575	–	R. HUM (prox.)
HAL-VP-9/581	F	R. MAX (C-P4, partial M1, M2); L. MAX (M2-M3)
HAL-VP-9/587	–	L. LI2; R. LM1 or 2; R. + L. FEM (dist.); R. FEM (prox.); FEM (shaft frag.); TIB (prox.); TIB (shaft frag.); VER frag.; MTP frag,; misc. frags.
HAL-VP-9/588	F	Isolated R. + L. UM1-M3; isolated R. UI2-P3; isolated L. LP4; R. HUM (dist. w/ shaft); R. SCA frag. (w/ glenoid); L. HUM (prox.); HUM shaft frag.; R. RAD (prox.); multiple MTP frags.; misc. frags.
HAL-VP-9/591	–	R. HUM (dist.); R. ULN (prox.)
HAL-VP-9/596	–	R. OCX frag.; 2 OCX frags. (side indet.); FEM (dist.); L. FEM (prox.); L. TIB (prox.); L. TIB (dist.); multiple partial VER; long bone frags.
HAL-VP-9/599	–	L. dUM2
HAL-VP-9/600	M	L. UC; R. LC; L. UM2; L. UP4; R. LP4; L. ZYG frag.; L. ULN (prox.); RAD (prox.); R. SCA frag.; MTC; 2 partial MTC (dist.); R. + L. FEM (prox.); FEM (dist.); R. OCX frag.; R. + L. TIB (prox.); L. TIB (dist.); L. FIB (prox.); R. + L. FIB (dist.); L. TAL; TAR; partial SAC; 3 partial VER; RIB frag.; long bone frags.
HAL-VP-9/616 *	–	FEM (dist.)
HAL-VP-9/619 *	–	L. MAN (M1 or M2 erupting); isolated mesial portion of L. LdM2
HAL-VP-9/631	U	M3
HAL-VP-9/634	M	R. + L. MAN (R. P4-M2, R. I1-P3 roots, R. M3 roots; L. I1-M1 roots, partial L. M2, L. M3 roots); R. MAX (I2 root, C-M3); L. MAX (P4-M3)
HAL-VP-9/638	M	L. MAX (C-M3)
HAL-VP-9/641 *	–	L. ULN (prox.)
HAL-VP-9/650	M	MAX (L. I1-R. M3); L. MAX (I2-M3); palate; R. FRO; R. + L. TEM; R. + L. ZYG; NAS; SPH; OCC; MAN w/ symph. (L. I1-M3; R. I1-I2, partial R. C, R. P3-M1 (VER cemented to occlusal surface)); R. + L. SCA frags.; R. + L. HUM; R. CLA; CER (2 and

		3); 11 THO and LUM; 4 VER (caud.); RIB frags.; R. + L. ULN; R. + L. RAD; R. MTC2; R. + L. OCX; R. + L. FEM; R. + L. TIB; R. FIB (dist.); R. CUB; R. CAL; L. TAL; R. MTT 3 and 4; 1 dist. PHX; 1 prox. PHX; 2 int. PHX; partial L. hand with prox. MTCs 1-5 and several carpals cemented together; R. scaphoid, LUN, TZM; STE
HAL-VP-9/652	U	L. MAN (M1 and M2 erupting)
HAL-VP-9/658 *	–	R. + L. TIB (prox.); L. TIB (dist.); FEM (dist.); 2 VER (caud.), 2 VER frags. (caud.); ULN (shaft frag.); long bone frags.; misc. frags.
HAL-VP-9/661	–	L. HUM (prox.); L. ULN (prox.); L. HUM (dist.); L. SCA (glenoid); RAD shaft
HAL-VP-9/663 *	–	R. RAD (prox.)
HAL-VP-9/664 *	–	R. + L. OCX; nearly complete TIB w/ TAL cemented to it; 18 VER frags.; 3 MTP; L. CAL; R. + L. FEM (prox. w/ shaft); misc. frags
HAL-VP-9/670	M	MAN (L. C, M1-M2; R. C-M1)
HAL-VP-9/678	U	MAN (R. M2-M3; L. P3-M3)
HAL-VP-9/680 *	–	L. TIB (dist.)
HAL-VP-9/688	U	MAN (L. P4); L. UM1 or 2
HAL-VP-9/697	–	R. HUM (prox.)
HAL-VP-9/700	U	L. MAX (dM1-M1)
HAL-VP-9/709	–	MAN (R. M1-M2)
HAL-VP-9/716	U	MAN (R. I1-M2, dM1; L. I1-I2, partial P3; P4-M2)
HAL-VP-9/717	U	L. MAN (M1-M2)
HAL-VP-9/734	M	L. MAN (M1-M3); R. LP3; R. + L. UC; L. UP4; L. UM1-M3; R. UM1; M1 frag.; I frags.; tooth frags.; R. + L. TIB; R. FEM; L. FEM (prox. w/ shaft); R. + L. HUM (prox., epiphyses unfused); R. + L. HUM (dist.); R. + L. ULN (prox., one with shaft and distal end); TAL; CAL; 2 podials; R. + L. FIB (dist.); R. + L. RAD frags.; PAT; 4 pelvic frags.; RIB frags.; CRA frags.; shaft frags.; misc. frags.
HAL-VP-9/738 *	–	L. TIB (prox.)
HAL-VP-9/740	–	L. FEM (prox.)
HAL-VP-9/742	M	L. MAX (P4-M2)
HAL-VP-9/748	–	L. LM3
HAL-VP-9/749	–	R. FEM (prox.)

HAL-VP-9/763	U	R. MAX (M1-M2)
HAL-VP-9/767	U	L. MAN (M2, M3 roots)
HAL-VP-9/773 *	–	R. MAN (M1)
HAL-VP-9/774	–	L. UM3
HAL-VP-9/798 *	–	L. MAN (L. dI1-dM2; R. dC-dM1); CRA frags. (imm.)
HAL-VP-9/813	–	R. HUM (dist.)
HAL-VP-9/828	M	MAN (R. I1-P4, M3; L. I1-P4, M2); R. MAX (I2)
HAL-VP-9/830	–	L. HUM (prox. w/ shaft)
HAL-VP-9/846	F	Nearly complete MAN (partial L. I1-C, P3 roots, partial P4-M1, M2-M3; partial R. I1-I2, C root, P3-M3); SAC frag.; 3 partial VER; 3 VER frags.; long bone and misc. frags.
HAL-VP-9/847	–	R. ULN (prox.)
HAL-VP-9/859	U	R. MAN w/ symph. (M1)
HAL-VP-9/862 *	–	MAN (edent.); R. OCX frag. (w/ acetabulum); 2 shaft frags.
HAL-VP-9/864	U	R. MAN (P4-M2, partial M3)
HAL-VP-9/865	F	R. MAX (I1-M3); L. MAX frag. (I1-I2); L. MAX frag. (P3-M3); MAN w/ symph. (L. P3-M3); R. MAN frag.; 3 TEM frags.; CRA frags.; R. + L. HUM (prox.); L. HUM (dist.); R. + L. ULN (prox.); R. ULN (dist.); R. RAD (dist.); carpals cemented together; FEM (head); TIB (prox.); PAT; L. TAL; RIB frags.; 5 partial VER; limb and misc. frags.
HAL-VP-9/868	M	R. MAN (P3)
HAL-VP-9/869	U	R. MAN (partial M2)
HAL-VP-9/872 *	–	R. MAN (edent.)
HAL-VP-9/873 *	–	R. FEM (prox.)
HAL-VP-9/874 *	–	MAN (L. dM1-M1)
HAL-VP-9/876	M	L. MAX (P4-M2); R. RAD (prox. and dist.); long bone frags.
HAL-VP-9/887	–	L. FEM (prox.)
HAL-VP-9/888	U	CRA frags. (FRO, PAR, MAX (L. P4-M2))
HAL-VP-9/898	U	L. MAN (M1-M3)
HAL-VP-9/934 *	–	L. MAX (M2)

HAL-VP-9/937 *	–	R. RAD (prox.)
HAL-VP-9/939 *	–	L. MAN (P4-M1)
HAL-VP-9/961	U	R. MAN (M1-M2)
HAL-VP-9/964	U	R. MAN (M1)
HAL-VP-9/991	U	L. MAN (M2-M3)
HAL-VP-9/996	F	L. MAN w/ symph. (R. P3; L. M2-M3); R. MAN (M1-M3); MAX (R. + L. I1); FRO w/ NAS; R. FEM (prox.); 3 OCX frags.; 2 limb bone shaft frags.
HAL-VP-9/1023	U	R. MAX (I1 erupting, dM1-M1)
HAL-VP-9/1026	F	L. MAX (M1-M3)
HAL-VP-9/1028	M	R. MAX (P3-M1); R. MAN (P3-M2)
HAL-VP-9/1031	M	L. MAN (P4-M3)
HAL-VP-9/1036 *	–	L. HUM (dist. shaft)
HAL-VP-9/1040	U	L. MAN (M2)
HAL-VP-9/1043	M	R. MAN (C); L. MAN (P3-P4)
HAL-VP-9/1049	F	R. MAN (P3-M3)
HAL-VP-9/1056	U	L. MAN (dM2)
HAL-VP-9/1058 *	–	R. + L. MAX (R. dM1-dM2, R. + L. I1 erupting)
HAL-VP-9/1059	U	R. MAN (P4-M3)
HAL-VP-9/1064 *	–	R. MAX (M1)
HAL-VP-9/1066	F	L. MAX (P3-M2)
HAL-VP-9/1069	M	MAN (L. M1-M3, partial R. P4, R. M1-M3)
HAL-VP-9/1079	F	R. MAX (P3-M2)
HAL-VP-9/1090 *	–	L. MAX (dM1-dM2)
HAL-VP-9/1103	U	R. MAX (P3-M2)
HAL-VP-9/1105	M	MAX (R. + L. I1-P3)
HAL-VP-9/1106	M	MAN (R. + L. P3-M3)
HAL-VP-9/1107 *	–	L. UI1
HAL-VP-9/1110	U	R. MAN (M1-M3); CRA frags.

HAL-VP-9/1111 *	–	L. FEM; L. TIB; pelvic frag.; 5 MTT; 2 TAR; misc. frags.
HAL-VP-9/1116	U	L. MAN (dM1-M1)
HAL-VP-9/1125	–	R. ULN (prox.)
HAL-VP-9/1137	U	Isolated L. LM1-M3; L.FEM (prox.); FEM (dist.); TIB (dist.); 2 partial VER; shaft frags.
HAL-VP-9/1142	U	L. MAN (M1-M3)
HAL-VP-9/1143	U	L. MAN (M1-M2); L. MAX (P4); L. UM2-3; R. MAN (edent.)
HAL-VP-9/1144	U	L. MAN (dM2); R. CAL; 2 VER (sacral); partial L. OCX; FEM (dist.); ULN shaft; HUM shaft; 10 VER frags.; 2 possible CRA frags.; limb bone frags.
HAL-VP-9/1148 *	–	L. MAX (M2)
HAL-VP-9/1151	–	R. HUM (prox.)
HAL-VP-9/1154	F	Partial MAN (L. P3-M1, R. P3-M3, partial R. C, L. I2-C roots); R. + L. partial OCX; L. HUM (prox.); MAN (condyle); R. + L. partial SCA; R. + L. FEM (dist.); L. TAL; R. HUM (dist.); R. + L. FEM (prox.); R. CAL; 17 partial VER; 3 shaft frags.; misc. frags.
HAL-VP-9/1166 *	–	FEM (dist.)
HAL-VP-9/1197 *	–	LI
HAL-VP-9/1198 *	–	R. UI2
HAL-VP-9/1200 *	–	L. UI1
HAL-VP-9/1201 *	–	L. LI2
HAL-VP-9/1381 *	–	L. CAL
HAL-VP-9/1396	U	L. MAN (M2)
HAL-VP-9/1440	F	MAN (L. P4-M1, L. I1-P3 roots; R. I1-P3)
HAL-VP-9/1443	U	L. MAX (P3-M1)
HAL-VP-9/1452	M	MAX (R. I1-M1; L. I1-M2); MAN (R. I1-M3; L. I1-C, P4-M3)
HAL-VP-9/1456	F	MAN (L. I1, P3-M2; R. P3-M2)
HAL-VP-9/1462	M	MAN (L. I1-2, P3-M3; R. I1, C-M2)
HAL-VP-9/1464	–	R. ULN
HAL-VP-9/1482	M	L. MAN (P3-P4); L. UM1-M2

HAL-VP-9/1484	U	R. MAX (P3-M2)
HAL-VP-9/1486	U	R. MAN (M2-M3)
HAL-VP-9/1487	M	R. MAN (P3-M3)
HAL-VP-9/1556 *	–	TIB (prox.)
HAL-VP-9/1563	–	L. FEM (prox.)
HAL-VP-9/1576	M	L. MAN (C-P4, partial M1, complete M2-M3); isolated R. LM2; L. MAX (partial C and P3)
HAL-VP-9/1582	–	Pelvis; R. + L. FEM (prox.); HUM (dist.); RAD (prox.); ULN (prox.); long bone frags.
HAL-VP-9/1583 *	U	Isolated LM; FEM (prox. end w/o unfused epiphysis); HUM (prox. end w/o unfused epiphysis); SCA frag.; TAL; misc. frags.
HAL-VP-9/1595 *	–	R. HUM (dist.)
HAL-VP-9/1608	–	L. MAX (M1, imm.)
HAL-VP-9/1609	–	L. HUM (dist.)
HAL-VP-9/1612 *	–	SCA (glenoid fossa)
HAL-VP-9/1613 *	–	RAD (dist.)
HAL-VP-9/1614 *	F	L. MAN (C root, partial P3, P4-M3); R. MAN (C root, partial P3, P4-M3); R. MAX (C root, P3-M3); L. MAX (partial C, P3-M3)
HAL-VP-9/1616	–	TIB (prox.); HUM (dist.)
HAL-VP-9/1617	F	R. + L. MAN (R. I1-C, P4, M2-M3; L. I1-M3); isolated R. M1
HAL-VP-9/1620 *	–	OCX
HAL-VP-9/1624 *	–	L. OCX frag.; FEM (dist.)
HAL-VP-9/1626 *	M	L. MAN (C, M1-M3)
HAL-VP-9/1627 *	U	L. MAN (M1-M2)
HAL-VP-9/1628 *	–	R. + L. OCX (partial); R. FEM (prox.); ULN (prox.)
HAL-VP-9/1630	–	FEM (prox.); ULN (prox.); TIB (prox.); TIB (dist.); RAD (dist.); SAC frag.; CAL; TAL
HAL-VP-9/1637 *	U	R. + L. HUM; R. + L. TAL; R. + L. ULN (prox.); TIB; L. FEM; long bone frags.; OCX frag; R. RAD and ULN (dist.) cemented together

HAL-VP-9/1641	U	L. MAN (M2-M3); R. MAN (M2)
HAL-VP-9/1647	–	L. UI
HAL-VP-9/1650	U	R. MAX (P3-P4)
HAL-VP-9/1651 *	M	L. MAN (C-P4)
HAL-VP-9/1652	–	R. ULN (prox.)

Note: see Supporting Information Table S2 for anatomical abbreviation key.
*Specific referral to cf. *Chlorocebus* rather than a more inclusive taxon is based on association with the broader assemblage and morphological congruence with more complete specimens.
Sex abbreviations: F, female; F?, probable female; M, male; M?, probable male; U, uncertain.

Appendix 2. Inventory of specimens from Chai Baro referred to cf. *Chlorocebus.*

Specimen ID	Sex	Element(s)
HAL-VP-5/8	–	R. FEM (dist.)
HAL-VP-5/10	–	R. MAN (P4); 2 VER; ULN (dist.)
HAL-VP-5/13 *	–	R. FEM (prox); R. TIB (prox); 3 VER frags.
HAL-VP-5/19 *	–	R. MAN (edent.)
HAL-VP-5/25	U	L. MAN (dM2-M1, M2 in crypt)
HAL-VP-5/26	M	R. + L. MAX (R. I1-2, R. P4-M3, L. I2, partial L. C, L. P3); MAN (L. I1, partial L. P3-P4, L. M1-M3, R. I2-M1, partial R. M2-M3)
HAL-VP-5/27	U	R. MAN (M2-M3)
HAL-VP-5/29	M	R. MAN (P3-M1)
HAL-VP-5/43	F	FRO w/ NAS; R. MAX (C-M3); L. MAN w/ symph. (R. I1-L. P3); 3 postcranial frags.
HAL-VP-5/63	M	L. MAX (P3-M3)
HAL-VP-5/75	U	R. MAN (M1-M3)
HAL-VP-5/77	M	R. + L. MAN (R. I1, P3, M1-M3; L. P4-M3)
HAL-VP-5/81	U	R. + L. MAN w/ symph. (L. I1-I2, P3-M2; R. I1-I2, P3-P4, M2-M3, partial R. LC and R. LM1); CRA vault frag.
HAL-VP-5/83	M	R. MAX (C-P3)
HAL-VP-5/99	U	R. MAN (M2-M3); L. MAN (P4-M3)
HAL-VP-5/101	U	L. MAN (edent.); R. FEM (prox. and dist. frags.)
HAL-VP-5/102	U	L. UdM1-dM2 and M1 (unerupted); HUM (prox., imm.)
HAL-VP-5/103	F	L. MAN (P3-M3)
HAL-VP-5/107	F	L. MAN (P3-M2)
HAL-VP-5/108	F	L. MAN (P3-M3)
HAL-VP-5/111	F	R. MAN (P3-M3); TIB (dist.)
HAL-VP-5/112 *	–	R. + L. MAN (R. P4)
HAL-VP-5/113	M	L. MAN w/ symph. (partial R. C, R. I1-L. I2, partial L. C, L. P3-M3); R. HUM (dist); 2 MTP frags.; 3 VER frags.; associated frags.
HAL-VP-5/116 *	–	TIB (prox.)
HAL-VP-5/121 *	–	L. UdC
HAL-VP-5/122 *	–	R. UdM1

HAL-VP-5/123 *	–	TIB (prox. epiphysis)
HAL-VP-5/131	U	L. MAX (P3-M2); R. MAX (partial C, P3-M2); R. MAN (P4-M2)
HAL-VP-5/132	M	L. MAX (partial L. C, P3-M2, M3 roots); MAN symph. (R. + L. partial C, L. P3-P4)
HAL-VP-5/134	U	R. LP4
HAL-VP-5/137	U	R. MAN (M1-M3)
HAL-VP-5/150	F	CRA (R. UC, R. UM1-M3 (M3 erupting); L. UI2, L. UP3-M3 (M1 is partial, M3 erupting))
HAL-VP-5/152 *	–	R. MAN (dM1-dM2)
HAL-VP-5/157	U	L. MAX (dI2-dM2, M1)
HAL-VP-5/158 *	–	R. + L. MAN (L. dM1-dM2; R. dM1)
HAL-VP-5/160	U	R. MAN (M1-M3)
HAL-VP-5/164	F	R. MAX (I1, C-M2)
HAL-VP-5/165	U	L. MAN (M1-M2); isolated C tip
HAL-VP-5/174 *	–	R. CAL
HAL-VP-5/176	M	R. + L. MAN (R. C; L. C-M1)
HAL-VP-5/182	U	L. MAN (M1-M3)
HAL-VP-5/192 *	–	L. FEM (prox., imm.)
HAL-VP-5/197	–	L. UC
HAL-VP-5/198 *	–	R. TIB (dist. w/ shaft); FEM (dist.); 2 shaft frags.
HAL-VP-5/199	U	L. MAN (M2-M3)
HAL-VP-5/202	F	MAN (L. I1, partial L. I2, L. P3-M2, R. I1-I2, partial R. C, R. P4-M2, M3's unerupted)
HAL-VP-5/204	U	L. MAN (M2-M3)
HAL-VP-5/207 *	M	MAN symph. frag. (L. I2, partial L. C and L. P3, partial R. C); L. HUM (dist. + shaft); ULN (prox., cemented to shaft of HUM)
HAL-VP-5/218	M	R. + L. MAN (R. C-P3; L. C)
HAL-VP-5/219	U	L. MAN (M1-M3)
HAL-VP-5/222	U	R. MAN (M2)
HAL-VP-5/234	M	R. + L. MAN (roots of R. C-M1, partial L. C, roots of L. P3-P4, roots of L. M3)
HAL-VP-5/241	–	R. FEM (prox.)

HAL-VP-5/248 *	–	R. ULN (prox.)
HAL-VP-5/249 *	–	R. ULN (prox., 2 frags.)
HAL-VP-5/252	–	L. FEM (prox.)
HAL-VP-5/254 *	–	FEM (dist.)
HAL-VP-5/259 *	–	L. CAL
HAL-VP-5/262 *	–	R. ULN (prox.)
HAL-VP-5/264	–	L. MAN (dM2, M2)
HAL-VP-5/285	–	L. ULN (prox.)
HAL-VP-5/286	–	L. LC
HAL-VP-5/287	–	R. HUM (dist.)
HAL-VP-5/288	–	L. FEM (prox.)
HAL-VP-5/290	–	R. + L. MAN (L. C)
HAL-VP-5/293	F	CRA (lacking posterior part of vault, w/ R. P3-M2, L. C-M3); CRA frags.
HAL-VP-5/296	U	R. LM2-M3; HUM (dist.)
HAL-VP-5/299	–	L. MAN (dM2-M1, M2 in crypt)
HAL-VP-5/300	–	R. HUM (dist.)
HAL-VP-5/306 *	–	R. TAL
HAL-VP-6/51	–	R. FEM (prox.)
HAL-VP-6/82 *	–	L. MAN (dM1-dM2); 2 small shaft frags.
HAL-VP-6/104	U	R. MAN w/ symph. (R. C-P3, M1-M3); L. MAN (M1-M3)
HAL-VP-6/105	–	RAD; R. HUM (dist. frags.)
HAL-VP-6/108	U	L. UM3
HAL-VP-6/112	–	L. HUM (dist.)
HAL-VP-6/120	U	Coprolite w/ FEM head and L. UP4-M1
HAL-VP-6/137 *	–	R. CAL
HAL-VP-6/138	U	R. MAX (M1-M3)
HAL-VP-6/140	U	L. MAN (I2-M1); R. MAN (C, P3, M1-M3); isolated R. LI1
HAL-VP-6/144	F	R. MAX (I1-M2)
HAL-VP-6/152	M	L. MAX (C-M2)

HAL-VP-6/231	–	FEM (prox.)
HAL-VP-6/236	–	R. FEM (prox. + shaft)
HAL-VP-6/238	F	L. MAN (M2)
HAL-VP-6/246	–	R. FEM (prox.)
HAL-VP-6/257	M	L. MAN (P3-M3); R. MAN (P4-M3)
HAL-VP-6/263	U	R. MAX (P4-M3)
HAL-VP-8/20	–	R. UM3
HAL-VP-8/24	–	L. FEM (prox.)
HAL-VP-8/56 *	–	L. OCX frag.; 1 misc. frag.
HAL-VP-8/74	U	R. MAX (M2-M3)
HAL-VP-8/100	M	L. MAX (partial P4 and M2; complete M1 and M3); R. MAN w/ partial symph. (partial L. I1 and R. I1-P3, complete R. P4, M1, and M3, partial R. M2)
HAL-VP-8/118	U	R. MAX (M1-M3)
HAL-VP-8/119	U	L. LM1 or 2
HAL-VP-8/124	U	L. MAN (M1)
HAL-VP-8/126	U	R. MAN (M1-M2)
HAL-VP-14/20	–	R. HUM (dist.)
HAL-VP-14/23	–	L. UM1 or 2
HAL-VP-17/5	–	R. HUM (prox.)
HAL-VP-22/16	F	R. MAN (I1-P3)
HAL-VP-22/30 *	–	TIB (prox.)
HAL-VP-22/53	U	R. MAN (P4-M3)
HAL-VP-22/64 *	–	R. TIB (prox.)
HAL-VP-22/73	U	R. MAN (M2-M3)

Note: see Supporting Information Table S1 for anatomical abbreviation key.
*Specific referral to cf. *Chlorocebus* rather than a more inclusive taxon is based on association with the broader assemblage and morphological congruence with more complete specimens.
Sex abbreviations: F, female; F?, probable female; M, male; M?, probable male; U, uncertain.

Appendix 3. Element inventory table for Faro Daba indeterminate Cercopithecidae.

Specimen ID	Element(s)
HAL-VP-2/5	R. HUM (dist. shaft)
HAL-VP-2/6	R. LC
HAL-VP-2/20	FEM (dist.) + shaft frags.
HAL-VP-2/21	FEM (dist. shaft); partial OCX; VER (may not be cercopithecid); shaft frags.
HAL-VP-2/30	Postcranial frags. (L. + R. OCX, dist. FEM); long bone shaft frags.
HAL-VP-2/39	TIB (prox. + shaft frag.)
HAL-VP-2/41	VER (caud.)
HAL-VP-2/46	L. OCX + FEM (head)
HAL-VP-2/71	VER (caud., frag.)
HAL-VP-2/80	R. TIB (shaft); L. partial ILI; 3 complete caud. VER; 4 partial caud. VER + 3 frags.
HAL-VP-2/82	TIB (prox.)
HAL-VP-2/90	R. FEM + OCX (imm.)
HAL-VP-2/99	FEM (shaft)
HAL-VP-2/101	VER (caud.)
HAL-VP-2/102	FEM frag. (shaft)
HAL-VP-2/106	L. HUM (dist. + shaft)
HAL-VP-2/114	FEM frag. (shaft)
HAL-VP-2/124	L. TAL
HAL-VP-2/125	R. UM
HAL-VP-2/139	VER (caud.); shaft frag.
HAL-VP-2/162	R. FIB (prox.)
HAL-VP-2/166	SAC (complete); R. + L. OCX frags.; 2 VER (cemented); 11 complete VER; 1 caudal VER; 5 VER frags.; RIB frags.
HAL-VP-2/168	R. LC
HAL-VP-2/171	L. TIB (dist. + shaft)
HAL-VP-2/192	R. MAX (R. UI1 and R. UC roots)
HAL-VP-2/194	R. MAN frag. (edent., imm.)
HAL-VP-2/197	MC; PHX
HAL-VP-2/198	HUM (dist. + shaft)
HAL-VP-2/199	RAD (prox.)
HAL-VP-2/200	FEM + OCX
HAL-VP-3/18	TIB (prox.)

HAL-VP-3/29	SAC frag.; R. ULN (prox.); L. TAL; 3 partial VER; small frag.
HAL-VP-3/52	R. TIB (dist.)
HAL-VP-3/69	L. HUM (dist.)
HAL-VP-3/81	R. UI1
HAL-VP-3/84	L. HUM (prox.)
HAL-VP-3/101	L. FEM (prox.)
HAL-VP-3/143	TIB (dist.)
HAL-VP-3/148	R. HUM (dist.)
HAL-VP-3/157	R. MAN (C-M2 roots)
HAL-VP-3/175	L. HUM (dist.)
HAL-VP-3/177	L. TIB (dist.)
HAL-VP-3/244	L. LdM1
HAL-VP-3/248	R. HUM (prox.)
HAL-VP-9/217	R. TEM
HAL-VP-9/218	R. FEM (prox.)
HAL-VP-9/219	L. MAN (edent.)
HAL-VP-9/223	R. LC
HAL-VP-9/224	L. UC frag.
HAL-VP-9/261	R. MAN (C)
HAL-VP-9/278	L. LdM1
HAL-VP-9/286	L. TIB (dist.)
HAL-VP-9/318	R. + L. OCX
HAL-VP-9/326	L. LC
HAL-VP-9/339	R. FRO
HAL-VP-9/341	L. OCX (2 frags.); TIB (prox. frags.)
HAL-VP-9/344	L. HUM (dist.)
HAL-VP-9/347	FEM (dist.)
HAL-VP-9/349	L. OCX (2 frags.)
HAL-VP-9/387	L. SCA (glenoid)
HAL-VP-9/389	R. + L. OCX; FEM (dist.)
HAL-VP-9/398	R. CAL
HAL-VP-9/399	TIB (prox.)
HAL-VP-9/402	PHX (dist. w/ shaft)
HAL-VP-9/415	L. CAL frag.
HAL-VP-9/418	R. FEM (prox.); partial VER (caud.); 3 long bone frags.

HAL-VP-9/436	R. SCA frag. (w/ glenoid)
HAL-VP-9/452	R. HUM (dist.)
HAL-VP-9/456	R. LC
HAL-VP-9/473	L. CAL
HAL-VP-9/529	L. UC
HAL-VP-9/542	R. OCX frag.; L. FEM (prox.); shaft frags. (incl. ULN frag. that appears too large for this individual)
HAL-VP-9/544	MAN symph. frag; R. SCA (w/ glenoid); R. RAD (prox.); misc. frags.
HAL-VP-9/615	TIB (prox.); FEM (dist.)
HAL-VP-9/626	PHX (prox.)
HAL-VP-9/629	L. TIB (dist.)
HAL-VP-9/633	R. HUM (dist.)
HAL-VP-9/648	R. TAL
HAL-VP-9/760	Partial SAC
HAL-VP-9/776	L. TIB (dist.)
HAL-VP-9/787	2 int. PHX
HAL-VP-9/792	R. CAL; partial L. TAL; R. + L. ULN (prox. frags.); 6 VER frags.; MTP (prox.); 3 podials; misc. frags.
HAL-VP-9/800	L. TIB (prox. and dist.); OCX frag. (ischium); 2 shaft frags.
HAL-VP-9/802	Partial SAC; partial R. + L. OCX; LUN; VER frags.; long bone frags.; misc. frags.
HAL-VP-9/821	R. TIB (prox.)
HAL-VP-9/851	R. TIB (prox.)
HAL-VP-9/852	R. TIB (dist.)
HAL-VP-9/853	L. FEM (prox.)
HAL-VP-9/860	R. TIB (prox. and dist.); MTP
HAL-VP-9/861	TIB (prox.)
HAL-VP-9/885	4 partial VER; 2 VER frags.
HAL-VP-9/890	R. HUM (dist.)
HAL-VP-9/911	R. TIB (dist.)
HAL-VP-9/916	L. CAL
HAL-VP-9/945	R. FEM (prox.)
HAL-VP-9/962	L. HUM (dist.)
HAL-VP-9/976	R. UC
HAL-VP-9/981	L. HUM (dist.)
HAL-VP-9/982	R. HUM (dist. and shaft frags.)

HAL-VP-9/993	R. RAD (prox.)
HAL-VP-9/1009	R. TIB
HAL-VP-9/1010	L. CAL
HAL-VP-9/1011	R. CAL
HAL-VP-9/1067	L. UC
HAL-VP-9/1072	L. FEM (prox.)
HAL-VP-9/1132	L. TIB (dist., shaft frag.)
HAL-VP-9/1160	L. TIB
HAL-VP-9/1162	R. UC
HAL-VP-9/1199	UM3 germ
HAL-VP-9/1379	L. UC
HAL-VP-9/1405	R. CAL; shaft frag.
HAL-VP-9/1429	L. FEM (prox.)
HAL-VP-9/1483	R. MAX (I1-C roots, broken C tip)
HAL-VP-9/1521	R. UC
HAL-VP-9/1532	HUM (dist.)
HAL-VP-9/1588	R. HUM (dist.)
HAL-VP-9/1599	MAN (condyle)
HAL-VP-9/1600	L. HUM (dist.)
HAL-VP-9/1603	MTP (dist.)
HAL-VP-9/1606	PHX (dist.)
HAL-VP-9/1621	FEM (prox.)
HAL-VP-9/1645	R. LdM2
HAL-VP-9/1648	R. LC
HAL-VP-9/1649	L. LdC

Note: Individuals assigned to indeterminate Cercopithecidae did not preserve enough morphology to be assigned to a more specific taxon. Sex is uncertain for all individuals.

Appendix 4. Element inventory table for Chai Baro indeterminate Cercopithecidae.

Specimen ID	Element(s)
HAL-VP-5/21	R. HUM (dist. 3/4)
HAL-VP-5/89	PHX (dist. + shaft)
HAL-VP-5/93	L. OCC
HAL-VP-5/106	FEM (dist.)
HAL-VP-5/115	MTP (prox.)
HAL-VP-5/148	L. HUM
HAL-VP-5/153	R. OCX
HAL-VP-5/185	R. LC
HAL-VP-5/245	MTPs (cemented)
HAL-VP-5/304	L. HUM (dist.); L. ULN (prox.)
HAL-VP-5/307	L. FEM (prox.)
HAL-VP-6/145	SAC frag.
HAL-VP-8/50	L. ULN (prox.)
HAL-VP-8/102	MAN symph. (partial L. I1-C)
HAL-VP-8/117	VER (caud.)
HAL-VP-14/45	L. UI2
HAL-VP-17/3	L. HUM (dist.)
HAL-VP-22/55	HUM

Note: Individuals assigned to Cercopithecidae did not preserve enough morphology to be assigned to a more specific taxon. Sex is uncertain for all individuals.

Appendix 5. Element inventory table for cf. Cercopithecidae (all from Faro Daba).

Specimen ID	Element(s)
HAL-VP-9/408	RAD (prox.)
HAL-VP-9/476	R. TIB (prox., imm.)
HAL-VP-9/771	R. HUM (prox.)
HAL-VP-9/1041	R. ULN (dist.)

Note: Individuals in this category are too fragmentary to be confidently assigned to Cercopithecidae. Sex is uncertain for all individuals.

Supplementary materials

Table S1 Anatomical abbreviations used in specimen inventory

Elements	
CRA	Cranium
FRO	Frontal
MAX	Maxilla
ZYG	Zygomatic
TEM	Temporal
OCC	Occipital
NAS	Nasal
MAN	Mandible
I1 – I2	First – second incisor
C	Canine
P3 – P4	Third – fourth premolar
M1 – M3	First – third molar
dI1 – dI2	Deciduous first – second incisor
dC	Deciduous canine
dM1 – dM2	Deciduous first – second molar
CER	Cervical vertebra
THO	Thoracic vertebra
LUM	Lumbar vertebra
VER	Vertebra
SAC	Sacrum
OCX	Os coxae
STE	Sternum
RIB	Rib
SCA	Scapula
CLA	Clavicle
HUM	Humerus
ULN	Ulna
RAD	Radius
FEM	Femur
PAT	Patella
TIB	Tibia
FIB	Fibula

CAR	Carpal
LUN	Lunate
CAP	Capitate
MTP	Metapodial
MTC	Metacarpal
MTC1 to 5	Metacarpal 1 to 5
PHX	Phalanx
CAL	Calcaneus
TAL	Talus
NAV	Navicular
CUB	Cuboid
MTT	Metatarsal
MTT1 to 5	Metatarsal 1 to 5
SES	Sesamoid
Descriptive terms	
Caud.	Caudal
Dist.	Distal
Edent.	Edentulous
Frag.	Fragment
Frags.	Fragments
Imm.	Immature
L.	Left
L	Lower
Misc.	Miscellaneous
Prox.	Proximal
R.	Right
Symph.	Symphysis
U	Upper

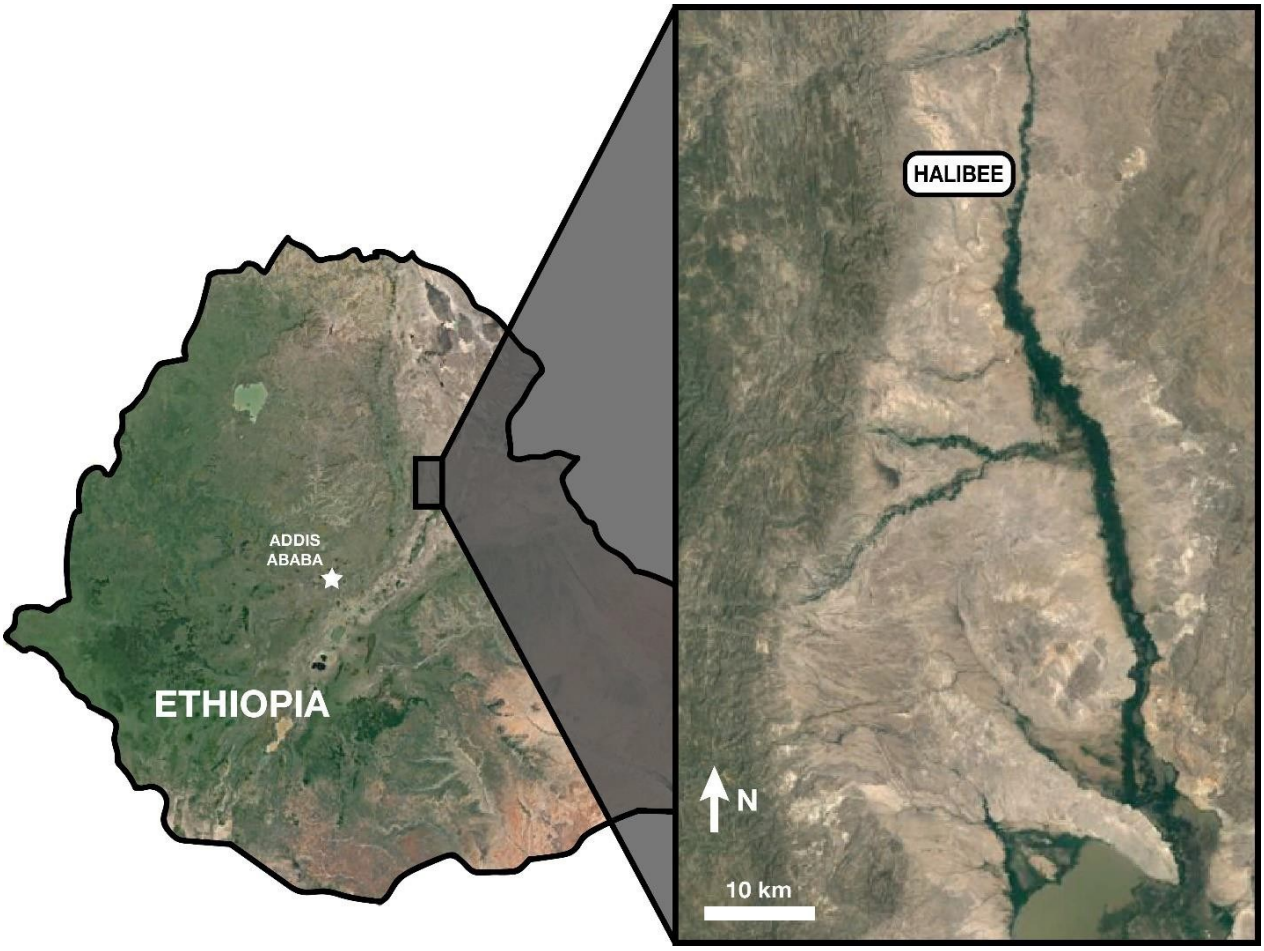

Figure 1. Map showing the location of the Middle Awash study area, indicated on the left by the grey rectangle. The research area is enlarged in the inset map on the right with the location of the Halibee area indicated. The modern Awash River is visible as the dark green strip of vegetation running approximately north-south. Map data ©2018 Google.

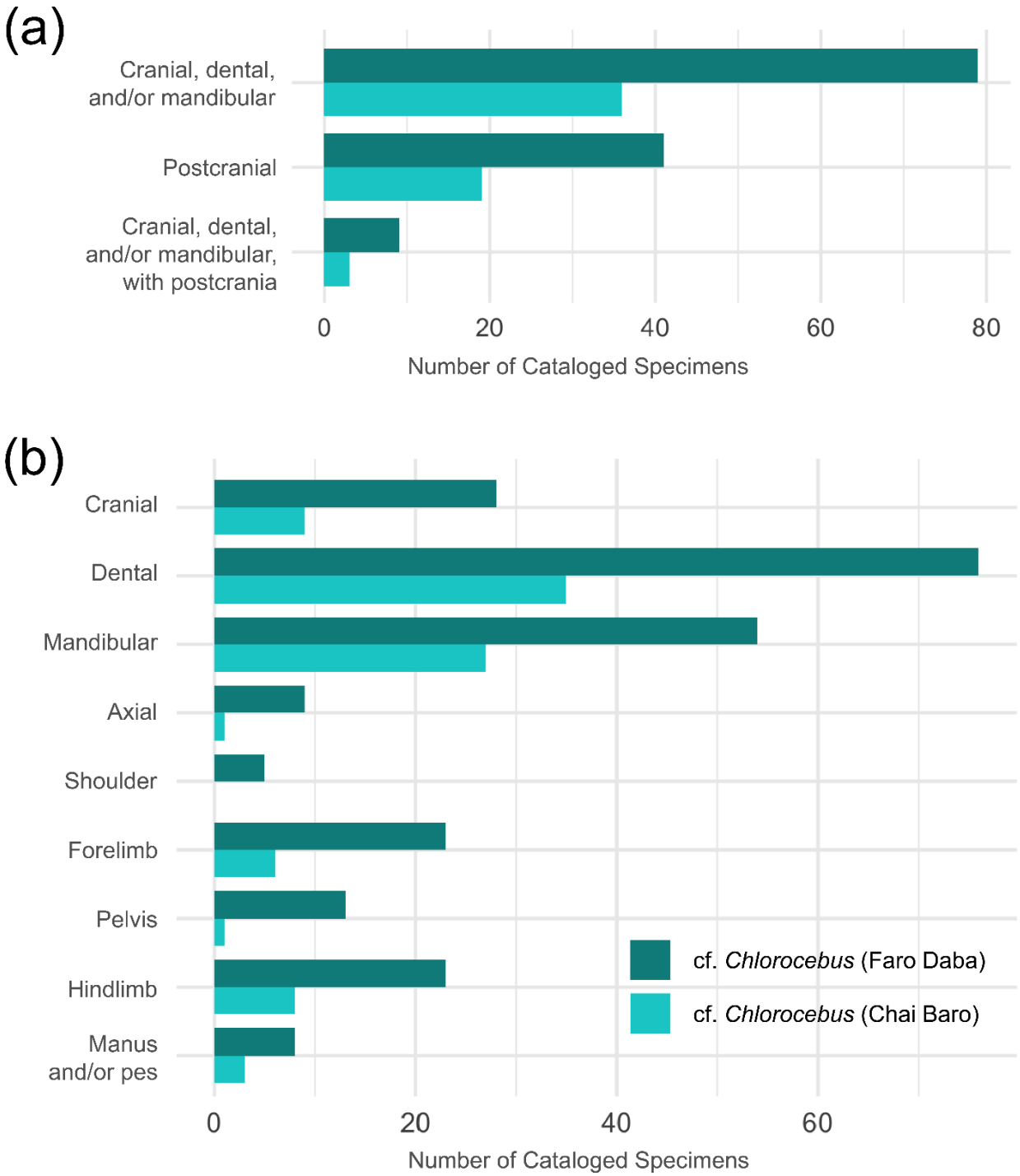

Figure 2. Element counts for Faro Daba and Chai Baro cf. *Chlorocebus*. (a) Element preservation by type. Each specimen is included once. (b) Element count by region – if an individual preserves fossils from multiple regions, they are included in each region count.

Figure 3. The partial male skeleton HAL-VP-9/650 from Faro Daba.

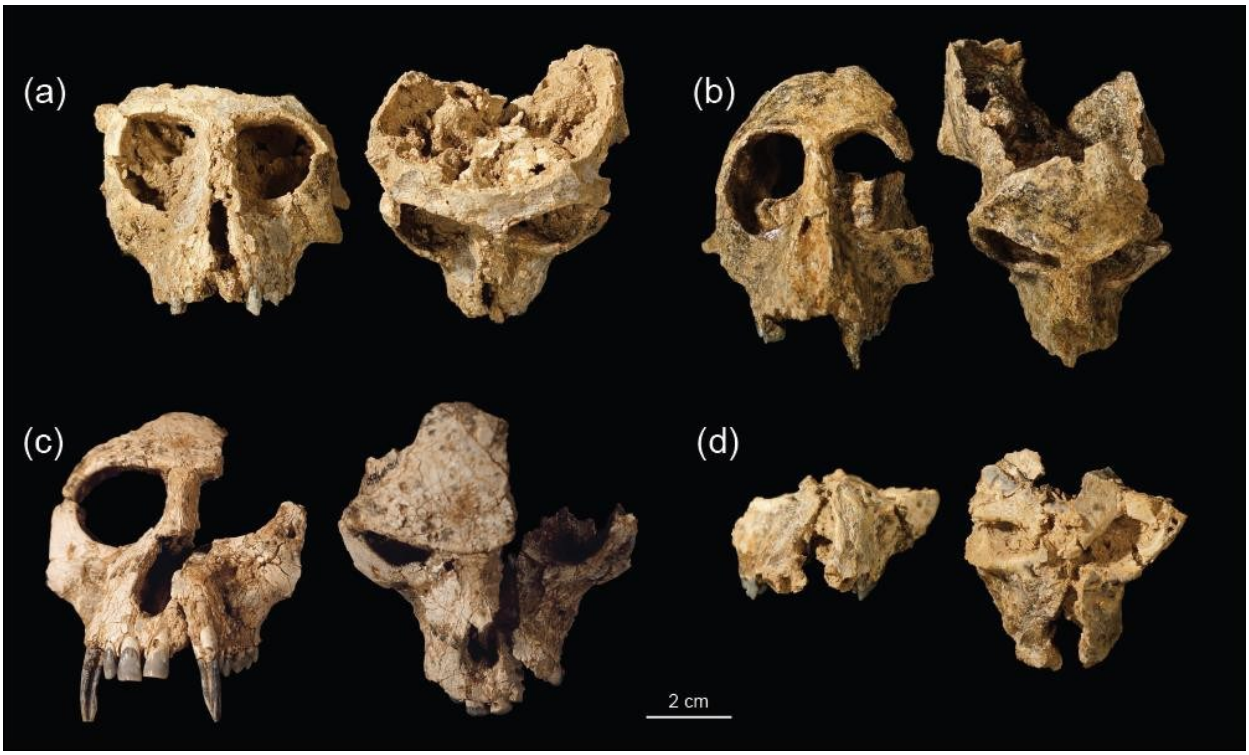

Figure 4. Crania from Chai Baro (a &b) and Faro Daba (c & d). Each individual is shown in anterior (left) and superior (right) views. a) HAL-VP-5/150, female; b) HAL-VP-5/293, female; c) HAL-VP-9/650, male; d) HAL-VP-9/13, sex uncertain.

Figure 5. Maxilla and mandible of HAL-VP-9/634, male from Faro Daba in lateral view (left) and occlusal view (right).

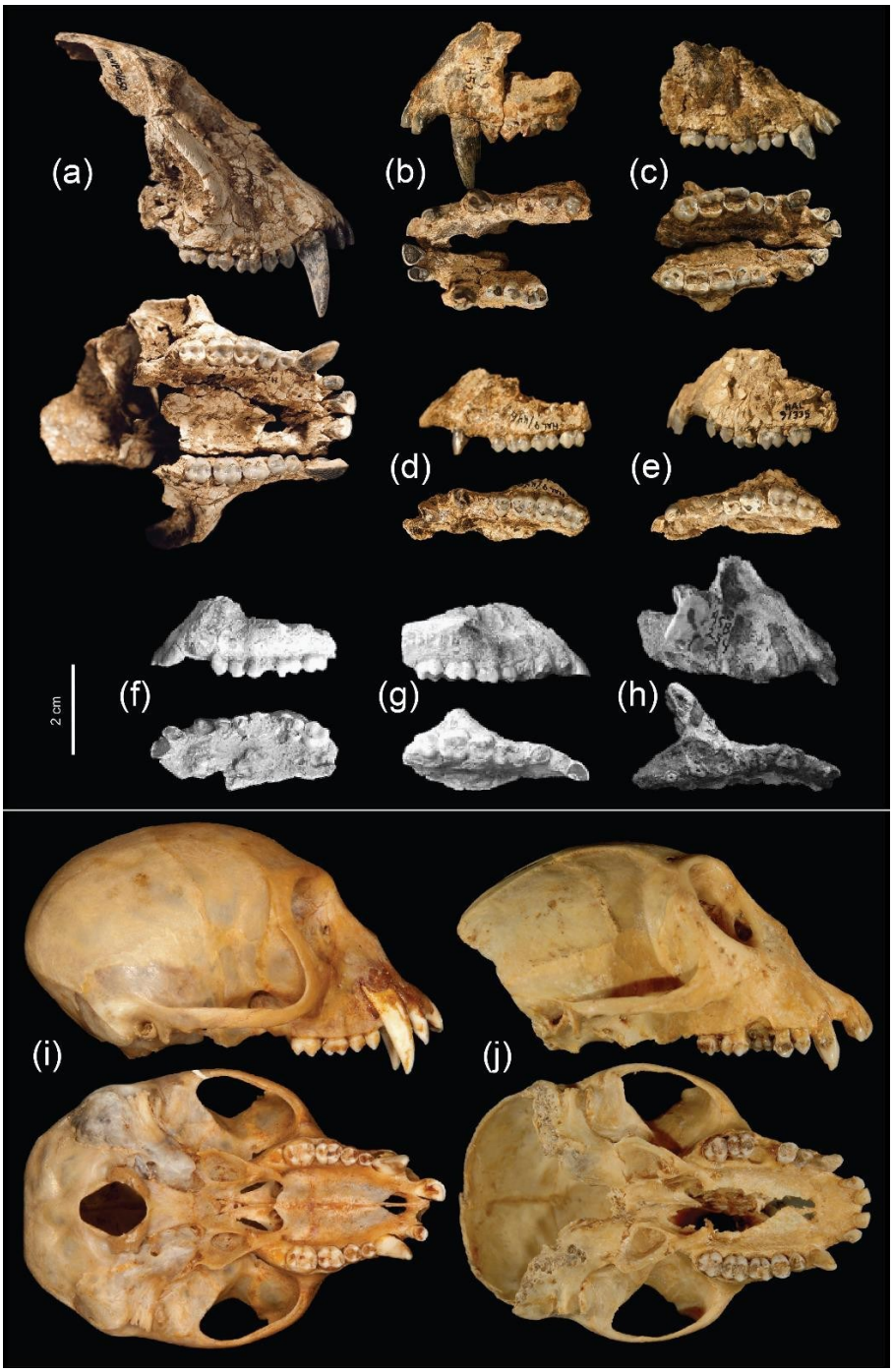

Figure 6. Maxillae from Faro Daba with fossil and extant comparisons. Each individual is shown in lateral view (top) and occlusal view (bottom). (a) HAL-VP-9/650, male; (b) HAL-VP-9/1452, male; (c) HAL-VP-9/865, female; (d) HAL-VP-9/446, female; (e) HAL-VP-9/335, female; (f) ASB-87-1, female; (g) ASB-89, male; (h) ASB-254-1; (i) Michigan Museum of Zoology 9207 (*Chlorocebus pygerythrus*), male; (j) MMZ 86350 (*Cercopithecus mona*), sex uncertain. Photos for (i) and (j) photos by Phil Myers (licensed http://creativecommons.org/licenses/by-nc-sa/3.0/). Scale is the same for both panels.

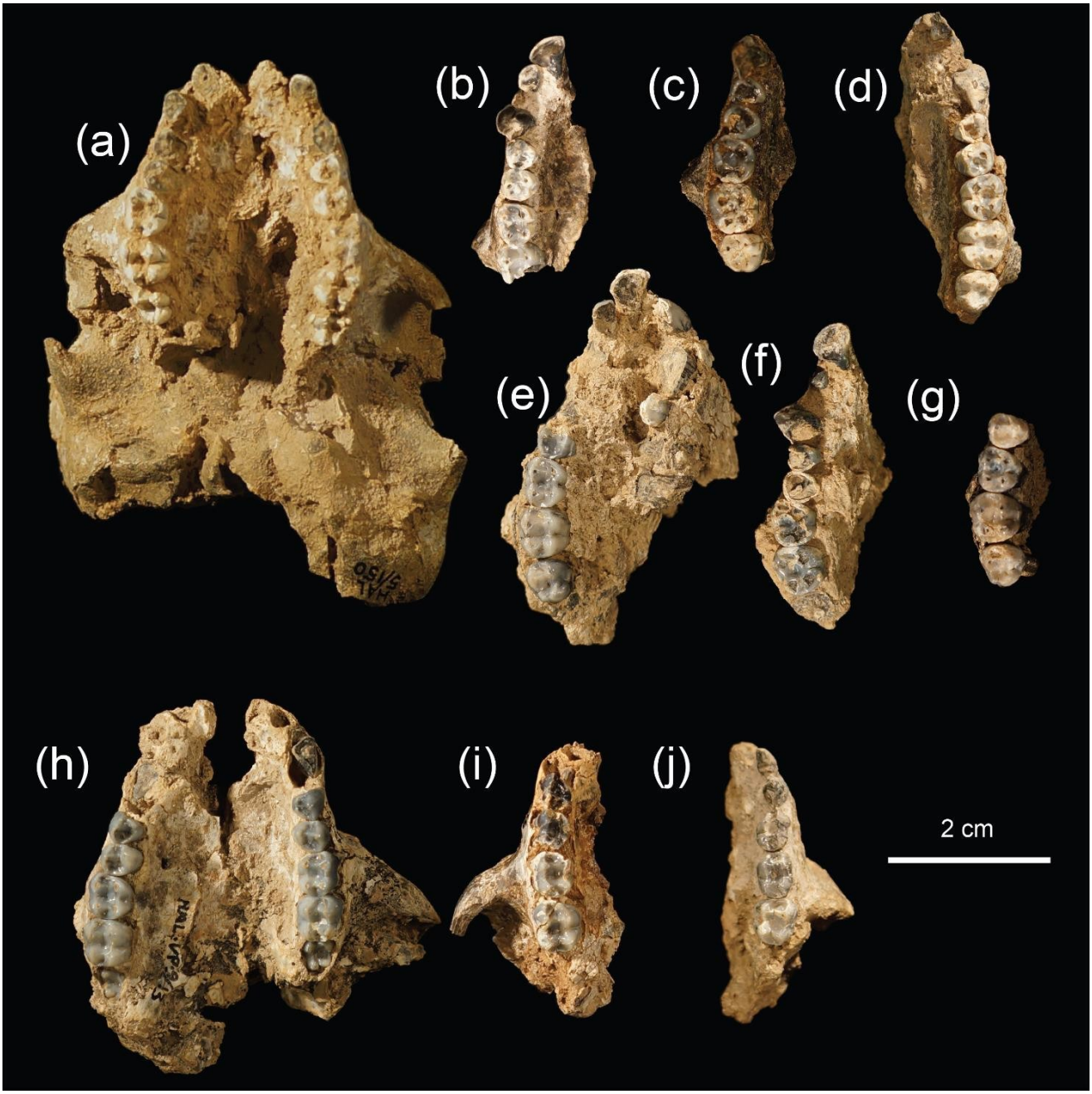

Figure 7. Occlusal views of maxillae from Chai Baro (a-g, j) and Faro Daba (h & i). Anterior is up. Bottom row individuals are juveniles. (a) HAL-VP-5/150, female; (b) HAL-VP-6/144, female; (c) HAL-VP-5/43, female; (d) HAL-VP-5/63, male; (e) HAL-VP-5/26, male; (f) HAL-VP-5/164, female; (g) HAL-VP-6/263, sex uncertain; (h) HAL-VP-9/13, male; (i) HAL-VP-9/385, sex uncertain; (j) HAL-VP-5/157, sex uncertain.

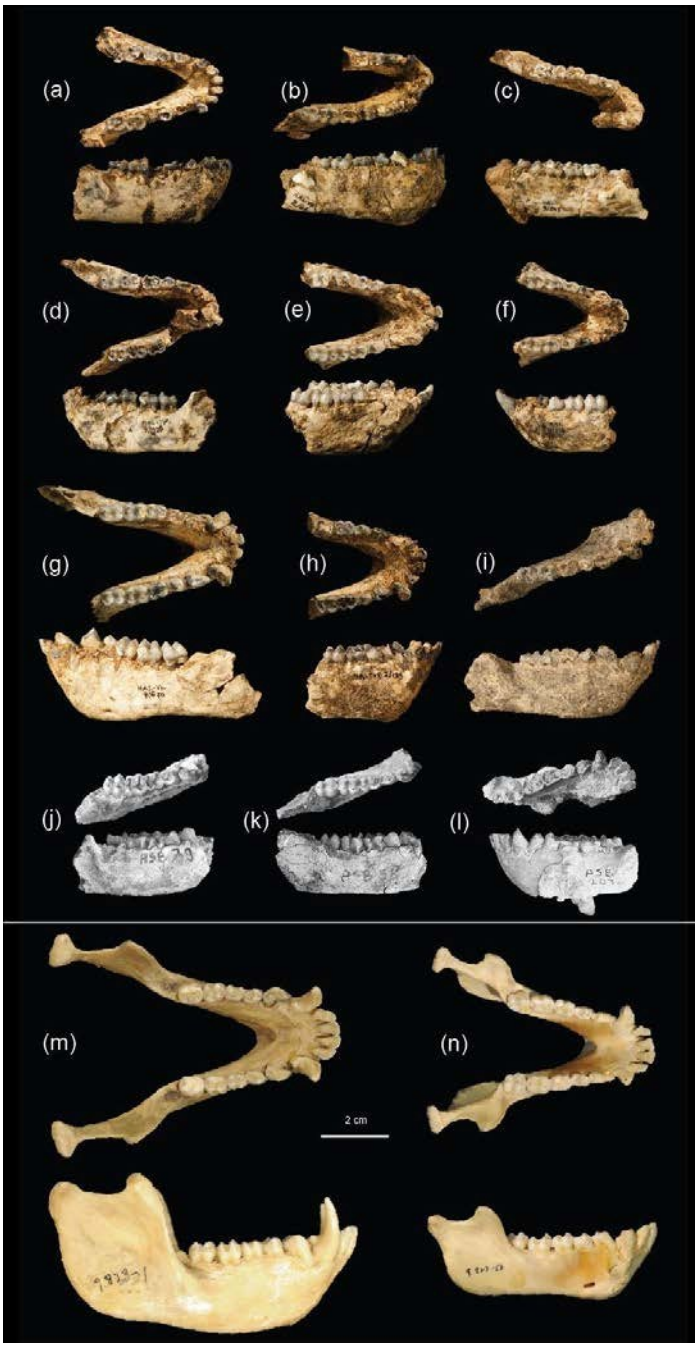

Figure 8. Mandibles in occlusal (top) and lateral (bottom) views from Faro Daba (a-h), Chai Baro (i), Asbole (j-l), and extant cercopithecins (m, n). Anterior is to the right except for lateral views of (c), (d), (f), (g), and (l). (a) HAL-VP-9/1617, female; (b) HAL-VP-2/67, female; (c) HAL-VP-9/865, female; (d) HAL-VP-9/439, female; (e) HAL-VP-9/446, female; (f) HAL-VP-9/716, sex uncertain; (g) HAL-VP-9/670, male; (h) HAL-VP-2/135, male; (i) HAL-VP-8/100, male; (j) ASB-79 (*Chlorocebus* aff. *aethiops*), female; (k) ASB-58 (*Chlorocebus* aff. *aethiops*), female; (l) ASB-254-3 (*Chlorocebus* aff. *aethiops*), female; (m) HTB 0147 (*Cercopithecus mona*), male; (n) HTB 0827 (*Chlorocebus aethiops*), female. Scale is the same for both panels. H – j are taken from Frost and Alemseged (2007).

Figure 9. Mandibles from Chai Baro and Faro Daba in occlusal view. Anterior is up. Top row, from left to right: HAL-VP-5/108, Chai Baro, female; HAL-VP-9/846, Faro Daba, female; HAL-VP-5/102, Chai Baro, female; HAL-VP-5/81, Chai Baro, sex uncertain. Bottom row, from left to right: HAL-VP-9/313, Faro Daba, sex uncertain; HAL-VP-5/77, Chai Baro, male; HAL-VP-6/257, Chai Baro, male; HAL-VP-5/26, Chai Baro, male.

Figure 10. Humeri from Faro Daba (a & c) and Chai Baro (b) with extant comparisons (d – f); medial and lateral views. (a) HAL-VP-9/650, male; (b) HAL-VP-5/148, sex uncertain; (c) HAL-VP-9/865, female; (d) HTB 2138 (*Cercopithecus mitis*), male; (e) HTB 0147 (*Cercopithecus mona*), male; (f) HTB 1162 (*Chlorocebus aethiops*), female.

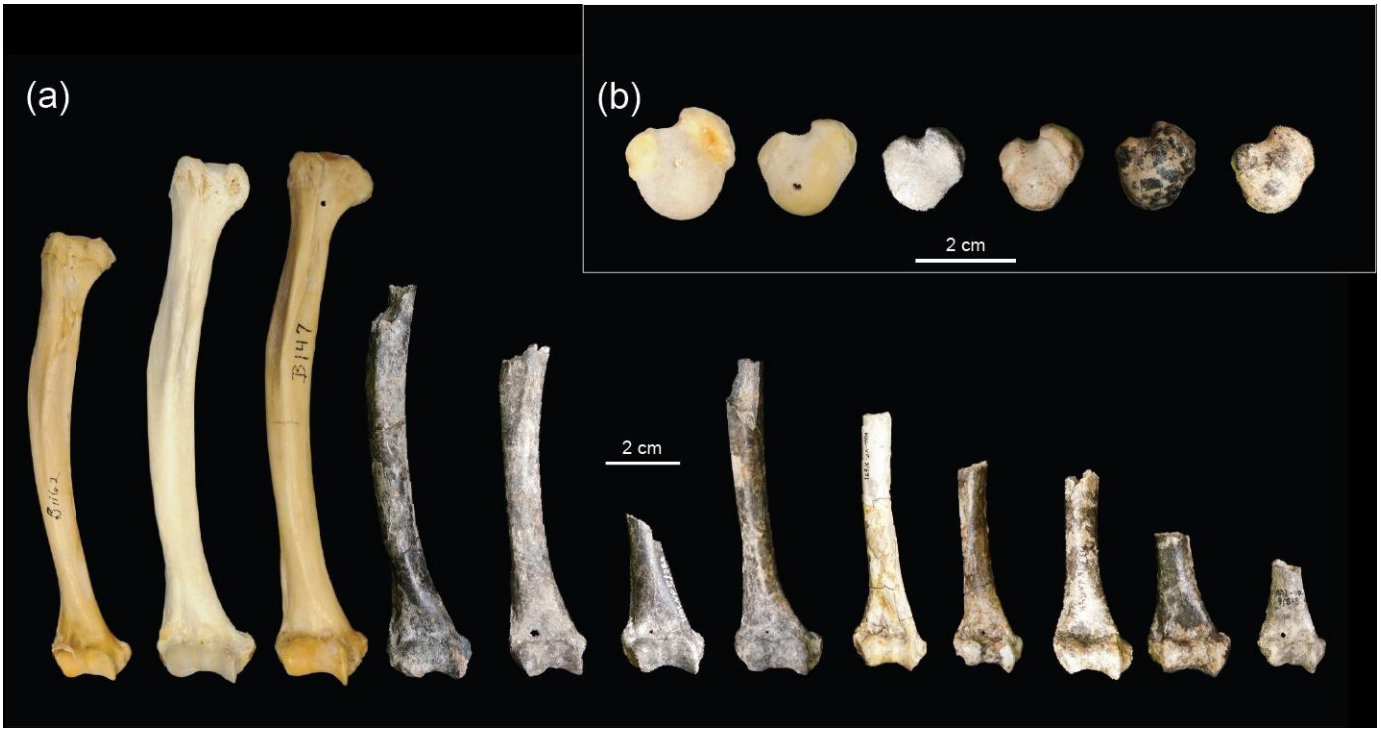

Figure 11. Fossil and extant humeri in (a) anterior and (b) proximal views. (a) Fom left to right: HTB 1162 (*Chlorocebus aethiops*), female; HTB 2138 (*Cercopithecus mitis*), male; HTB 0147 (*Cercopithecus mona*), male; HAL-VP-5/21, Chai Baro, sex uncertain; HAL-VP-5/300, Chai Baro, sex uncertain; HAL-VP-5/287, Chai Baro, sex uncertain; HAL-VP-9/416, Faro Daba, sex uncertain (mirrored); HAL-VP-9/591, Faro Daba, sex uncertain; HAL-VP-9/661, Faro Daba, sex uncertain (mirrored); HAL-VP-9/734, Faro Daba, male; HAL-VP-9/508, sex uncertain; HAL-VP-9/813, sex uncertain. (b) from left to right; HTB 2138 (*Cercopithecus mitis*), male; HTB 1162 (*Chlorocebus aethiops*), female; HAL-VP-5/148, Chai Baro, sex uncertain; HAL-VP-9/697, Faro Daba, sex uncertain; HAL-VP-9/650, Faro Daba, male; HAL-VP-9/1154, Faro Daba, sex uncertain.

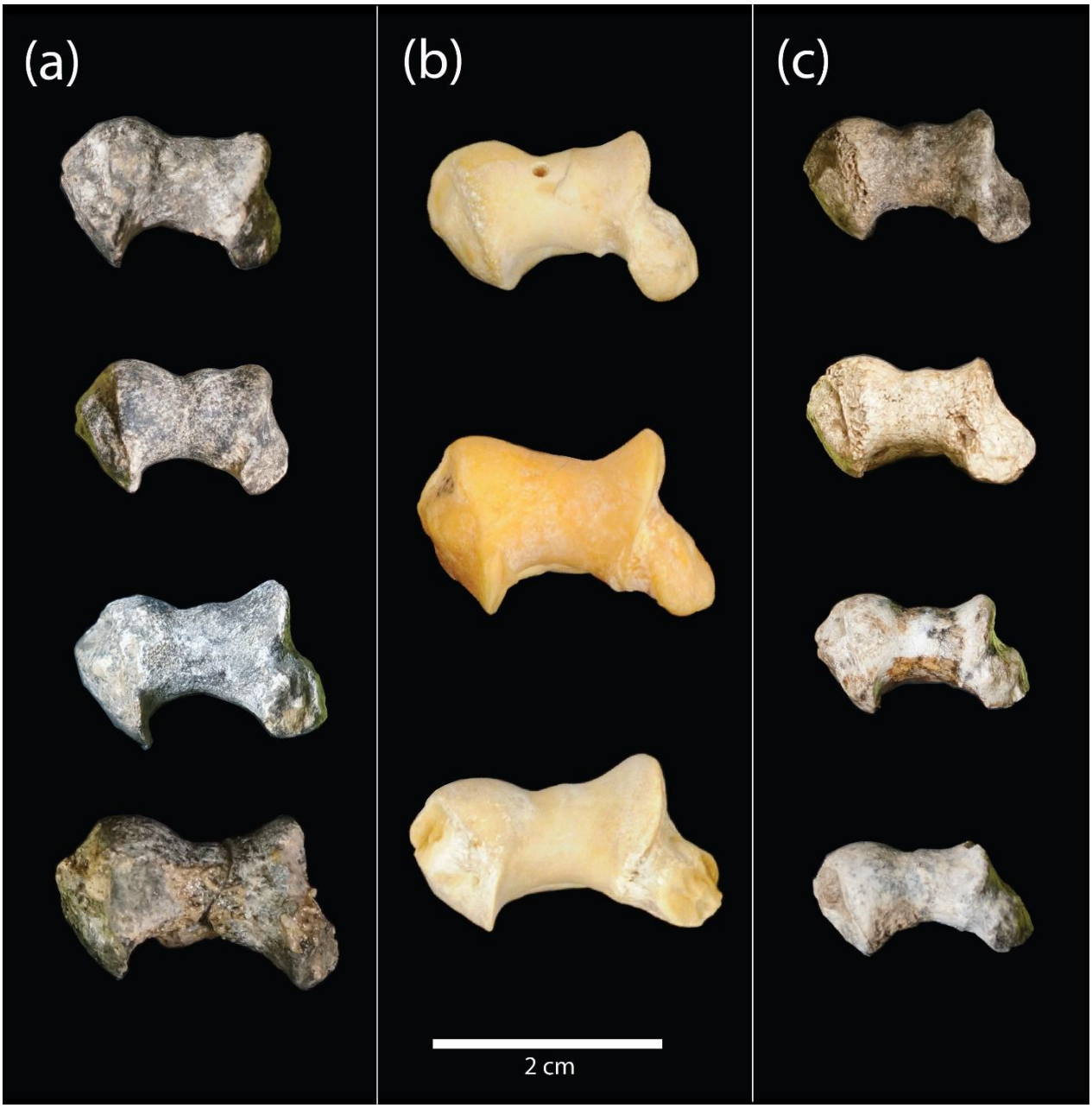

Figure 12. Distal humeri in inferior view, anterior is up. All humeri are from the right side unless otherwise stated. Sex is uncertain unless otherwise indicated. Column (a) from top to bottom (Chai Baro): HAL-VP-6/112 (mirrored); HAL-VP-6/105; HAL-VP-5/287; HAL-VP-5/113, male. Column (b) from top to bottom: HTB 1044 (*Chlorocebus aethiops*), male; HTB 0147 (*Cercopithecus mona*), male; HTB 2138 (*Cercopithecus mitis*), male. Column (c) from top to bottom (Faro Daba): HAL-VP-9/813; HAL-VP-9/1154, female; HAL-VP-9/661; HAL-VP-14/20.

Figure 13. cf. *Chlorocebus* ulnae from Faro Daba in lateral view, seriated by size from largest (left) to smallest (right). From left to right: HAL-VP-9/600, male; HAL-VP-9/650, male; HAL-VP-9/734, male; HAL-VP-2/147, female; HAL-VP-9/865, female; HAL-VP-9/1637, sex uncertain.

Figure 14. Femora from Faro Daba (left panel), Chai Baro (middle panel), and extant comparative specimens (right panel). Sex is uncertain unless otherwise indicated. (a) HAL-VP-9/740; (b) HAL-VP-9/1137; (c) HAL-VP-9/734, male; (d) HAL-VP-9/1154; (e) HAL-VP-9/1637; (f) HAL-VP-6/231; (g) HAL-VP-5/288; (h) HAL-VP-5/241; (i) HAL-VP-6/246; (j) HAL-VP-5/101; (k) HTB 0147 (*Cercopithecus mona*), male; (l) HTB 0827 (*Chlorocebus aethiops*), female.

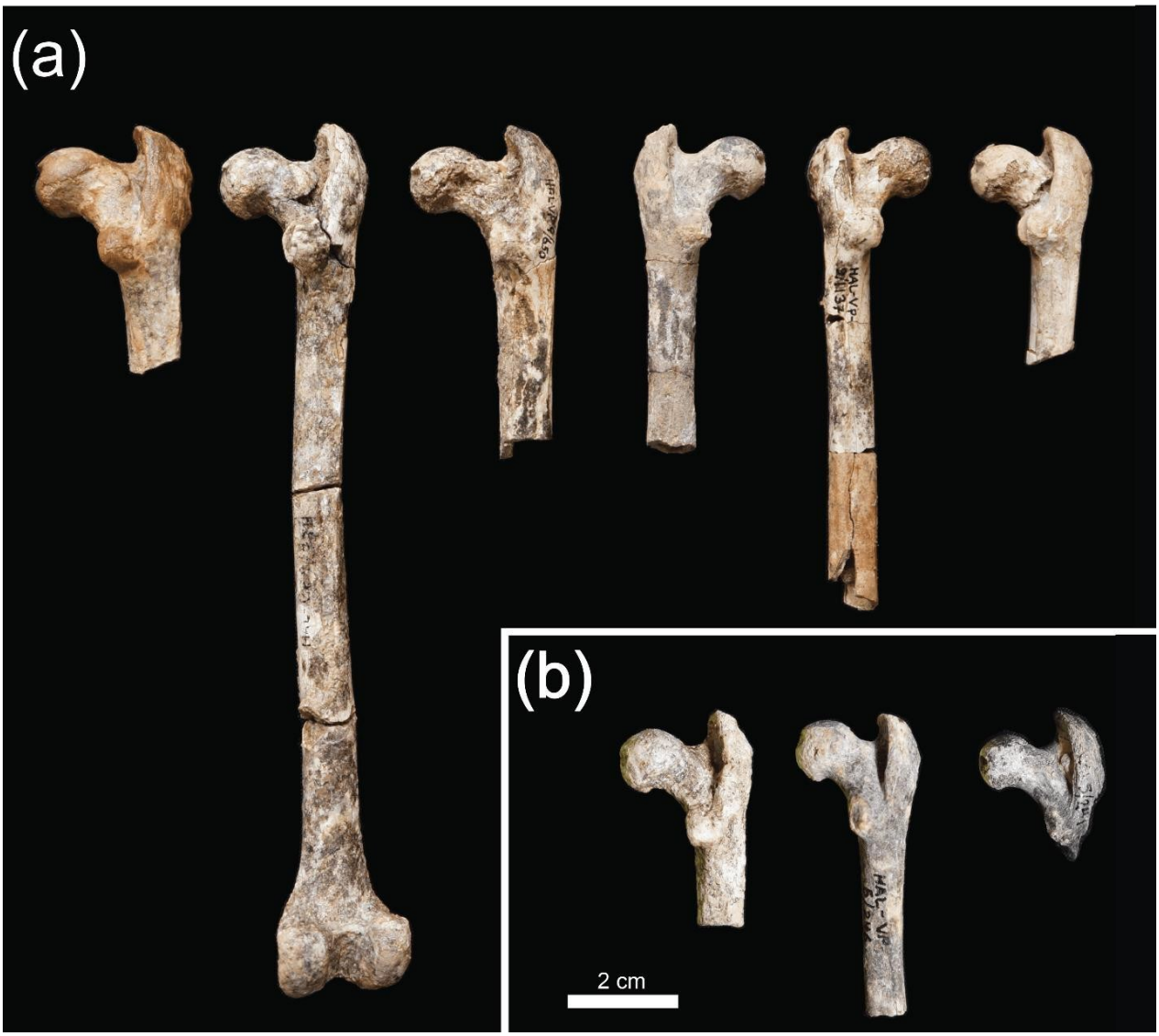

Figure 15. cf. *Chlorocebus* femora from Faro Daba (a) and Chai Baro (b) in posterior view, seriated by size from largest (left) to smallest (right). Sex is uncertain unless otherwise indicated. Left to right (largest to smallest): HAL-VP-9/600; HAL-VP-9/734, male; HAL-VP-9/650, male; HAL-VP-9/1637; HAL-VP-9/1137; HAL-VP-9/1154. HAL-VP-6/51; HAL-VP-6/246; HAL-VP-5/241.

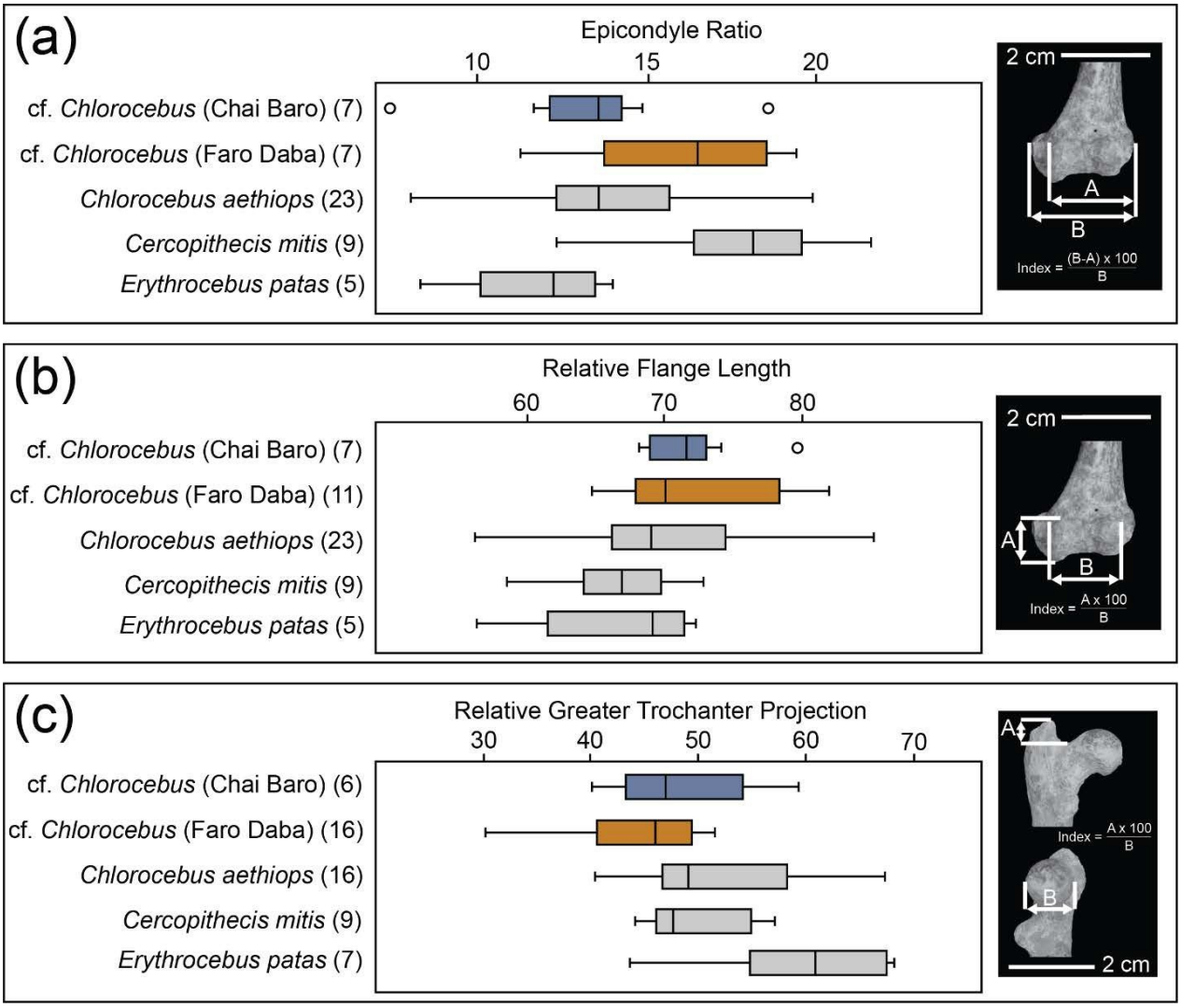

Figure 16. Three traits often considered indicative of locomotor habitus in cercopithecid monkeys with visual descriptions of each measurement on the right. The Faro Daba means fall closer to the arboreal end of the extant species, whereas the Chai Baro fossils are more similar to extant terrestrial and semi-terrestrial taxa. However, considerable overlap exists, complicated by the small sample sizes of both the extant and fossil taxa. Boxplots for modern species are modified from Frost et al. (2020b).

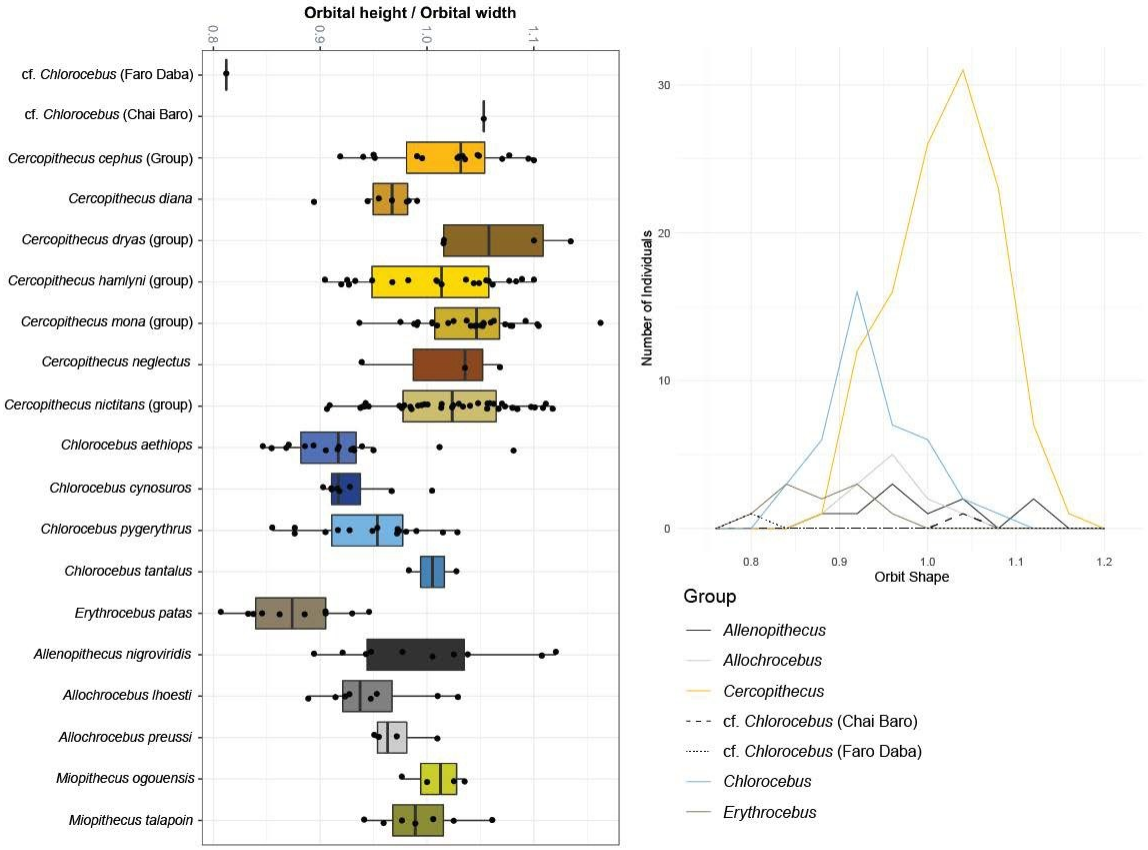

Figure 17. Boxplot of orbital shape (orbital height/orbital width, left) and distribution plot (right).

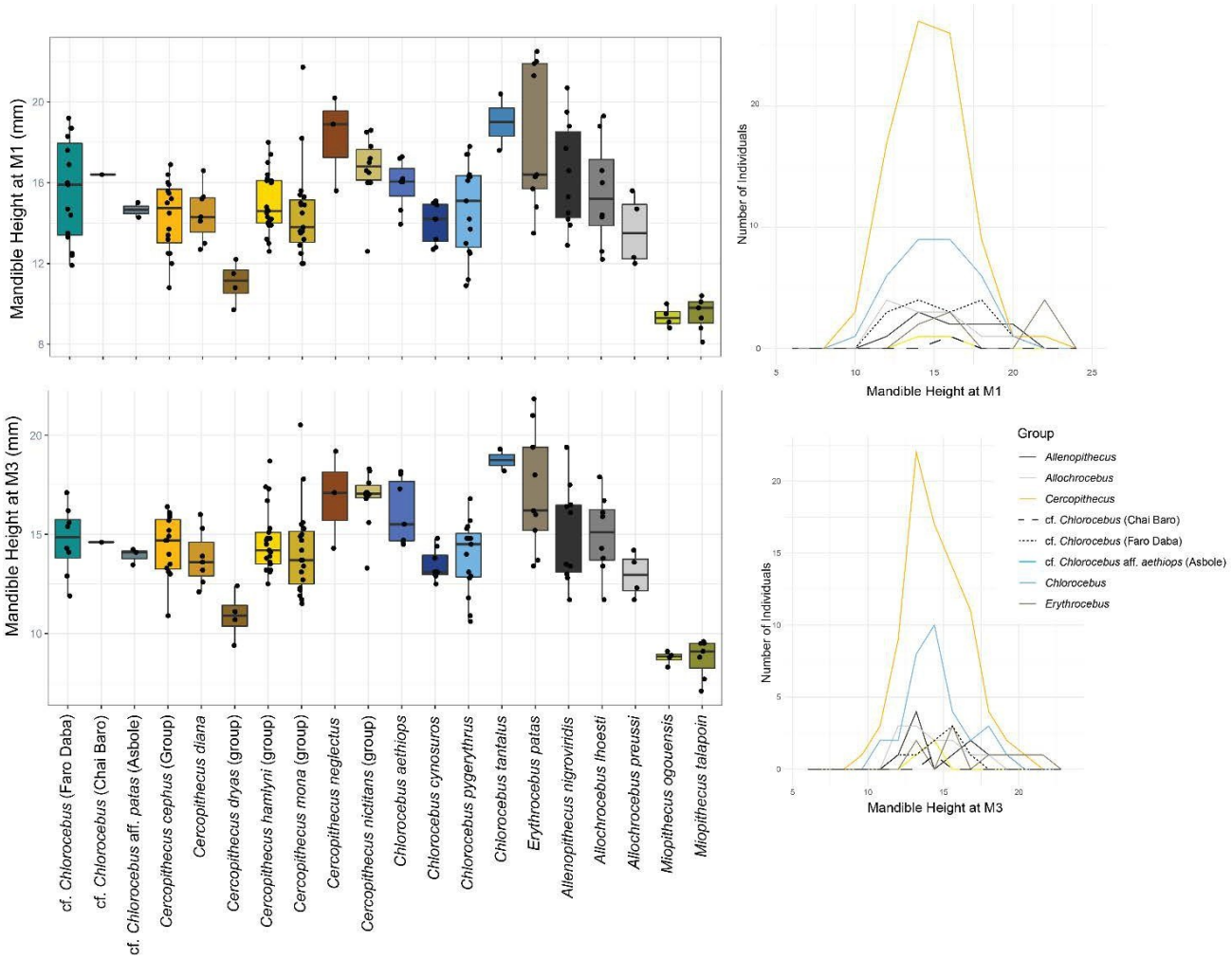

Figure 18. Boxplots of mandibular corpus height at the midpoint of M_1 (top left) and M_3 (bottom left) with corresponding distribution plots (right).

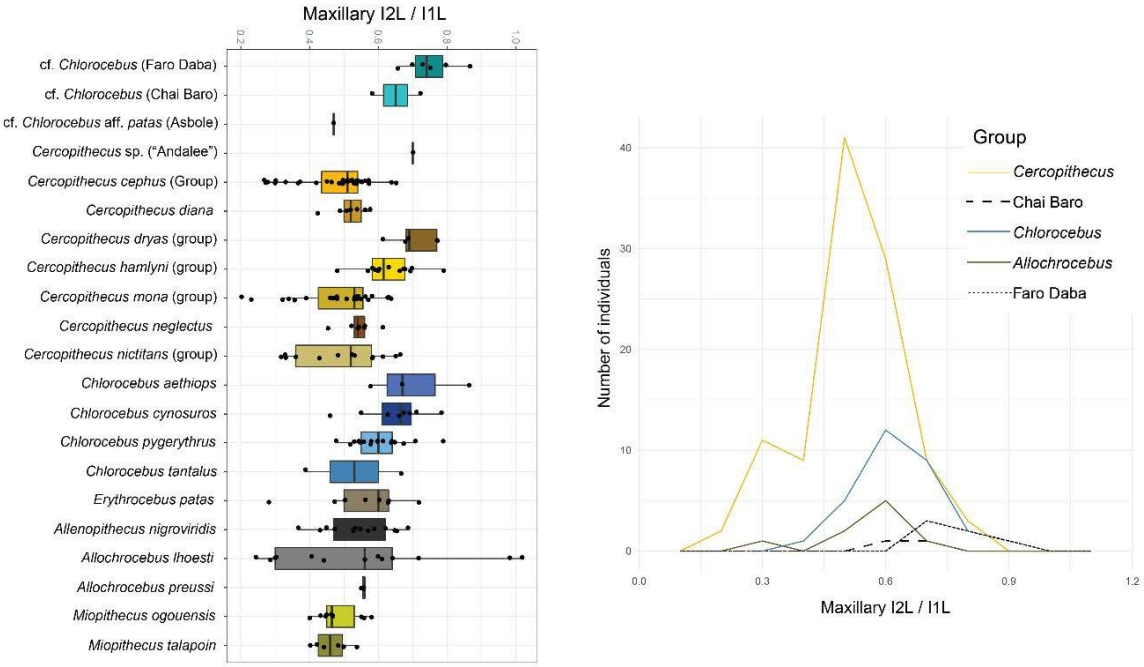

Figure 19. Boxplot of relative I^2 size (maxillary I^2 mesiodistal length / I^1 mesiodistal length; left) and corresponding distribution plot (right).

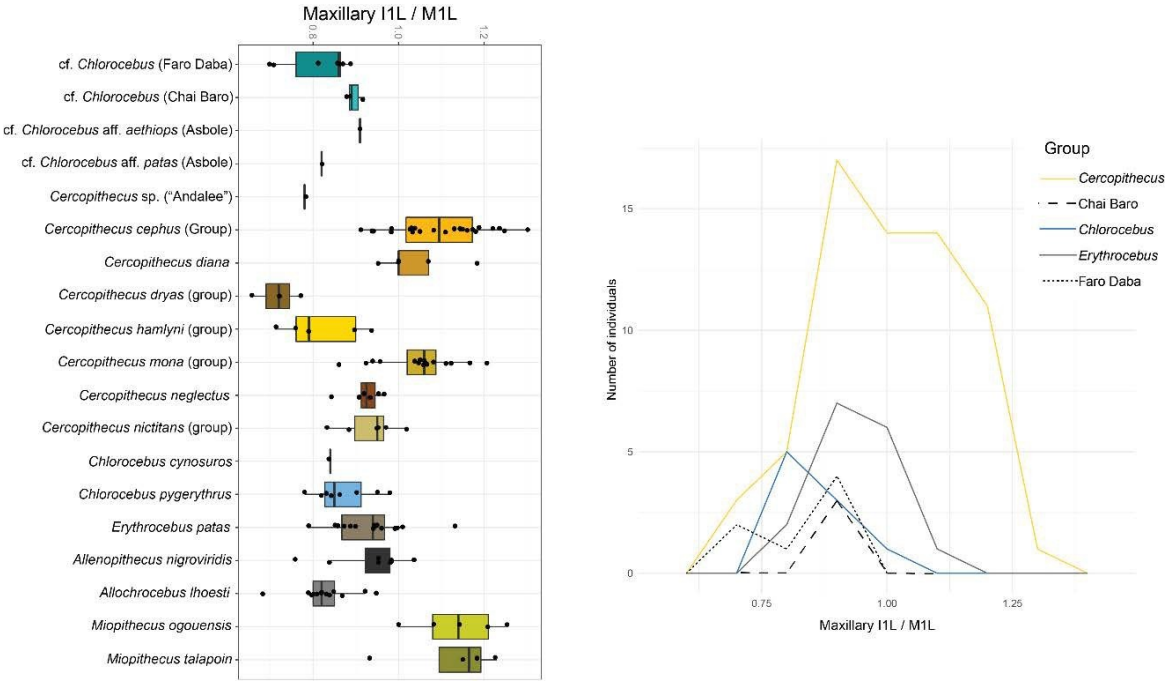

Figure 20. Boxplot of relative I^1 size (maxillary I^1 mesiodistal length / M^1 mesiodistal length; left) and corresponding distribution plot (right).

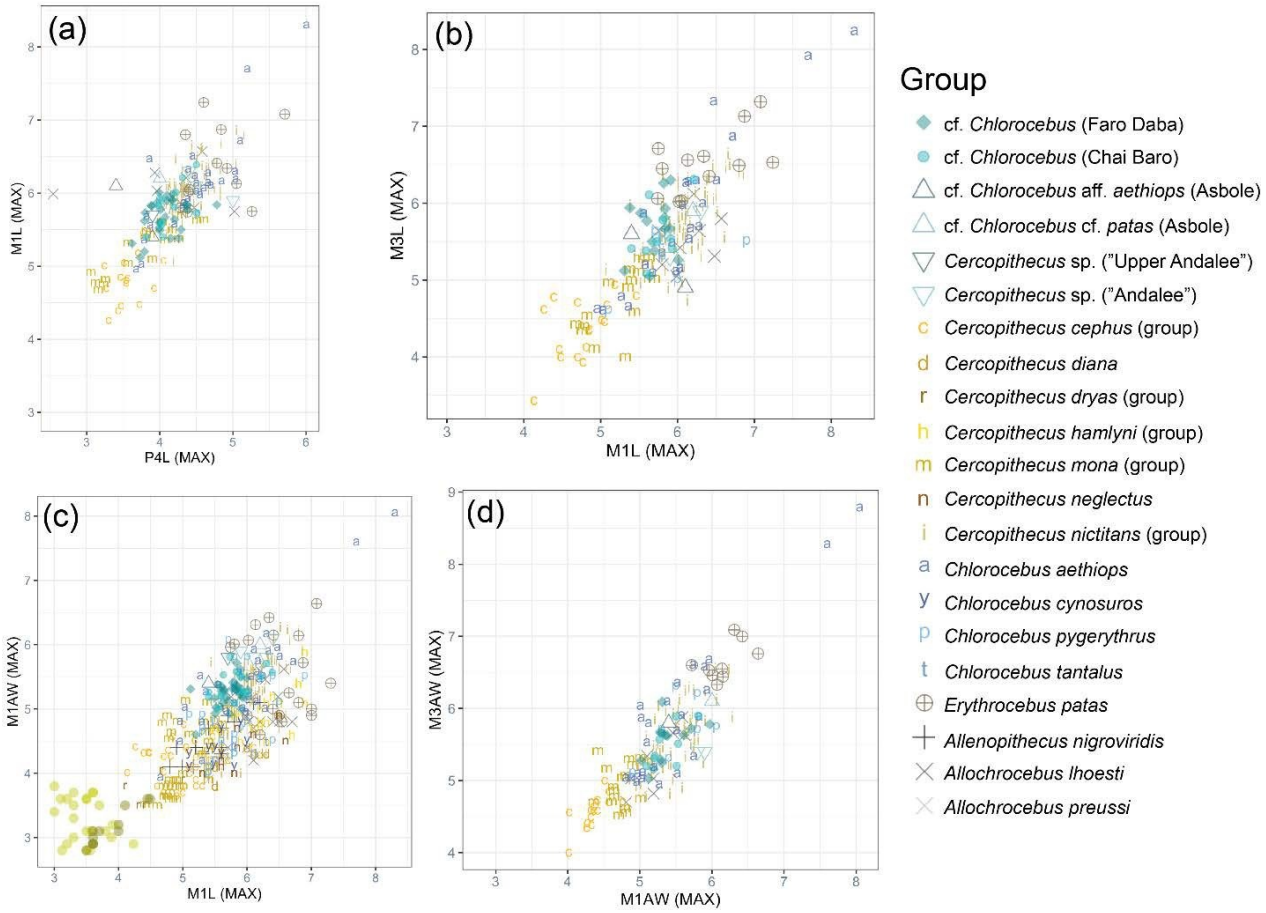

Figure 21. Maxillary dental plots of the Middle Awash fossil assemblages and fossil and extant comparative data. Measurements are in millimeters. A) M^1 maximum length vs. P^4 maximum length. B) M^3 maximum length vs. M^1 maximum length. C) M^1 anterior width vs. M^1 length. D) M^3 anterior width vs. M^1 anterior width. Abbreviations: L is mesiodistal crown length; AW is buccolingual width of the anterior loph; P4, M1, M2, and M3 refer to the fourth premolar and first, second, and third molars, respectively.

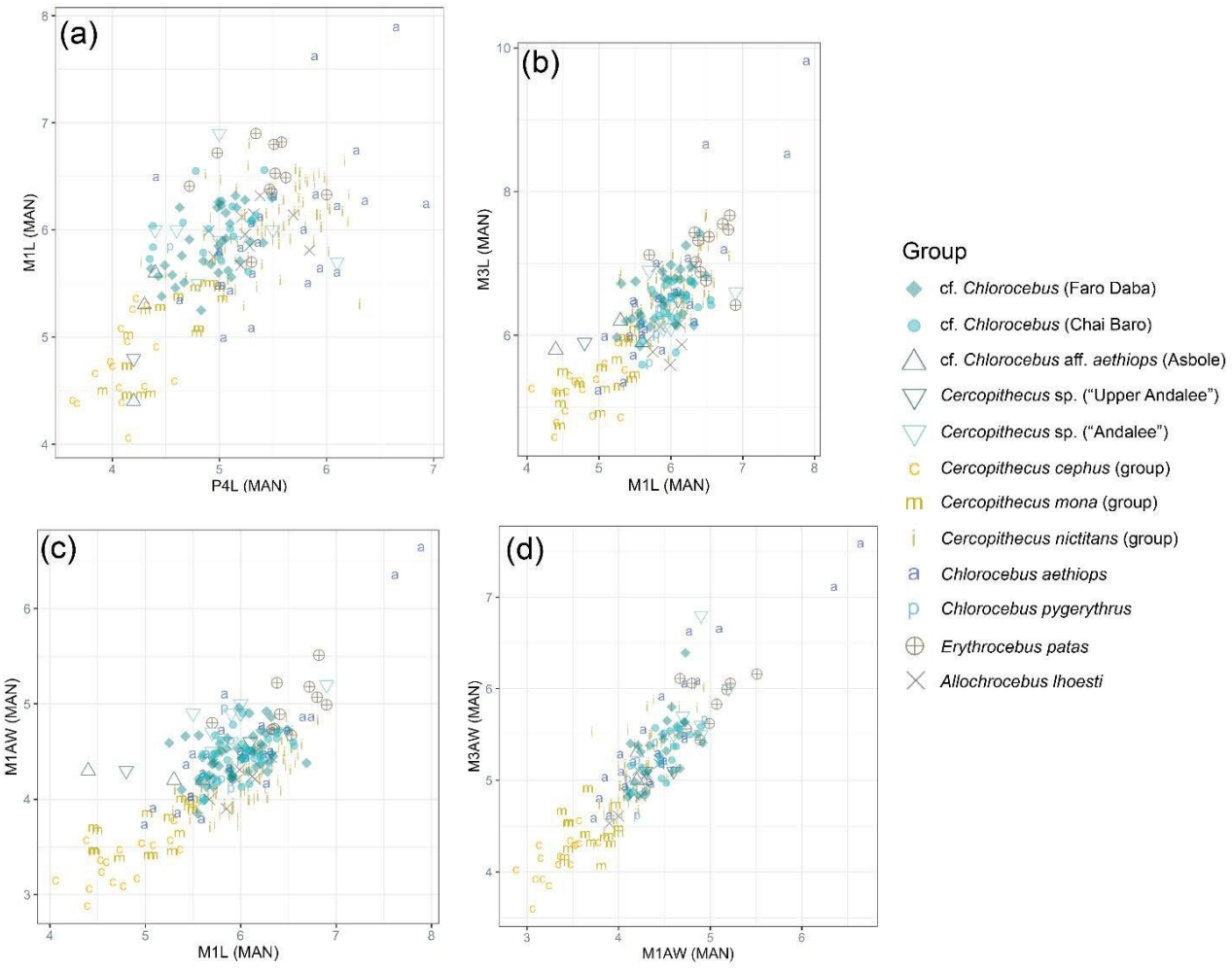

Figure 22. Mandibular dental plots of the Middle Awash fossil assemblages and comparative fossil and extant data. Measurements are in millimeters. A) M_1 maximum length vs. P_4 maximum length. B) M_3 maximum length vs. M_1 maximum length. C) M_1 anterior width vs. M_1 length. D) M_3 anterior width vs. M_1 anterior width. Abbreviations: L is mesiodistal crown length; AW is buccolingual width of the anterior loph; P4, M1, M2, and M3 refer to the fourth premolar and first, second, and third molars, respectively.

	Faro Daba cf. *Chlorocebus*				Chai Baro cf. *Chlorocebus*			
	Relative I1 Size	Relative I2 Size	Orbital Shape	Facial Length	Relative I1 Size	Relative I2 Size	Orbital Shape	Facial Length
Allenopithecus nigroviridis	**0.041**	**0.020**	0.090	–	0.471	0.315	0.390	0.547
Allochrocebus lhoesti	0.984	**0.002**	0.304	–	0.380	0.175	0.134	0.340
Allochrocebus preussi	–	–	0.196	–	–	–	0.269	0.990
Cercopithecus albogularis	–	–	**0.017**	–	–	–	0.629	0.077
Cercopithecus ascanius	**<0.001**	**<0.001**	**0.018**	–	**0.008**	**0.009**	0.876	0.642
Cercopithecus campbelli	–	–	**0.020**	–	–	–	0.803	0.492
Cercopithecus cephus	**0.001**	**0.030**	0.054	–	0.052	0.311	0.693	0.823
Cercopithecus denti	**<0.001**	**<0.001**	**0.033**	–	**0.021**	**0.014**	0.791	0.290
Cercopithecus diana	**0.002**	**0.002**	0.242	–	0.081	0.091	0.181	0.571
Cercopithecus dryas	0.410	0.976	**0.025**	–	0.162	0.625	0.953	0.413
Cercopithecus erythrotis	–	–	0.109	–	–	–	0.770	0.494
Cercopithecus hamlyni	0.980	0.120	**0.035**	–	0.446	0.570	0.618	0.127
Cercopithecus lomamiensis	–	–	0.31	–	–	–	0.17	**0.04**
Cercopithecus mitis	0.090	**0.006**	**0.039**	–	0.600	0.170	0.558	0.055
Cercopithecus neglectus	0.151	**0.010**	0.075	–	0.747	0.211	0.589	0.147
Cercopithecus petaurista	0.207	**0.026**	0.248	–	0.714	0.226	0.214	0.483
Cercopithecus pogonias	**0.011**	**0.001**	**0.044**	–	0.714	0.066	0.637	0.727
Cercopithecus wolfi	**<0.001**	**0.005**	**0.010**	–	0.049	0.166	0.927	0.525
Chlorocebus aethiops	–	–	0.464	–	–	–	0.062	0.503
Chlorocebus cynosuros	0.994	**0.035**	–	–	0.616	0.139	0.074	0.675
Chlorocebus pygerythrus	0.525	0.223	–	–	0.720	0.810	0.897	0.897
Erythrocebus patas	**0.043**	**0.023**	–	–	0.585	0.339	–	–

Supplementary Table 1. Results of Kruskal-Wallis non-parametric statistical analyses. P values are presented and bolded when the result is statistically significant ($p<0.05$).